WSRC-OS-2002-0051

3D GEOLOGICAL MODELING
OF THE
GENERAL SEPARATIONS AREA, SAVANNAH RIVER SITE
- A PRELIMINARY WORKFLOW AND MODEL -

- AUGUST 2002 -

GUILLAUME JEAN – E.N.S.GEOLOGIE, FRANCE
JEFFREY M.YARUS, RICHARD L. CHAMBERS - QGSI
M. K. HARRIS, G.P. FLACH, M. MILLINGS, F. SYMS - WSRC

EXECUTIVE SUMMARY

Quantitative Geosciences, LLP was solicited by the Savannah River Site to build a three dimensional geological model of a specific area within the site known as the General Separations Area (GSA) using the modeling tools of the petroleum industry. The main objective is identify useful technologies employed by the petroleum industries for aquifer characterization and flow transport and transfer the technology to SRS by building a full 3D high resolution model that can be used in a flow simulator for the purpose of tracking ground water contaminants.

Workflow

The data set used for this 3D model contains data from more than 600 locations, including Cone Penetrometer Test data and percentage of mud from visual description of core. The surface well picks were defined from core description. Core descriptions from more than 100 wells were studied to identify depositional facies.

The first step was to build key marker horizons from well tops using Kriging, a geostatistical interpolation algorithm. Unlike traditional estimation procedures, Kriging uses spatial modeling to minimize error variances to improve estimates by incorporating distance and orientation in its weighting procedures. The spatial models, called variograms, allow resulting maps to capture the geological fabric often obscured by more commonly used techniques.

Next, based on sequence stratigraphic principles, a 3D grid was constructed representing the discretized volume. The maximum flooding surface was used as a reference to create stratigraphic gridding in each sequence. The depositional facies from 114 well logs were distributed within the grid using indicator based conditional simulation. Multiple realizations (200 for each sequence) were run and the results accurately depicted the main oriented scales of the depositional environments.

Finally, multiple realizations of petrophysical properties derived from Cone Penetration Tests and percent mud from core data were distributed separately within the depositional facies. The main simulated property was percentage of mud. The CPT data were used to assist in the percent mud modeling. Basic summary statistics were computed from the realizations.

Result

The construction of the different structural horizons was not simple, requiring complex, multi-directional variogram models. Several modeling attempts were required for each surface before the final surface was created. Artifacts, commonly referred to as

"pimples" occur at several well locations suggesting that the well picks require additional editing.

The experimental depositional facies variograms interpretations were difficult when first computed. So, 2D variogram maps were computed to find the spatial correlation scales and directions of the facies. However, the 2D maps represent a composite of the interval and it was not possible to accurately determine any correlation structure for the depositional facies. When 3D variogram maps were used it was very easy to see some structures. For the simulations, only the major facies were retained for each formation as delimited by the structural surfaces. These facies are: 1) Fluvial and Floodplain/Overbank muds for the Upland, 2) Tidal Flat/Lagoonal and Barrier Beach for the Barnwell Group, 3) Siliciclastic Shelf, Middle Shelf (low energy), Middle Shelf (high energy) and Open/outer Shelf for the Santee, 4) Open/outer Shelf, Lower Shoreface and Innerbay/Lagoonal for the Green Clay, and 5) Lower Shoreface and Innerbay/Lagoonal for the Congaree. After generating 200 simulations, the most common facies per cell (mode) was calculated, producing reasonable results. However, two problems with this approach are that the most common facies is biased towards the major facies in terms of global proportions within the formation, and the resulting map does not have the finer-scale heterogeneity of a simulation.

Petrophysical variograms and variogram maps show subtle structures, however, the results of the 200 simulations look reasonable. The correlation between friction ratio from CPT data and the mean of percent mud (from the 200 simulations) were calculated separately in each depositional facies (from most common facies maps). The correlation found was very low, with a correlation coefficient greater than 0.2 in only one facies. This implies that the CPT data had very little impact in this phase of the project.

The project results are encouraging enough to build a full 3D model. In the next phase of the project, simulation ranking will be completed to improve the model, in terms of depositional facies and petrophysics. The TCCZ formation will be added to the model, the permeability will be calculated from the petrophysics, and some streamlines flow simulations will be performed.

Table of Contents

Table of Figures

Introduction

The Savannah River Site, located in South Carolina, contains nuclear defense products and nuclear waste byproducts as result of national defense operations dating to the 1950's. The facility has been the subject of a variety of scientific investigations focusing on potential ground water transportation of nuclides and other hazardous materials through the different aquifers within the site. The area of particular interest, and the subject of this report, is the General Separations Area.

The modeling of fluid flow through porous media is not unique to the environmental industry. In fact, the mathematical characterization of porous and permeable rock has been an area of substantial research and application in the petroleum industry, particularly over the past several decades. Although the emphasis in the petroleum industry has been to improve hydrocarbon production, the modeling objectives are similar to the environmental industry in its need to better understand the transportation of fluids and particularly through the subsurface.

The need to improve hydrocarbon production motivated the development of powerful computational techniques and software for modeling the surface, subsurface, and porous and permeable rock. Scientists from the Savannah River Site desire a better understanding of petroleum reservoir modeling technology and its potential implementation in their modeling efforts.

Quantitative Geosciences, LLP was solicited by the Savannah River Site to build a three dimensional geological model of a specific area within the General Separations Area (GSA) using petroleum industry reservoir modeling tools. The main objectives are to identify, recommend, and transfer useful technologies for aquifer characterization and fluid flow transport of ground water contaminants.

Presentation of the Savannah River Site

Background

The Savannah River Site (SRS) is a U.S. Department of Energy (DOE) facility occupying 300 square miles within Aiken, Barnwell, and Allendale counties in southwestern South Carolina (Figure 1). The site was set aside in 1950 as a controlled area for production of nuclear materials for national defense. More specifically, the SRS processes and stores nuclear materials in support of the national defense and U.S. nuclear non-proliferation efforts.

During the early 1950s SRS began to produce materials used in nuclear weapons, primarily tritium and plutonium-239. Five reactors were built to produce nuclear materials. Also built were support facilities including two chemical separations plants, a heavy water extraction plant, a nuclear fuel and target fabrication facility, a tritium extraction facility and waste management facilities.

More recently, the site has also developed and deployed technologies to improve the environment and treat nuclear and hazardous wastes left from the Cold War.

The DOE and its contractors are responsible for the operation of the SRS. Westinghouse Savannah River Company (WSRC) currently manages and operates the site.

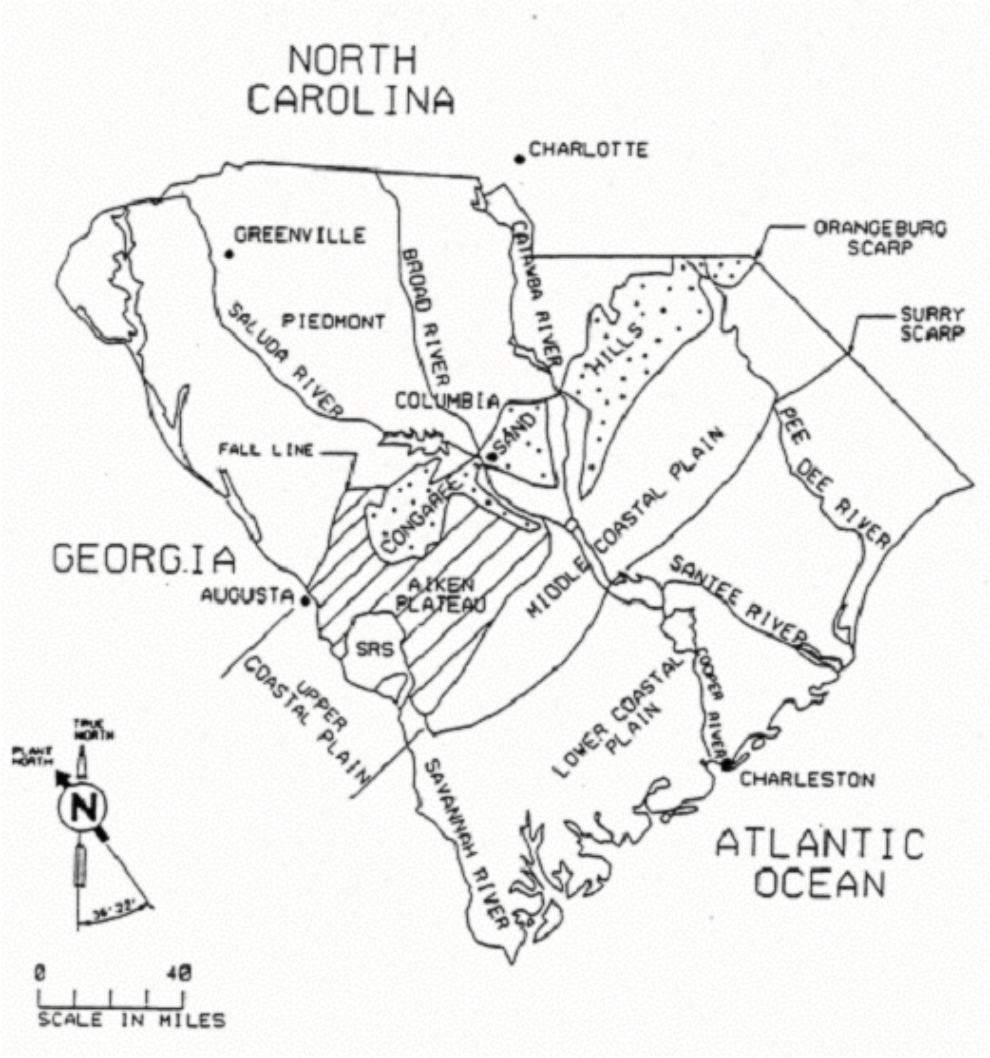

Figure 1: Location of the Savannah River Site and Physiography of the Surrounding Region (Smits, Harris, Hawkins, and Flach, 1997)

The SRS has been the focus of numerous geological and hydrogeological investigations dating from the initial geotechnical work associated with site construction in the early 1950's. The past 10 years mark resurgence in geological work at the SRS, primarily hydrogeological investigations related to waste-site characterization and remediation.

The General Separations Area (GSA) includes the F- and H-Areas, S-Area, Z-Area (including the area formerly referred to as "Y-Area") (Figure 2). The area contains several waste sites that are undergoing environmental assessment and/or closure under State and Federal regulations. The assessment process includes evaluation of the hydrogeology of the site and modeling of ground-water flow and potential transport of contaminant releases from the waste sites. The models require an extensive knowledge of the geology of the media through which the water is moving. Subsurface geologic mapping is one method by which such knowledge may be obtained. The area has

received intense geologic and hydrologic study during recent years and contains numerous borings and monitoring wells.

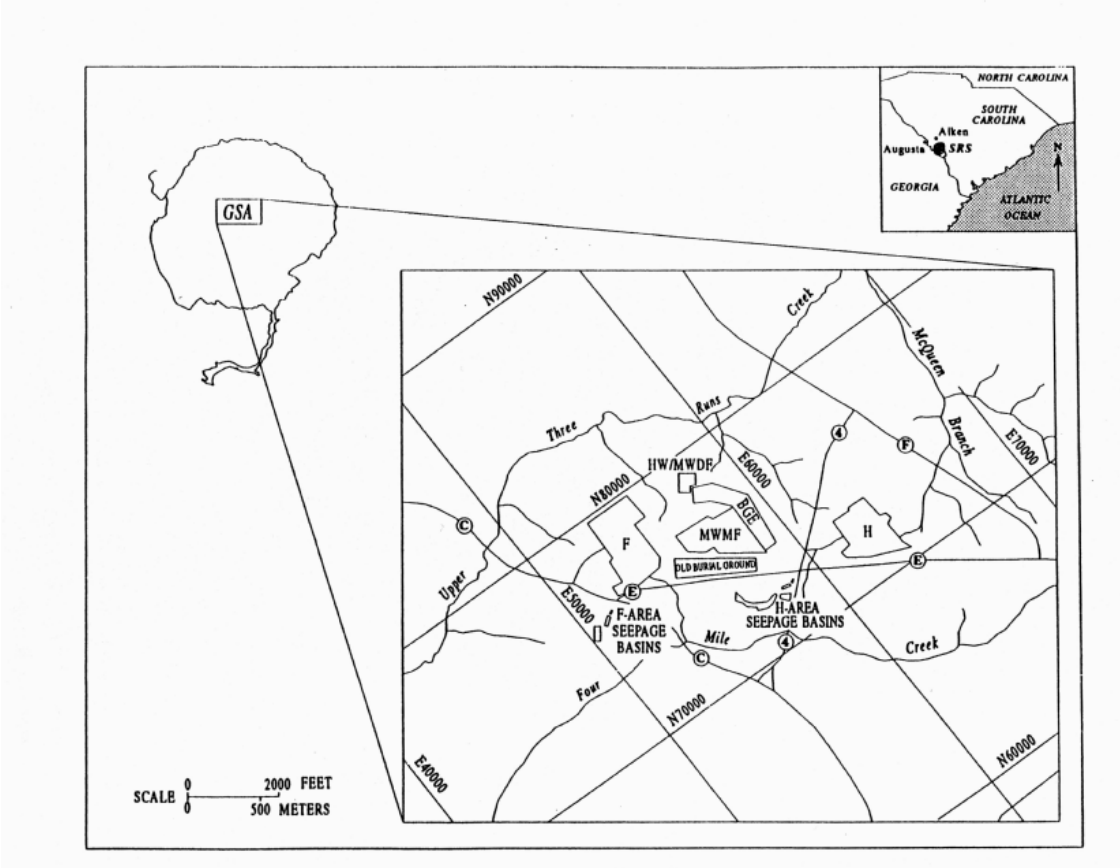

Figure 2: Location of the General Separations Area, Savannah River Site, South Carolina (Smits, Harris, Hawkins, and Flach, 1997)

Description of the study area

The SRS is centered 22.5 miles southeast of Augusta, Georgia, approximately 100 miles from the Atlantic Coast within the Upper Atlantic Coastal Plain Physiographic Province (Figure 1). The SRS is situated on the Aiken Plateau of the Atlantic Coastal Plain at an approximate elevation of 300 feet msl. Overall, the plateau has a highly dissected surface and is characterized by broad inter-fluvial areas with narrow, steep-sided valleys. Local relief can attain 280 feet. The Aiken plateau is generally well-drained, although many poorly drained sinks and depressions exist, especially in the "upland" unit. The SRS is bounded on the southwest by the Savannah River (Figure 1).

The study area comprises approximately 15 square miles of the central SRS in the GSA (Figure 2). The GSA has low to moderate topographic relief and is drained by several unnamed perennial streams. The study area is bordered by three streams with several intermittent streams present within the area boundary. Upper Three Runs forms

the northern boundary of the study area with an average elevation of 150 feet msl, Fourmile Branch forms the southern boundary with an average elevation of 200 feet msl, and McQueen Branch forms the northeastern boundary with elevations ranging from 160 to 250 feet msl. There is no natural drainage at the west margin of the area. An arbitrary boundary is established west of C Road by connecting Upper Three Runs to Fourmile Branch. The model area is shown in Figure 3.

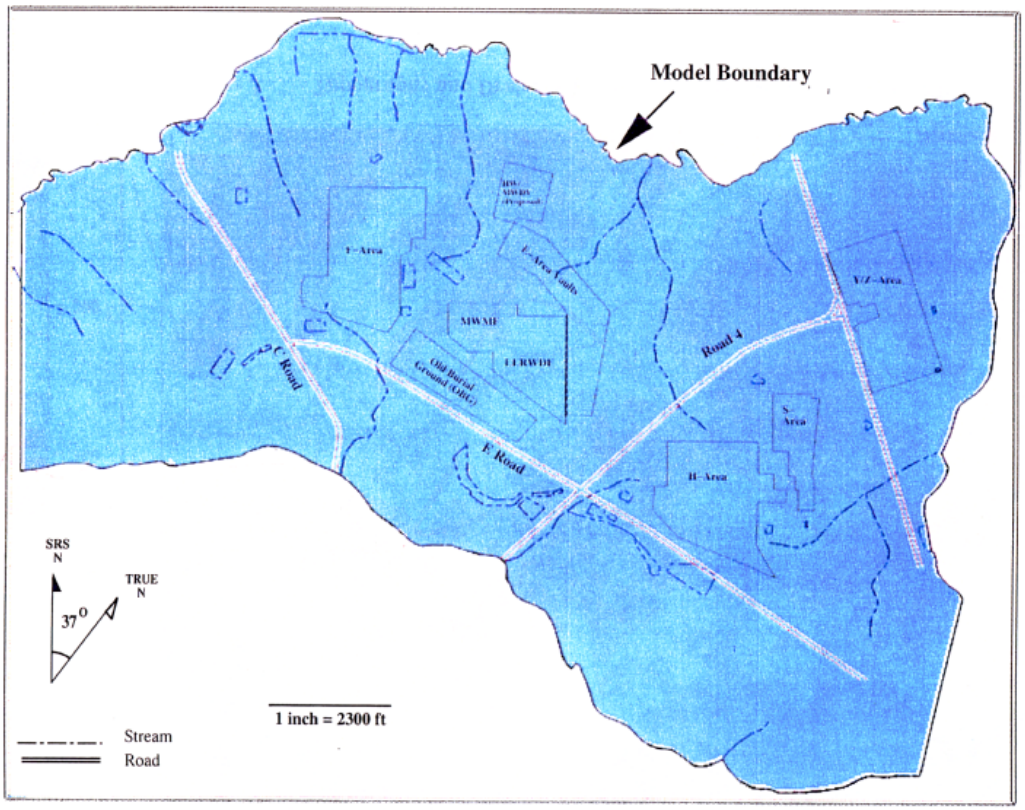

Figure 3: Model Boundaries (Smits, Harris, Hawkins, and Flach, 1997)

General Geology

The SRS area is underlain by sediment of the Atlantic Coastal Plain (Figures 1 and 4). The Atlantic Coastal Plain consists of a southeast-dipping wedge of unconsolidated and semi-consolidated sediment that extends from its contact with the Piedmont Province at the Fall Line to the edge of the continental shelf (Figure 1). The sediment ranges from Late Cretaceous to Miocene in age and comprises layers of sand, muddy sand, and mud with subordinate calcareous sediment (Figure 4). The sediment rests unconformably on crystalline and sedimentary basement rock.

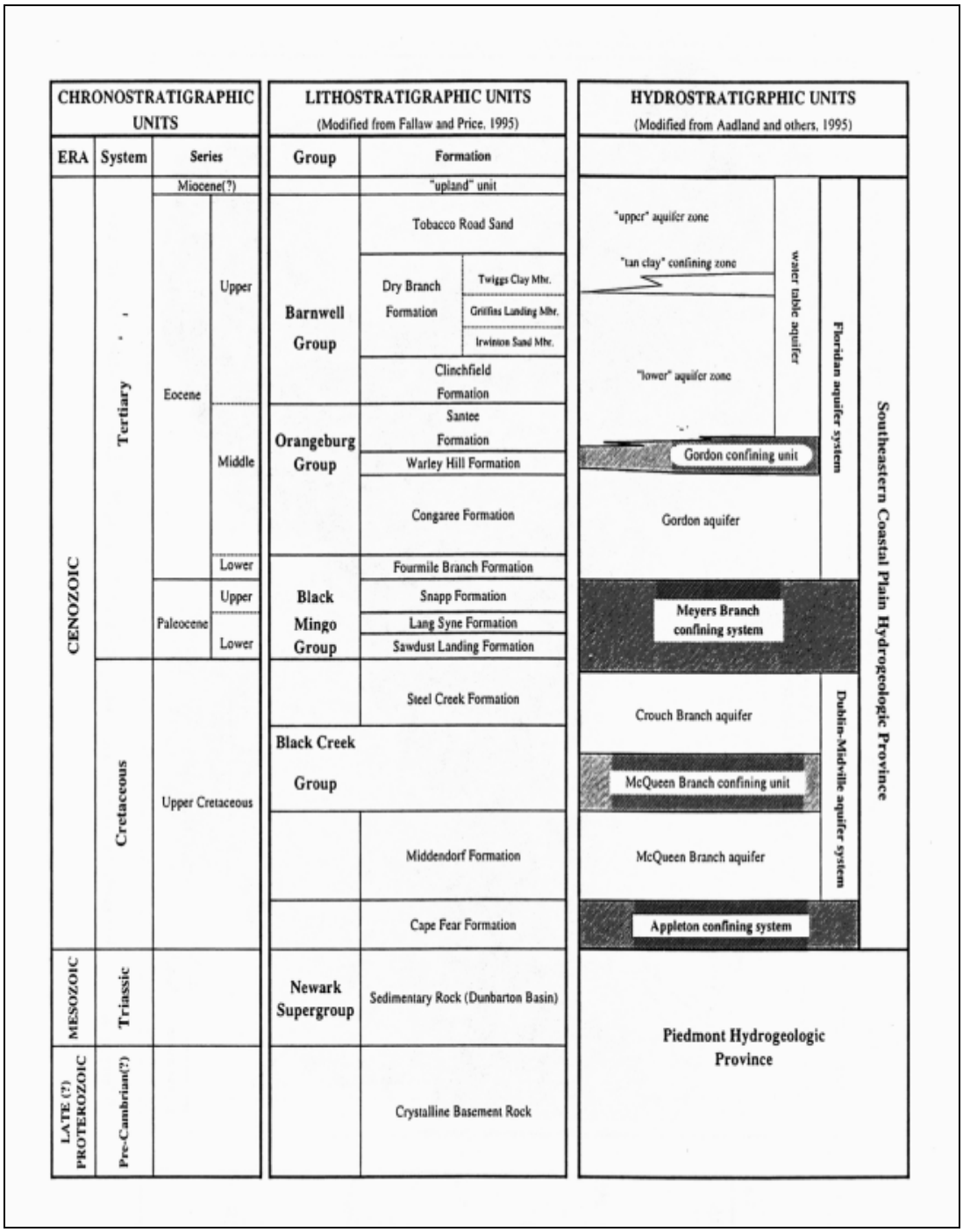

Figure 4: Comparison of lithostratigraphic and hydrostratigraphic units at SRS (Smits, Harris, Hawkins, and Flach, 1997)

Geology of Modeled Units (Smits, Harris, Hawkins, and Flach, 1997)

Tertiary Sediments

Orangeburg Group

The Orangeburg Group (Figure 4) crops out at lower elevations within the central part of the SRS area, along creek beds, and the Savannah River. The Orangeburg Group thickens from approximately 75 feet at the northwestern SRS boundary to about 150 feet near the southeastern SRS boundary (Colquhoun, 1991). Across the SRS region, the upper surface of the Orangeburg Group dips southeast at approximately 10 feet/mile. At the South Carolina coast, the Orangeburg Group is about 300 feet thick (Colquhoun and others, 1983) and represents outer-shelf depositional environments (Boylan, 1982). The dominant lithology of the Orangeburg Group includes sand, muddy and sandy limestone, calcareous mud, calcareous sand, clay, and glauconitic sand and clay. In the GSA, the Orangeburg Group includes, in ascending order, the Congaree, Warley Hill and Santee Formations (Figure 4). The sand and mud are generally unconsolidated and friable, whereas the limestone is usually moderately to well-indurated.

Congaree Formation

The term "Congaree Phase" was first introduced by Sloan (1907, 1908) to describe the shale, sands, and "buhrstone" of early and middle Eocene age sediments overlying the "Black Mingo Phase" and underlying the "Warley Hill Phase" at Warley Creek in Calhoun County, South Carolina. Cooke and MacNeil (1952) assigned the Congaree an early middle Eocene age and raised it to formational rank, correlating it with the Tallahatta Formation of Alabama. The Congaree Formation has been traced from the Congaree valley in east-central South Carolina into the SRS area by Colquhoun and others (1982, 1983). At SRS, the Congaree crops out along the Upper Three Runs near the juncture with Tinker Creek (Nystrom and Willoughby, 1982a; Willoughby, 1983, 1985, 1986; Nystrom, 1986; Nystrom and others, 1989).

At the SRS, the Congaree Formation consists of yellow, orange, tan, gray, and greenish gray, iron-stained, moderately to poorly sorted, medium to fine-grained sand with discontinuous lenses of montmorillonite-rich clay (Colquhoun and Johnson, 1968). Layers rich in pebbles, clay clasts, calcareous sand, and glauconite are present, but sporadic in their position within the formation. The base of the formation is unconformable. The Congaree and other deposits of lower middle Eocene age become increasingly calcareous between the SRS and the Atlantic coast, where they are primarily limestone (Colquhoun, and others, 1983; W.B. Harris and others, 1990; Harris and others, 1993).

Marine fossils, phosphate and glauconite indicate the Congaree Formation to be a marine-shelf deposit (Robertson and Thayer, 1992). The Congaree Formation averages 85 feet thick in the SRS area (Robertson, 1990). Robertson (1990) reported a local maximum of 110 feet for the thickness of the Congaree in this area at a location immediately south of the SRS. In the area northwest of the SRS, a unit equivalent to the Congaree is mapped as the Huber Formation (Nystrom and Willoughby, 1982a).

Warley Hill Formation

Sloan (1907) first used the term "Warley Hill Phase." Cooke and MacNeil (1952), coined the name "Warley Hill Marl" for glauconitic beds between the Congaree and McBean Formations. Pooser (1965) said that the overall lithology of the unit made the term "marl" inappropriate, and proposed that the name be changed to the Warley Hill Formation. Both the glauconitic sand and the clay at the top of the Congaree are assigned to the Warley Hill Formation (Fallaw and others, 1990; Fallaw and Price, 1995).

The Warley Hill Formation unconformably overlies the Congaree Formation and consists of approximately 15 feet of poorly to well-sorted quartz sand, often glauconitic, clay, sandy clay, and clayey sand (Fallaw and Price, 1995) (Figure 4). The sediment generally has a distinct dark green color due to accessory glauconite. The clay minerals that constitute the matrix of the sediment include illite and smectite (Dennehy and others, 1989). The green sand and clay beds are referred to informally as the "green clay" in many SRS reports. Northwest of the study area, the Warley Hill is missing or very thin, and the overlying Santee Formation rests unconformably on the Congaree Formation.

The lithology of the Warley Hill Formation indicates deposition in a shallow to deep water clastic shelf environment, generally deeper water than the underlying Congaree Formation (Pooser, 1965). Fallaw and Price (1995) note that the presence of glauconite, and the dinoflagellate assemblage are indicative of shallow marine conditions. The muddier sand in the Warley Hill indicates quieter water than that in which the Congaree was deposited (Fallaw and Price, 1995).

Santee Formation

Charles Lyell (1845) was the first to use the term "Santee" for limestone exposed along the Santee River in South Carolina. Sloan (1908) continued the use of the term, modified to the "Santee Marl". The terms "McBean Formation" and "Lisbon Formation" have been applied in the past to this unit but the term "Santee" has priority (Sloan, 1908). Cooke (1936) gave the unit formational status, assigned it an upper Eocene age, and re-named it the Santee Formation. Cooke and MacNeil (1952) correlated the Santee Formation with the middle Eocene Cook Mountain Formation of the Claiborne Group.

The Santee Formation (Figure 4) consists of moderately sorted, yellow and tan sand, calcareous sand and clay, and terrigenous clay. The lithology is consistent with deposition in a shallow marine, shelf environment. The carbonate lithology of the Santee Formation includes tan to white calcilutite, calcarenite, shelly limestone, and calcareous sand and clay. The carbonate content is highly variable. Limestone is much more abundant in down-dip areas, sporadic and pod-like in the middle of the study area, and missing in up-dip areas northwest of the study area. The carbonate sediment generally represents the limit of the transgression of the carbonate platform across the continental margin. This carbonate platform first developed in early Paleocene time near the South Carolina and Georgia coasts (Colquhoun and Johnson, 1968). The average thickness of the Santee is approximately 40 to 50 feet near the center of the study area.

Barnwell Group

The Barnwell Group (Figure 4) was named by Sloan (1908). The units assigned to the Barnwell Group were originally included in the Orangeburg Group by Siple and Pooser (1965). The Barnwell was raised to group status in Georgia by Huddlestun and Hetrick (1979). The Barnwell Group comprises three formations, the Clinchfield Formation, Dry Branch Formation, and Tobacco Road Sand. Colquhoun and others (1982, 1983) and Nystrom and Willoughby (1982a, 1982b) extended group status for Barnwell strata into South Carolina.

Clinchfield Formation

The Clinchfield Formation is the lowermost formation of the Barnwell Group (Figure 4). It consists of medium-grained, well-sorted, poorly consolidated, massively bedded quartz sand (Huddlestun and Hetrick, 1979). At the SRS, this unit has only been identified where carbonate strata of the Griffins Landing Member of the Dry Branch Formation and the Santee Formation are present, with sand of the Clinchfield between them. According to Fallaw and Price (1995) the sand is tan and yellow, poorly to well-sorted, and fine to coarse-grained at the SRS.

Dry Branch Formation

The Dry Branch Formation is the middle unit of the Barnwell Group (Figure 4). The Dry Branch crops out at the SRS and is approximately 45 feet thick near the northwestern site boundary and about 77 feet near the southeastern boundary (Fallaw and Price, 1995).

Huddlestun and Hetrick (1979) divided the Dry Branch into three lithofacies: the Twiggs clay, a marine, montmorillonite-rich clay; the Irwinton Sand, a distinctly bedded sand and clay; and the Griffins Landing Member, a massive "calcareous" and fossiliferous sand. The Griffins Landing Member represents the uppermost calcareous upper Eocene strata in the study area. The Griffins Landing contains the large oyster, *Crassostrea gigantissima*, and at up-dip (northwestern) locations the clay matrix appears very similar to the Twiggs Clay and is probably correlative with this unit. Distribution of the Griffins Landing is sporadic in up-dip locations, and the unit thickens to greater than 96 feet in the southern part of the SRS region.

The presence of *Crassostrea*-bearing beds indicates bay or lagoonal environments for the Griffins Landing Member. Sand of the Irwinton is interpreted to be inner neritic and barrier island deposits, whereas the clay is interpreted as a lagoonal or possible bay deposits (Fallaw and Price, 1995).

Tobacco Road Sand

The Tobacco Road Sand is the uppermost unit of the Barnwell Group (Figure 4). This sandy unit varies from fine-grained and well-sorted to poorly sorted sediment with pebbles. Variations in clay, chert, mica, carbonate, and heavy-mineral content exist locally (Huddlestun and Hetrick, 1979). Massive bedding and bioturbated strata characterize the formation (Logan and Euler, 1989).
Abundant *Ophiomorpha* and clay laminae in the Tobacco Road Formation indicate deposition in a low energy, transitional marine environment, such as a tidal flat (Fallaw and Price, 1995).

"Upland" Unit

The term "upland" unit has been widely used in the Coastal Plain of South Carolina for the poorly sorted, silty, clayey and pebbly sand present at higher elevations within the study area (Figure 4). At the SRS, the "upland" unit has been called the Hawthorn Formation (Siple, 1967), and the Altamaha Formation (Huddlestun, 1988; Nystrom and Willoughby, 1992; Fallaw and Price, 1995). As the age of the unit is still controversial, this report will use the informal name "upland" unit. It is believed that the unit is correlative with the Chandler Bridge Formation in the vicinity of the Atlantic Coast (Colquhoun and others, 1994).

The "upland" unit is considered by many to be a distinct unit separated from the underlying parts of the section by a significant unconformity (Nystrom and Willoughby, 1982a; Nystrom and others, 1989). Colquhoun and others (1994) demonstrate that the "upland" unit, Tobacco Road and Dry Branch Formations are similar in texture and composition. They believe that the unit is part of the same transgressive-regressive cycle as the Tobacco Road and Dry Branch Formations. The "upland" unit represents the most inland lithofacies, and the Dry Branch represents the most seaward lithofacies of the transgressive-regressive cycle.

Methods

Geostatistics provides numerous spatial analytical tools to interpolate or simulate variables at unsampled locations. These methodologies developed over the past 40 years (Isaaks and Srivastava, 1989; Krige, 1951; Krige, 1966; Matheron, 1963; Matheron, 1970; Matheron, 1978), represent a vast improvement over traditional interpolation techniques which are limited in their ability to capture spatial continuity (Hohn, 1988; Yarus and Chambers, 1994). For aquifer or reservoir characterization, the goal is to develop a model of spatial continuity from primary data, such as from wells, and use these data to infill the inter-well space with rock property attributes affecting fluid flow. Modeling can be done in 2 or 3 dimensions depending upon project objectives and the volume of data available.

The importance of geostatistical methodologies compared to classical statistical methods, is demonstrated by examining Figures 5 and 6. Based on univariate statistical measures, shown as a histogram and a table (Fig. 5), there is no difference in the two datasets. However, both maps look quite different (Fig. 6); one shows a strong NW-SE continuity, whereas the other image does not.

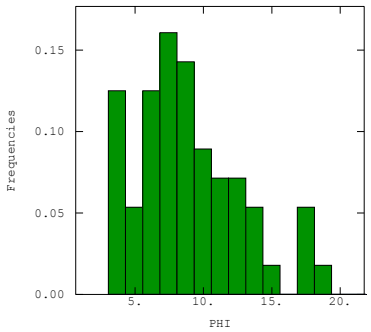

MIN = 3.1
0.25 = 6.2
0.5 = 8.4
0.75 = 11.5
MAX = 19.1
MEAN = 8.9
STD = 3.8
STD /MEAN = 0.428132

Figure 5: Porosity distribution

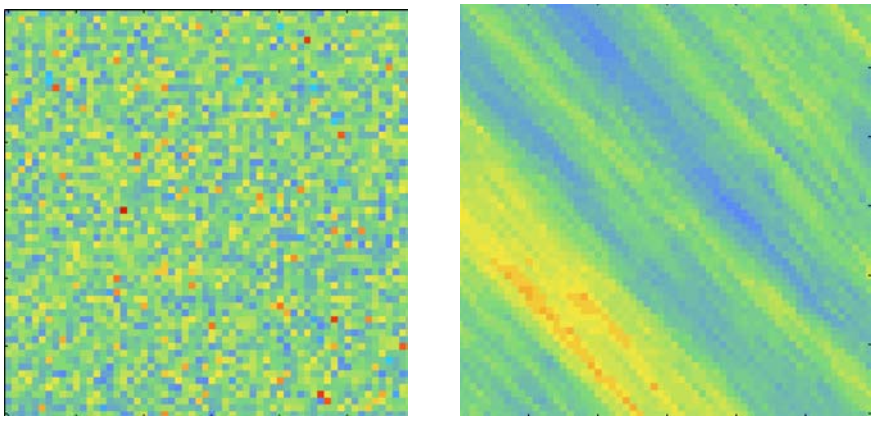

Figure 6: Porosity maps

The need to quantify the differences between the two data sets is clear. Classical statistical measures do not differentiate the spatial arrangement of the data, whereas geostatistical methods can quantify the spatial information in geoscience datas.

Variogram

The major innovation brought by geostatistics is the variogram, which measures the spatial correlation, or the degree of spatial continuity in data. The variogram is a two point statistic that summarizes the variance between pairs of data points separated by a distance, *h*. The data pairs are organized into incremental bins of h, and their orientation in geographical space. In this way, a comparison of variograms using the same separation intervals but different orientations or azimuths of sample pairs, can distinguish major directions of continuity, as displayed in Figure 6.

The theoretical variogram γ(h) in any direction D is:

$$\gamma(\mathrm{h}) = \frac{1}{2N(h)} \sum_{(i,j)|h_{ij} \approx h} (x_i - x_j)^2$$

where
h is the distance between data pairs, known as the lag distance
$N(h)$ is the number of data pairs (i, j) included in the sum for any given lag
x_k are data values,

For example, Figure 7 shows two experimental variograms calculated from a data set in two directions: N-S and E-W. The small blue crosses are data locations, and the blue lines represent connected data pairs for one lag.

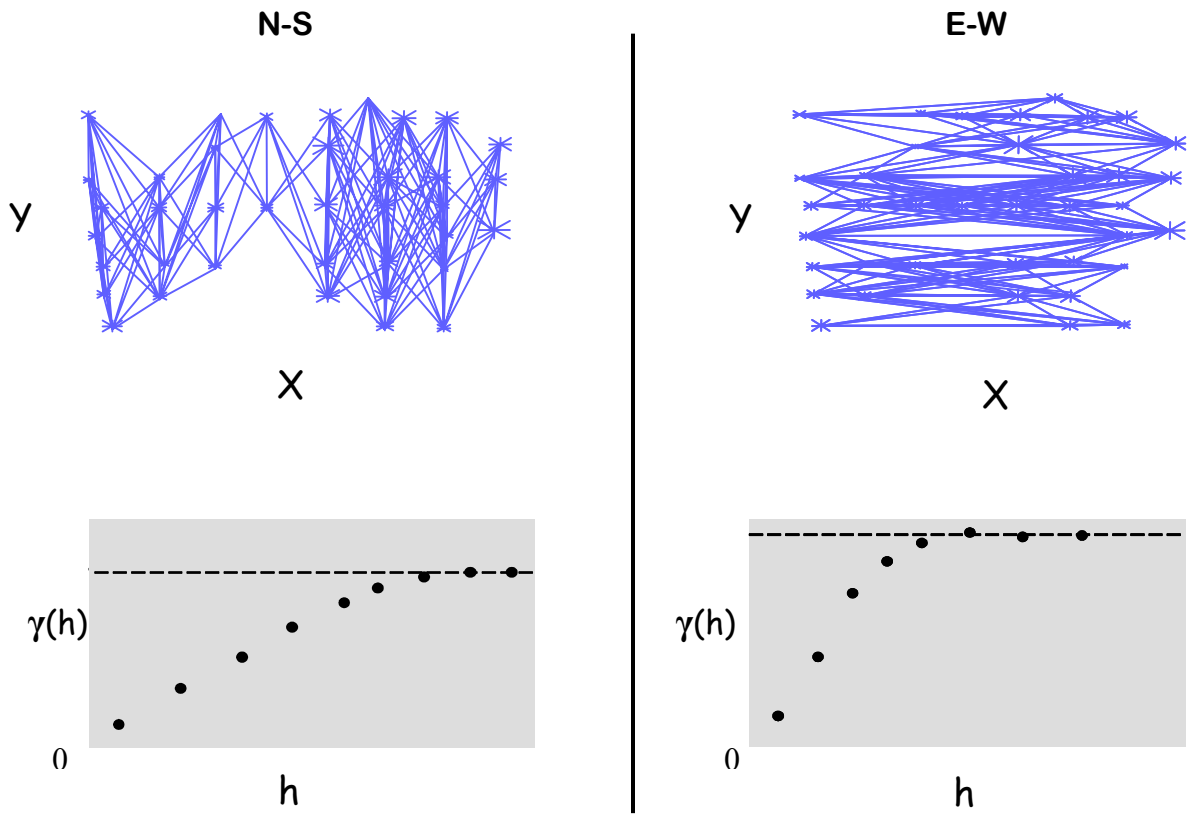

Figure 7: Calculation of a variogram in two different directions

For the direction N-S it can be seen that $\gamma(h)$ increases more slowly than for the direction E-W. This means that data are more correlated along the N-S direction than E-W. For example, if you compute the variograms from elevation data sampled along the strike of a N-S trending anticline, there are only small changes in the elevation, thus the computed variance changes slowly with distance, conversely the variance in the dip direction shows a more rapid change.

The basic variographic parameters are shown in Figure 8 below.

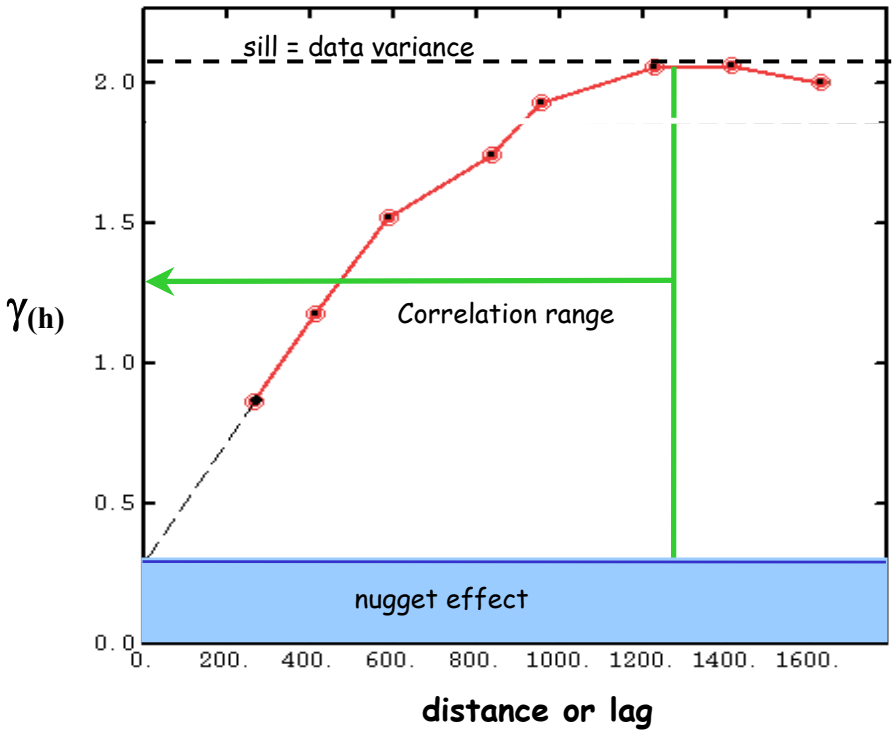

Figure 8: Variogram parameters

The sill is the global data variance computed from the data. The nugget is the apparent variance for *lag* equal to zero. The nugget allows the modeler to incorporate data uncertainty, into the spatial model (variogram model), at short distances from data points. The range of the variogram is the maximum distance separating pairs of correlated data points.

The statistical properties that are commonly used to describe or depict geological bodies or features are known as regionalized variables. They have properties that are both deterministic and random (Davis, 1986), and when mapped show interpretable patterns familiar to geologists. Such variables include porosity, surface elevation, facies, isopach thickness, and more. Regionalized variables can have directions of continuity that are not random, and in fact, often show dependencies among them. For example, splays tend to be perpendicular to channels, barrier bars tend to be parallel to the shoreline, etc. However, we often construct maps of lithofacies which makes no distinction of its genetic origin or the depositional environment. For example, a sand lithofacies could be composed of both tidal bars, and washover fans, both of which can have different orientations from one to another and different petrophysical characteristics. Thus, a simple map of "sand" may not adequately depict the accurate spatial distribution that is depositionally controlled. In this example, a "nested variogram" model, composed of two structures, one for tidal bars and the other for washover fans can be constructed. Both variograms have different ranges, different azimuths, and a different influence on the total data variance. Figure 9 shows a nested variogram model with two structures in addition to a nugget effect.

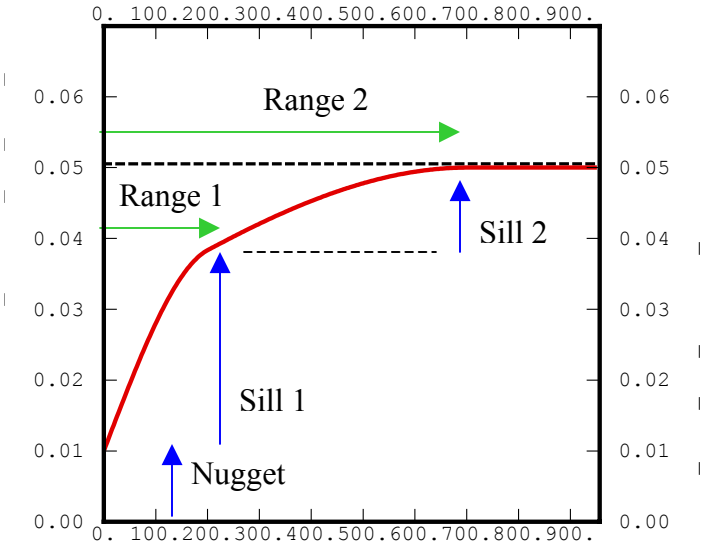

Figure 9: Nested variogram with two structures

When all the variograms are computed for every direction, the spatial correlation of the variable could be represented in a 3D space. On Figure 10 the black lines represent the ellipsoidal axes.

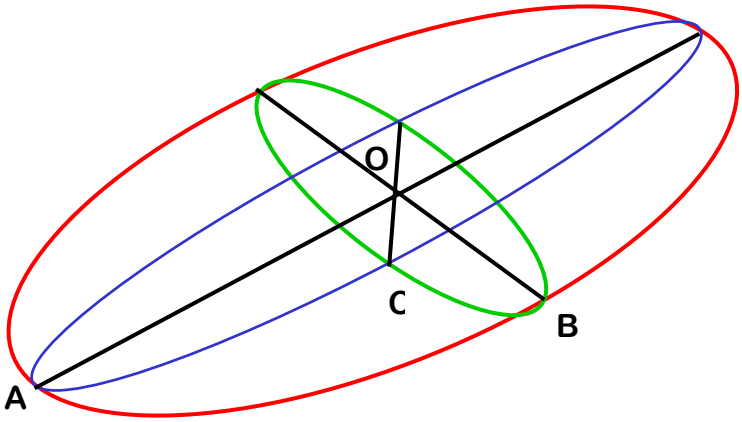

Figure 10: 3D variogram ellipsoid

OA is the longest correlation range; its orientation is defined by the azimuth and the dip
OB is the shorter correlation range; its orientation is orthogonal to OA's
OC is the vertical correlation range

The shape of the ellipsoid and its orientation represents the 3D spatial correlation model of the studied property.

In practice, the modeler must first calculate several experimental directional variograms from the data, and then mathematically model the experimental vertical

variogram and two experimental horizontal variograms (one with the shortest correlation range (small ellipsoid axis) and one with the longest (long ellipsoid axis)). The shapes of three commonly used mathematical models are shown in Figure 11.

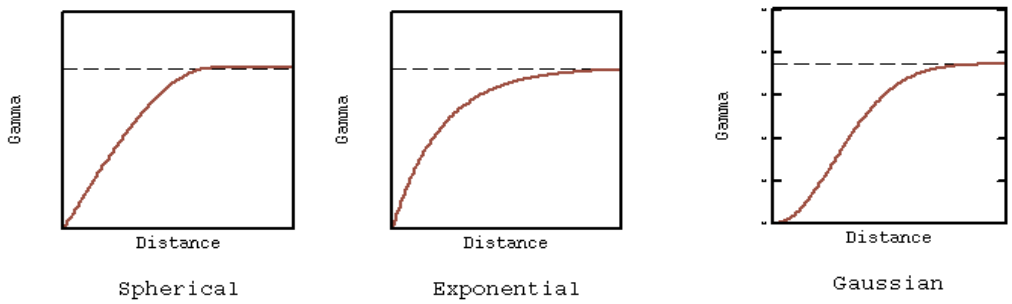

Figure 11: Examples of variogram models

Variogram Map

In some cases, it is difficult to determine different correlation structures and their parameters using only variograms that have been computed along one direction at a time. A display (Fig. 12) illustrating the combination of all the variograms computed for all azimuths is called the variogram map. The variogram map is a map of variance or a "**γ**(h) map", that can be in 2D or 3D. From this map it is very easy to determine the anisotropy ellipse.

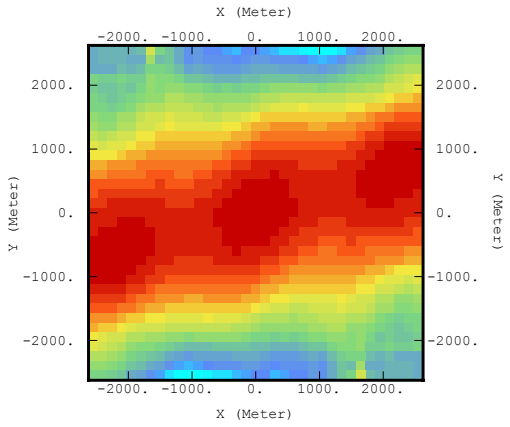

Figure 12: Variogram map calculated from well picks

In Figure 12, it is obvious that the main correlation data orientation is about N75E, because the same color means roughly the same variance. Looking closer at this figure, several structures with different ranges and different orientations are seen. Variogram maps make modeling easier and more representative of reality.

Data workflow summary for to defining the spatial model:

- Data quality control and exploratory data analysis (histogram, base map, crossplot …)

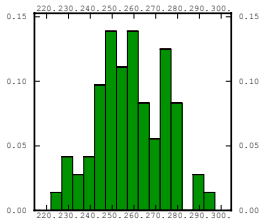

- Compute the variogram map of the data, define the longest correlation range azimuth D for each structure discovered

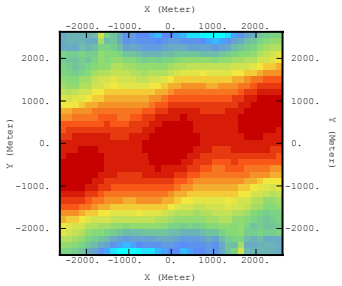

- Compute the experimental variogram from the data for the azimuth D and D+90º and the vertical experimental variogram

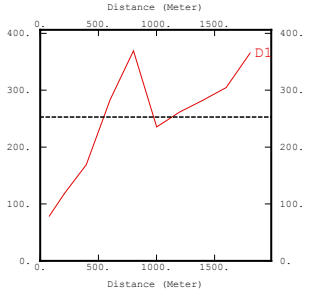

- Model the three variograms mathematically using the calculated experimental variograms, and the variogram map taking into consideration any other relevant data and your knowledge about the depositional system

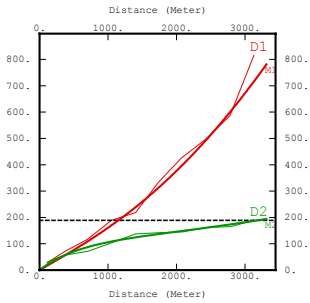

Kriging

Most commonly used interpolation methods (i.e. inverse distance, moving average) do not take into account the spatial location of the data points used during the interpolation process. This is an important point, because depositional patterns cannot be accurately reproduced using these methods without considerable effort. None of them use a model of spatial correlation (variogram). Kriging, a geostatistical mapping method, is the only interpolation method that uses a variogram model to determine weighting coefficients (λ_i). As the variogram model depends on the direction, λ_i depends on the direction too, this is the important advantage when compared to more commonly used interpolation methods like moving average or inverse distance A distinguishing feature of Kriging, compared to other methods, is its ability to minimize the error variance.

Kriging is also known as the best linear unbiased estimator (B.L.U.E.).

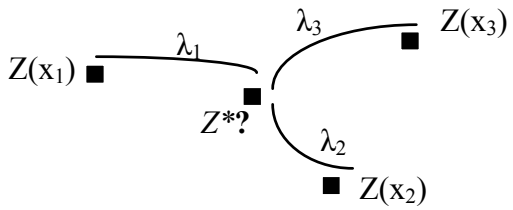

Kriging is linear:

$$Z^*(estimate) = \sum_i^n \lambda_i * Z(x_i)$$

Kriging is unbiased: $\sum_i^n \lambda_i = 1$

Kriging is the best estimator: the error variance is minimized.

Kriging honors perfectly all the data.

The particularity of Kriging is the way it calculates the weights λ_i. They are calculated by using the variogram model. As the variogram model depends on the direction, λ_i depends on the direction too, that is the important advantage compared to more commonly used interpolation method like moving average or inverse distance.

To decide which data point are used in the estimation, the modeler defines a neighborhood around the location of the estimated point. In this project the neighborhood was the whole area, all the data point were used at each estimation location.

Kriging has many options, including the integration of multiple variables. In this project, Ellenton picks were very few, so the Congaree Kriged surface was used as complementary data assuming a correlation factor between both surfaces. The Kriging based method using two variables is Collocated CoKriging. In practice, an Ellenton grid cell value is estimated by using Ellenton data picks plus the Congaree Kriged picks at the locations of Ellenton data picks. The influence of the soft data is specified by a correlation coefficient between –1 and 1.

Sequential Gaussian/Indicator Simulation

Kriging, like any interpolation method, does not reproduce heterogeneity. For facies and petrophysics modeling, it is advisable to use a method that reproduces heterogeneity. Kriging based simulation methods are available for this purpose. In fact simulations attempt to reproduce the variability around the estimated value provided by Kriging. The Kriging based method called Sequential Gaussian Simulation (SGS) was chosen to distribute the percentage of mud from core measurements. SGS is designed to simulate a continuous variable, such as porosity, permeability, percent mud, etc.

At any grid cell location, the SGS algorithm randomly samples a simulated value from a Gaussian probability distribution constructed for that particular cell. The mean of this Gaussian distribution is the Kriged result and the standard deviation is the Kriging variance. Sequential means that the previously simulated values are treated as data points for the simulation of subsequent points. Each simulation (characterized by a seed number) has a different path through the grid; which is why each simulation produces slightly different results.

Figure 13 illustrates SGS simulation schematically. In this figure we are looking at 9 cells from a grid mesh, which may contain thousands to millions of cells. Locally, for each cell, we define a probability distribution function based on neighboring data points for the grid node to be simulated. The center figure shows that the Kriged result (blue lines) represent the mean of the frequency distributions, whereas a simulated value comes from any location within the distribution. The left and right images, in Figure 13, represent two simulations from an infinite number of possible simulated values for the 9 cells.

Another form of SGS is Sequential Indicator Simulation (SIS), which is designed to simulate discrete variables, such as facies. These variables are coded with integer values, 1, 2, 3, etc. A value of 1.5 has no meaning, because the facies simulated is either 1, 2, or 3, for example.

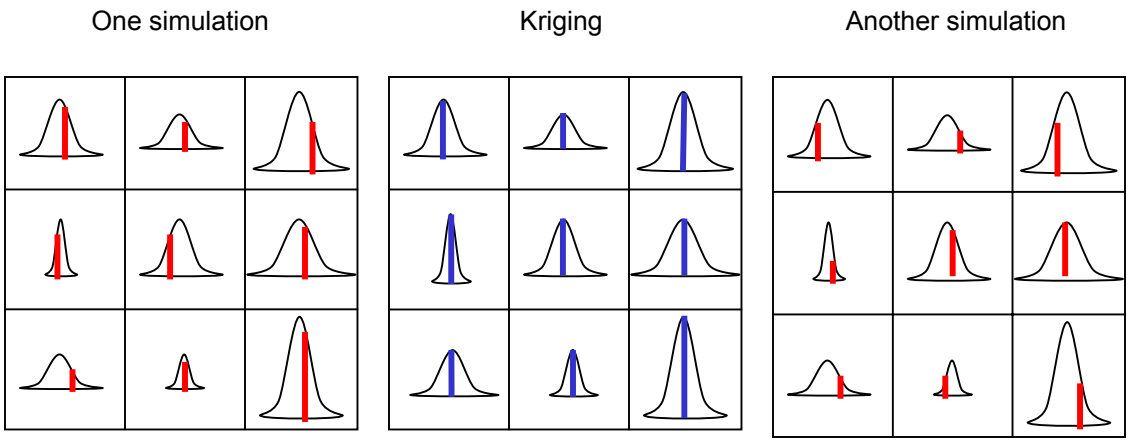

Figure 13: Comparison Kriging/Simulation for a 9 cells grid

Horizons Construction

Univariate and multivariate forms of Kriging were used to create the various horizons required for the 3D model. The Tobacco Road, the Santee, the maximum flooding surface, and the Congaree top were built with Ordinary Kriging (most commonly used form of Kriging). The Ellenton surface was built using Collocated Cokriging because the available tops for this horizon were sparse, when compared to the other surfaces, thus the Congaree Kriged surface was used as the soft data.

Stratigraphic Grid Construction

Before actually filling the inter-well space, the geologist needs to define the workspace in which he will work. For the construction of a surface from well tops the workspace would be a 2D grid, representing the spatial discretization of the surface. Each cell penetrated by a well would be initialized with the well picks, then the surface is created using Kriging from the discrete horizon tops throughout the entire grid. Modeling of a well log property requires a 3D workspace.

For a 2D grid, the only problem is to define the cell size and the number of cells in X and Y, but for a 3D grid, the stratigraphic layering geometries must be defined. The grid layering should be based on sequence stratigraphic analysis of the depositional system. Thus, the geologist must know whether the geological surfaces are conformable or non-conformable and bedding types (i.e. onlap, toplap, etc.). Then, based on this information, he can build the stratigraphic grid (Appendix 1: 3D grid layering examples).

The accuracy of the geological model really depends on the quality of the surfaces. In fact the Kriged horizons define the stratigraphic grid that constrains correlation layering for the inter-well space.

In the SRS project, the maximum flooding surface was found to be the only consistent surface. Therefore, the grid layering was defined to be parallel to the maximum flooding surface for the whole model. A grid was built between the Ellenton horizon and the ground surface with a horizontal layering parallel to the maximum flooding surface. This implies onlap, toplap, downlap, or erosional truncation boundaries with the other horizons. The 3D model cell sizes used was: X=Y=50m, and Z=0.61m (2ft).

Because the grid was built with the non-eroded Kriged horizons, the final grid was eroded by the ground surface. Figure 14 shows a vertical cross section of the grid, the brown is the Upland formation, the green is the Barnwell Group and the white is the Santee formation.

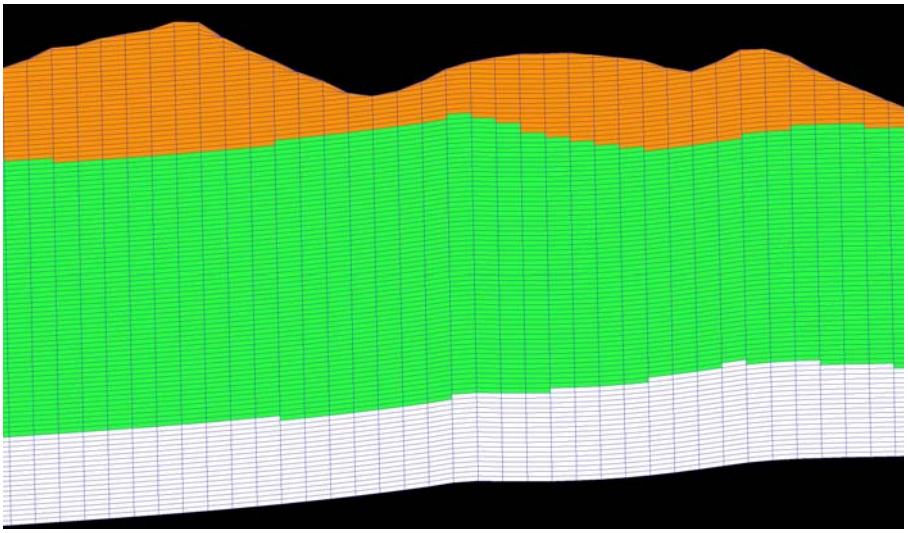

Figure 14: Vertical cross section of the grid from the maximum flooding surface up to the ground

Figure 15 shows a top view of a grid layer in the Upland formation after erosion by the ground surface.

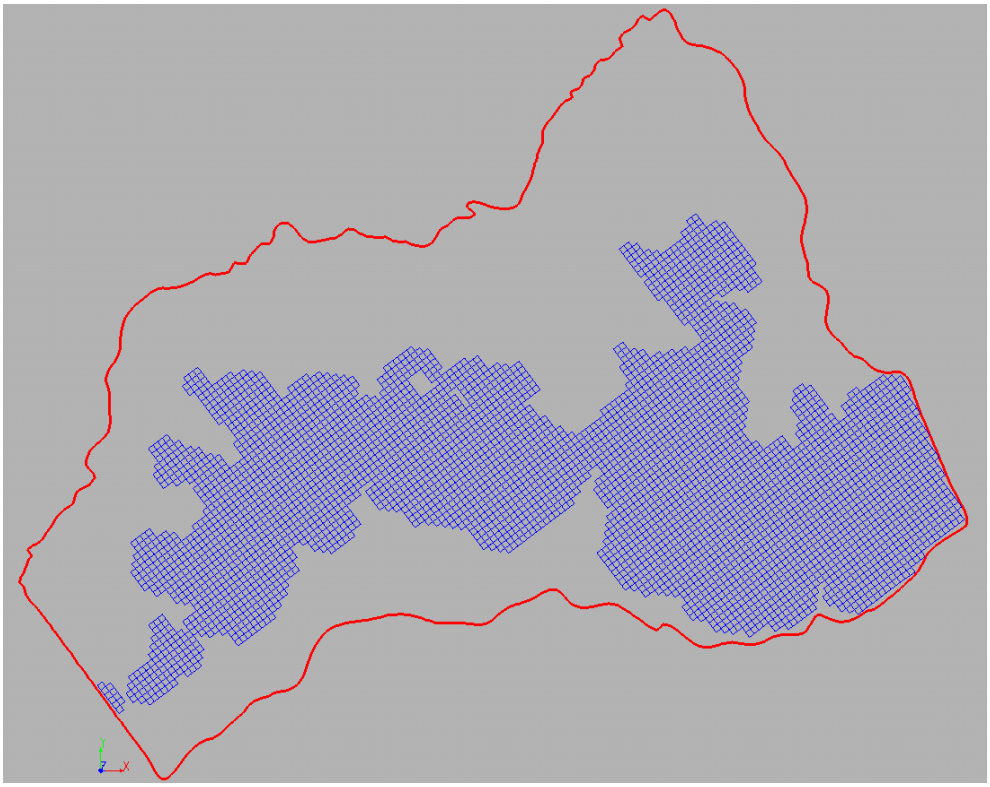

Figure 15: Top view of a grid layer within the Upland formation

Depositional Facies Modeling

Traditionally geological model were created based solely on mapping petrophysical data from well data, without any consideration of the depositional environment. Such an approach ignores most of the geological content of the data, as the model is based only physical rock properties. A barrier island sand has a different spatial distribution when compared to a fluvial sand. The geological model should use this information to be accurate, which is why the Savannah River Site geologists interpreted depositional facies from core data. Their analyses resulted in depositional facies indicator well logs.

For each formation and each depositional facies a variogram model was defined. Then depositional facies were distributed in the inter-well space using Sequential Indicator Simulation separately in each formation. One SIS simulation distributes **all** the facies within a selected formation, while honoring the variogram model and the well data.

Two hundred (200) simulations of depositional facies were run for each formation and each simulation is equiprobable. For the first simulation pass, the most common facies was computed in each cell from the 200 simulations. This is not necessarily the best solution, but it is easiest to use so that the geology of the area could be better understood. In fact in this case the most common facies 3D map does not honor the

spatial correlation dictated by the variogram model. The cell-by-cell post-processing breaks this correlation. This part of the workflow will be improved in the future.

The most common 3D facies map, created separately for each formation, was used in the petrophysical modeling.

Petrophysical Modeling

The petrophysics, mud percentage from core, and Friction Ratio from Cone Penetrometer Test were simulated using the depositional facies model as a template. In each formation and in each most common simulated facies, a variogram model was defined for percent mud using variogram maps and available geological information. For example, in the Upland formation, two depositional facies (Fluvial and Floodplain/Overbank muds) are present; one variogram for percent mud was calculated in the Fluvial facies using only the data occurring in this particular facies, and another variogram for Floodplain/Overbank muds). Then percent mud was distributed using Sequential Gaussian Simulation. Two hundred simulations were run separately in each most common simulated depositional facies for each formation. A cell-by-cell post-processing calculated the maximum, the minimum, the mean, and the standard deviation from the 200 simulations.

For each formation, the mean percent mud was computed at the well locations, then cross-plots of the friction ratio against the mean percent mud were generated and correlation coefficients between both variables were computed. If the correlation coefficient was greater than 0.2, Collocated CoKriging Simulations would be used in that particular facies to simulate percent mud using the friction ratio as soft data. Precisely the soft data would be the friction ratio mean from 200 simulations, exactly as it was done for percent mud.

Result

The construction of the different structural horizons was not simple, requiring complex, multi-directional variogram models. Several modeling attempts were required for each surface before the final surface was created. Artifacts, commonly referred to as "pimples" occur at several well locations suggesting that the well picks require additional editing.

The experimental depositional facies variograms looked strange when first computed. So, 2D variogram maps were computed to find the spatial correlation scales and directions of the facies. However, the 2D maps represent a composite of the interval and it was not possible to accurately determine any correlation structure for the depositional facies. When 3D variogram maps were used it was very easy to see some structures. For the simulations, only the major facies were retained for each formation as delimited by the structural surfaces. These facies are: 1) Fluvial and Floodplain/Overbank

muds for the Upland, 2) Tidal Flat/Lagoonal and Barrier Beach for the Barnwell Group, 3) Siliciclastic Shelf, Middle Shelf (low energy), Middle Shelf (high energy) and Open/outer Shelf for the Santee, 4) Open/outer Shelf, Lower Shoreface and Innerbay/Lagoonal for the Green Clay, and 5) Lower Shoreface and Innerbay/Lagoonal for the Congaree. After generating 200 simulations, the most common facies per cell (mode) was calculated, producing reasonable results. However, two problems with this approach are that the most common facies is biased towards the major facies in terms of global proportions within the formation, and the resulting map does not have the finer-scale heterogeneity of a simulation.

Petrophysical variograms and variogram maps show subtle structures, however, the results of the 200 simulations look reasonable. The correlation between friction ratio from CPT data and the mean of percent mud (from the 200 simulations) were calculated separately in each depositional facies (from most common facies maps). The correlation found was very low, with a correlation coefficient greater than 0.2 in only one facies. This implies that the CPT data had very little impact in this phase of the project.

General Project Workflow for 2D and 3D Modeling

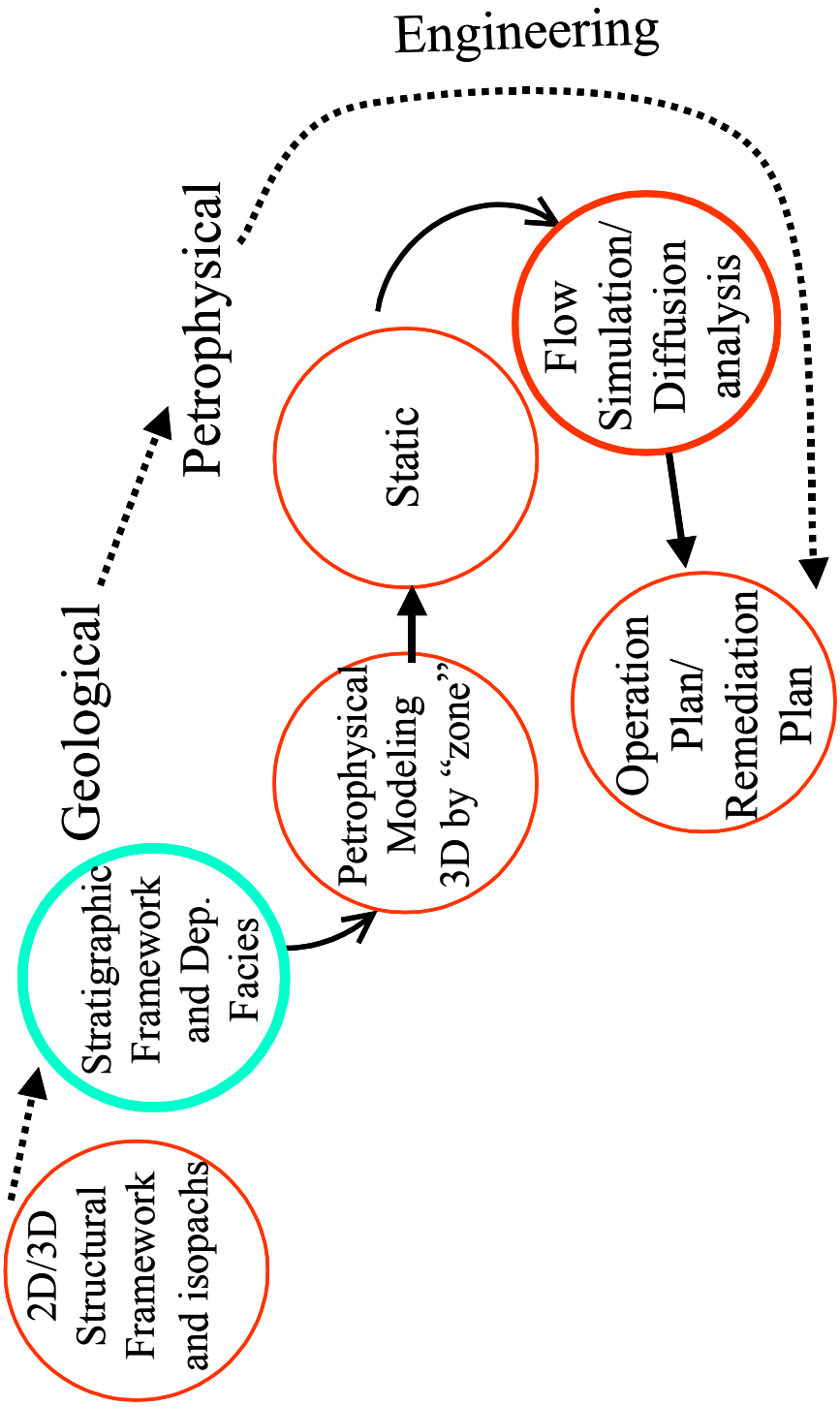

Figure 16: General workflow of the project

Sofware

Two different geostatistical software packages were used to create the 3D model.

ISATIS

ISATIS, a product of the Centre de Geostatistique, Paris, School of Mines, and marketed by Geovariances, is the best-in-class tool for data clean-up and spatial analysis and modeling. The primary use of ISATIS was for variograms, variogram maps and creating the structural surfaces by Kriging. Figure 17 shows typical displays and analytical tools available in the software for exploratory data analysis.

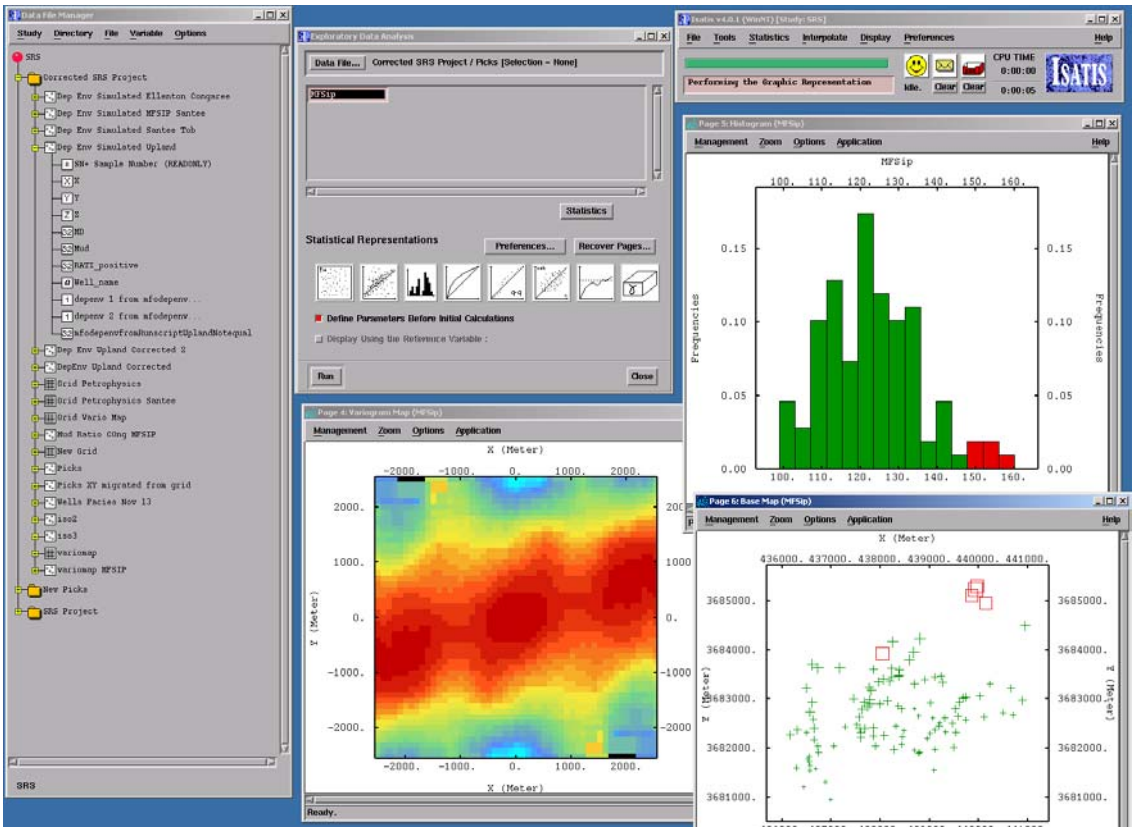

Figure 17: Isatis interface under Microsoft Windows

Gocad is a full 3D, stochastic, reservoir modeling software package. It has functionalities for structural, stratigraphic, and petrophysical property modeling using geostatistical methodologies. Gocad also has very good 3D graphical display capabilities. The G2 plugin was used for advanced geostatistical modeling. Gocad is distributed by T-Surf, another French company, based in Houston, Texas. Figure 18 shows the display capability of Gocad.

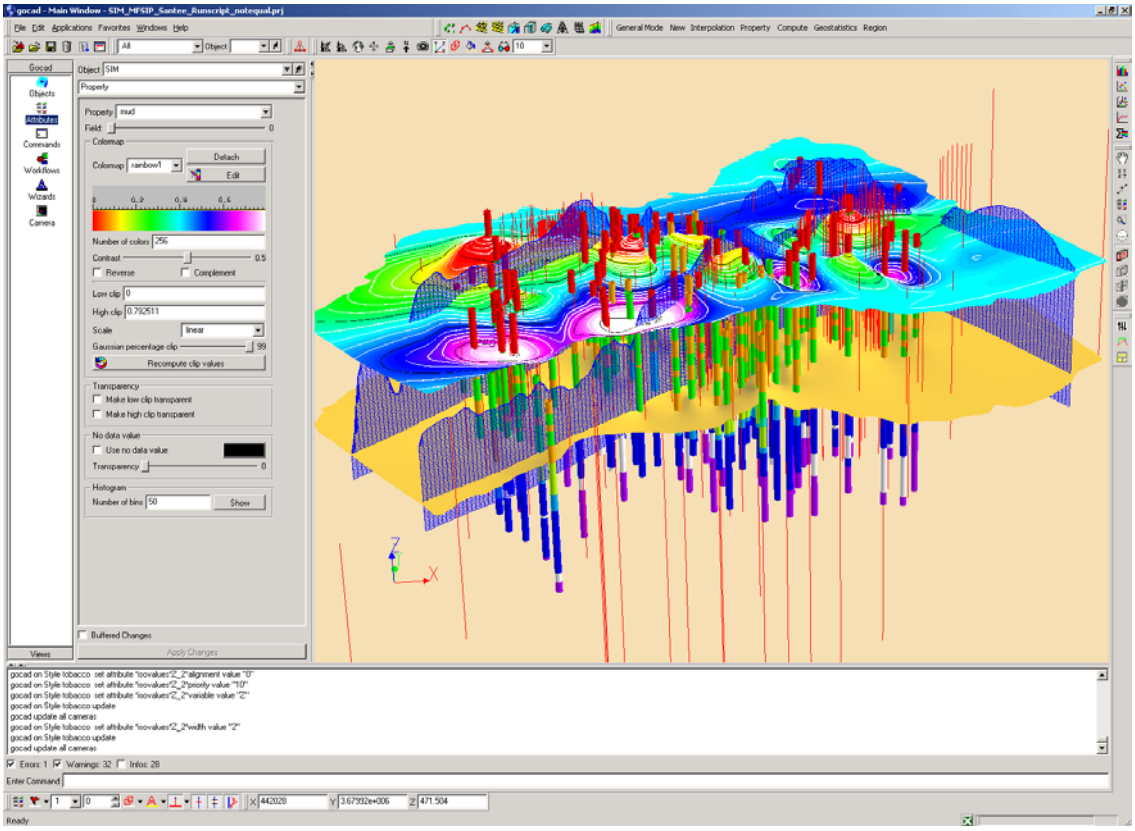

Figure 18: Gocad interface under Microsoft Windows

Results

Surface Modeling

The first step of every 3D geological modeling is the construction of the structural model, consisting of all the principle geological horizons and faults defining the reservoir. The accuracy of this model controls the whole 3D model.

In the General Separation Area, five horizons were interpreted based on core data: the Tobacco Road, Santee, maximum flooding surface, Congaree, and the Ellenton. The data density varies based on the depth of the horizon, with deeper horizons having fewer well penetrations. The Ordinary Kriging method was used to create all the surfaces, except the Ellenton where we used the Collocated CoKriging method.

First, an experimental variogram and a variogram map, for each horizon, was calculated from the well tops. Based on the experimental variogram, variogram map, and existing geological information, a nested variogram model was defined, integrating multiple structures with multiple orientations and multiple correlation ranges. The variogram model captures the geological fabric of the structural surface. Then, the variogram model is used with the Kriging algorithm to create the surface. The eroded portion or the surface is not taken in account at this point in the workflow.

The neighborhood used during the Kriging step includes all the surface included all the data points. Only one highly spurious data point (borehole BGO6A) was not used in the construction of the following surfaces: Congaree top, Santee top and maximum flooding surface.

Tobacco Road Top

Figures 19 to 21 show the data locations, the variogram map, and the modeled direction variogram for the Tobacco Road. The final variogram modeling parameters are:

- Structure 1: spherical, az = N70, sill = 180, range N70 = 500m, range N160 = 1000m
- Structure 2: spherical, az = N70, sill = 170, range N70 = 3500m, range N160 = 1400m

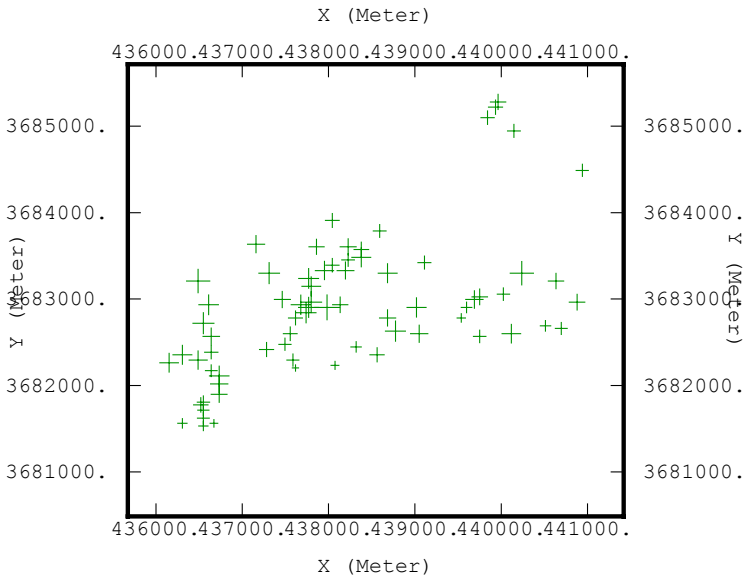

Figure 19: Tobacco Road top well picks location

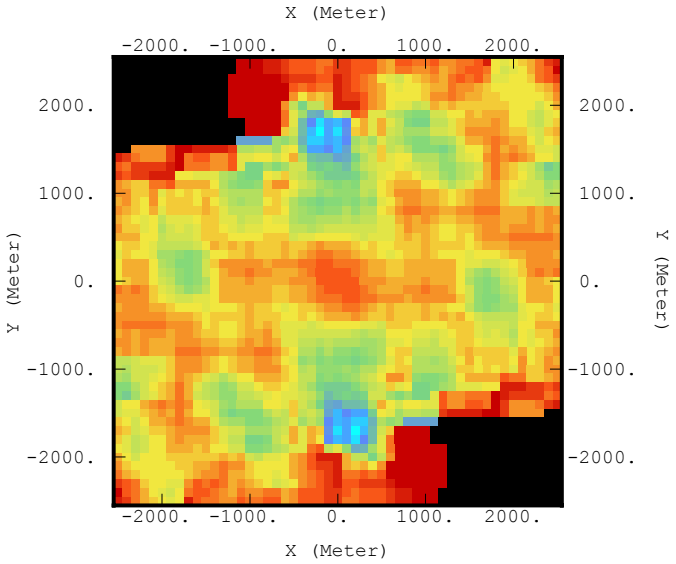

Figure 20: Variogram map of Tobacco Road top well picks

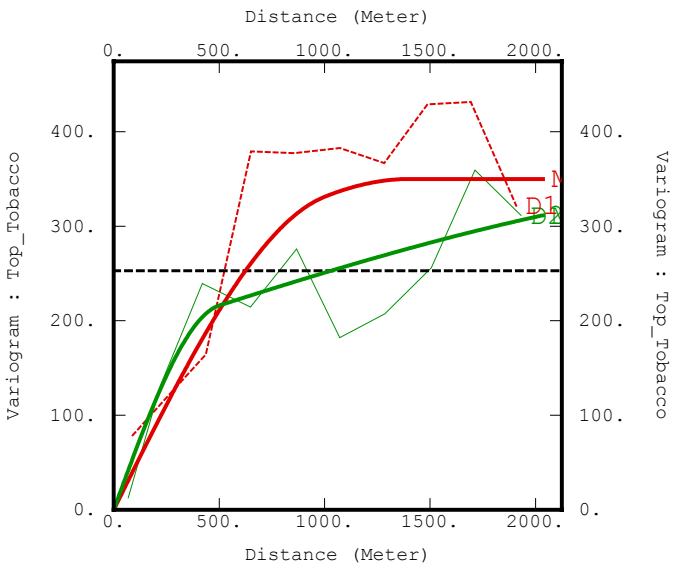

Figure 21: Experimental variogram and its model for the Tobacco Road top

elevation in ft

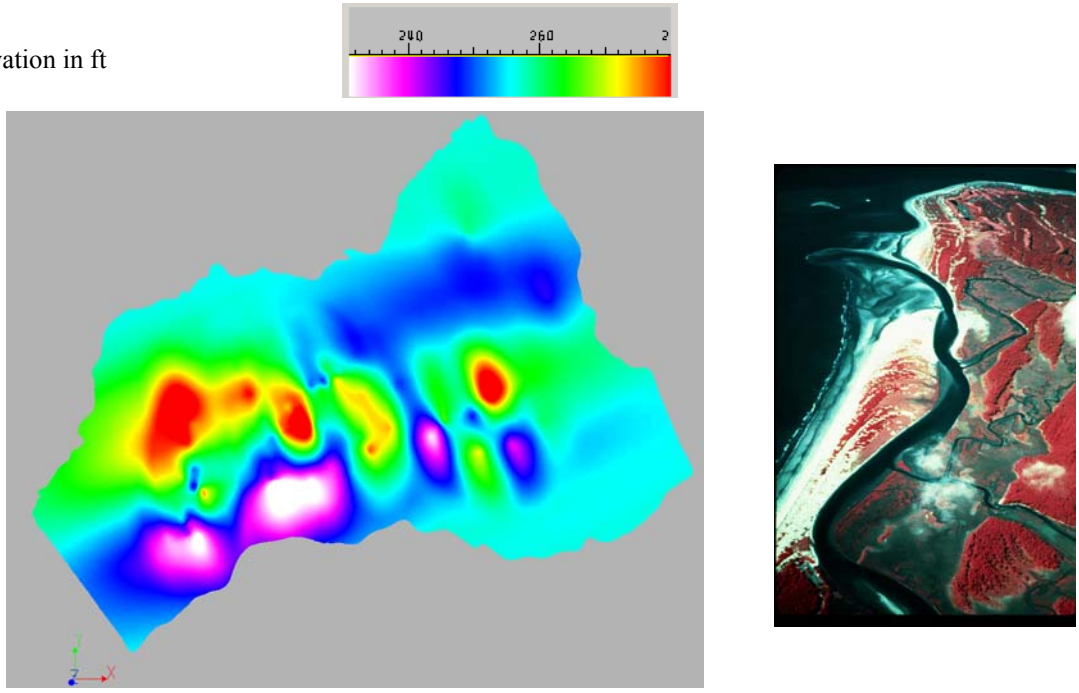

Figure 22: Elevation of the Kriged Tobacco Road top

The picture on the right in Figure 22 is a false color aerial photograph of the present-day coast of South Carolina, showing a tidal inlet and tidal flat. Compare this image to the Kriged surface of the Tobacco Road. The tow images look remarkably similar. The Kriged horizon appears to show an inlet connecting to the open ocean, with a tidal flat, as well as offshore sand bars. Figure 23 is an idealized conceptual depositional model for the Santee/Tinke, Dry Branch, and Tobacco Road Formations.

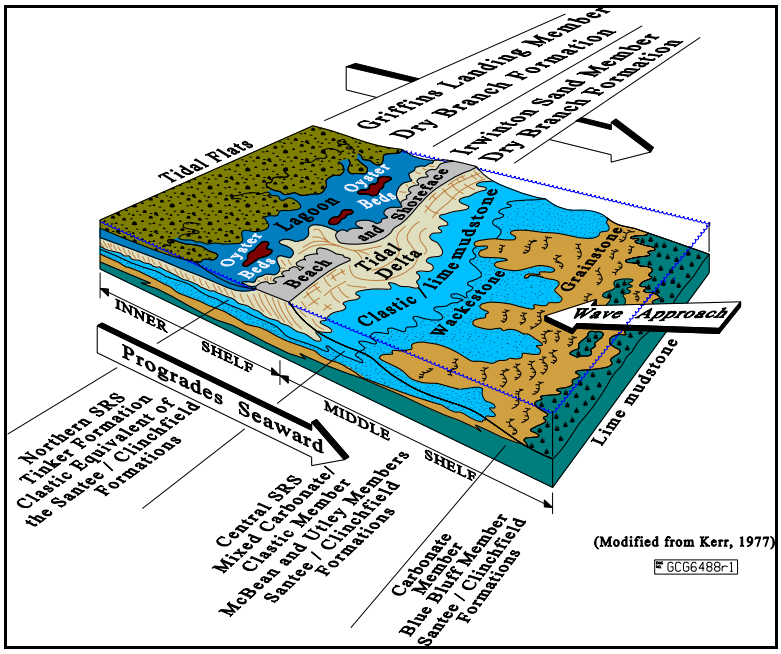

Figure 23: Idealized depositional model for the Santee/Tinker, Dry Branch and Tobacco Road Formations

Santee Top

Figures 24 to 26 show the data locations, the variogram map, and the modeled direction variogram for the Santee. The final variogram modeling parameters are:

- Structure 1: power (exp 1.8), az = N80, sill = 70, range N80 = 3500m, range N170 = 900m
- Structure 2: exponential, az = N170, sill = 130, range N170 = 3000m, range N80 = 1900m
- Structure 3: nugget, sill = 2

The Kriged horizon (Fig. 27) appears to show the effect of channeling perpendicular to the coastal plain. The localized "'dimples" suggests additional editing of the well top picks for the Santee.

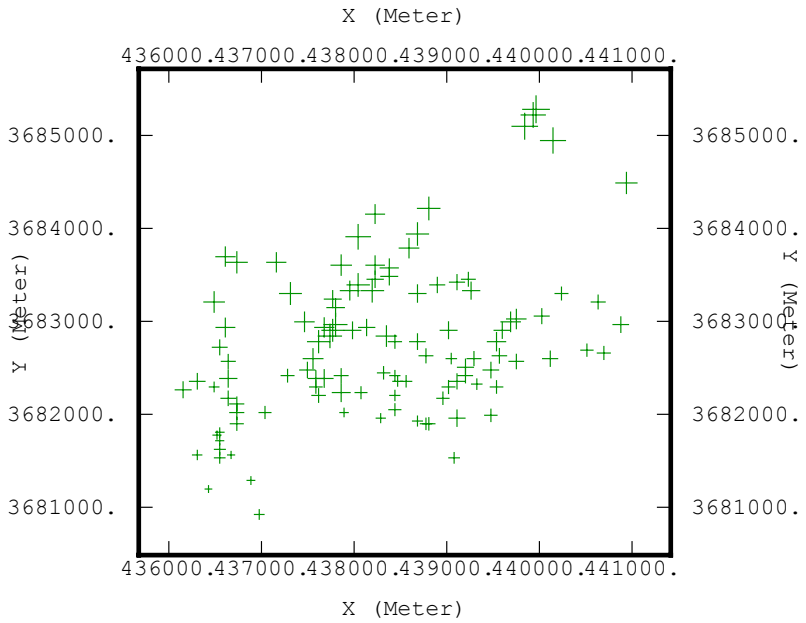

Figure 24 Santee top well picks location

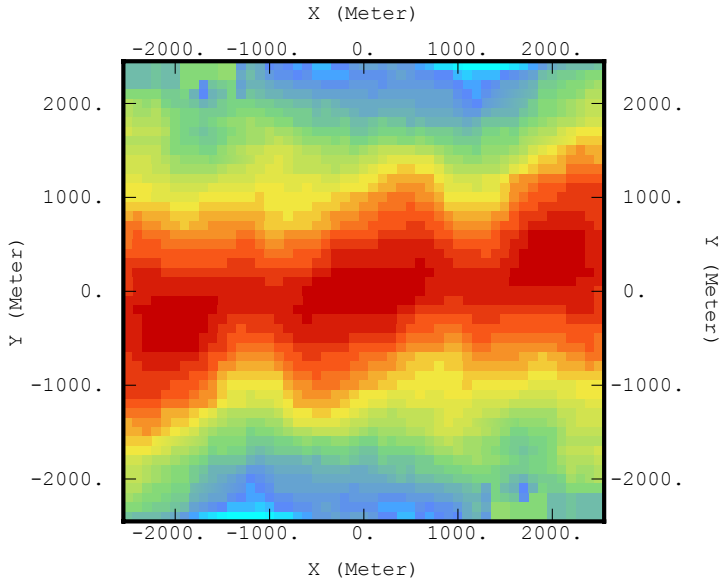

Figure 25: Variogram map of Santee top well picks

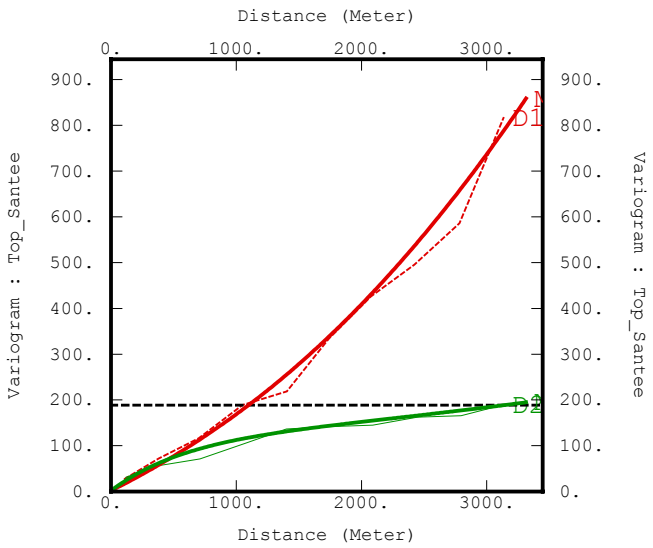

Figure 26: Experimental variogram and its model of the Santee top

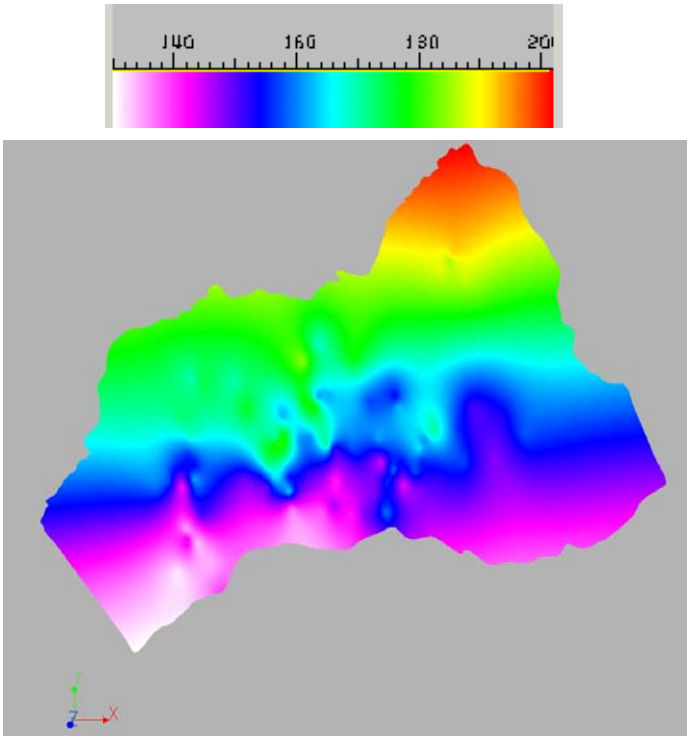

Figure 27: Elevation of the Kriged Santee top

Maximum Flooding Surface

Figures 26 to 28 show the data locations, the variogram map, and the modeled direction variogram for the Maximum Flooding Surface. The final variogram modeling parameters are:

- Structure 1: power (exp 2), az = N75, sill = 70, range N75 = 2800m, range N165 = 1000m
- Structure 2: exponential, az = N170, sill = 80, range N170 = 3800m, range N80 = 2200m
- Structure 3: nugget, sill = 2

The Kriged horizon (Fig. 31) appears to show the effect of channeling perpendicular to the coastal plain. The localized "dimples" suggests additional editing of the well top picks for the Maximum Flooding Surface.

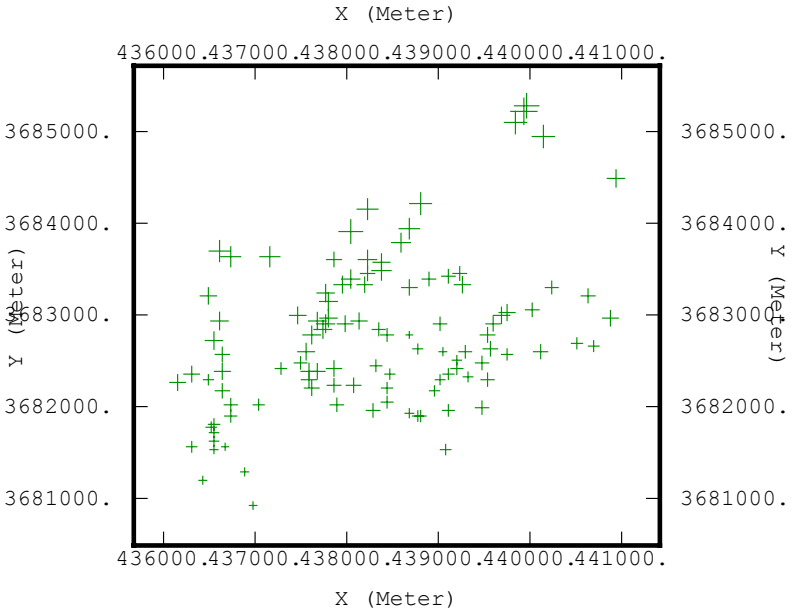

Figure 28: Maximum flooding surface well picks location

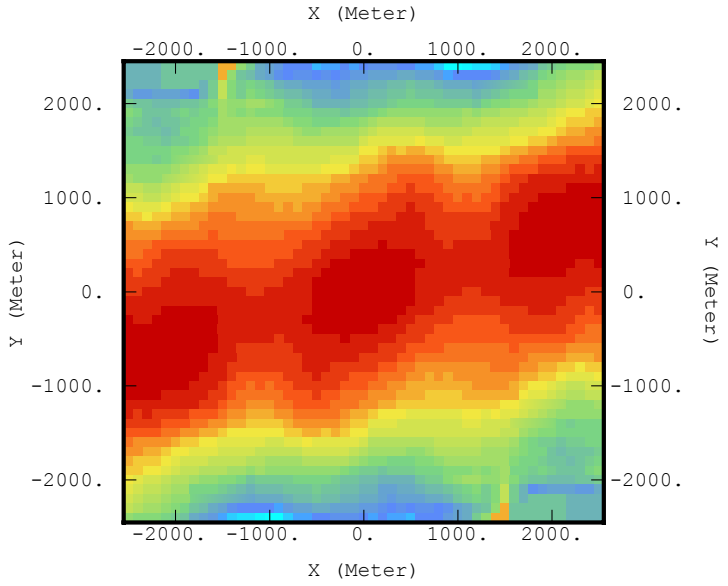

Figure 29: Variogram map of the maximum flooding surface well picks

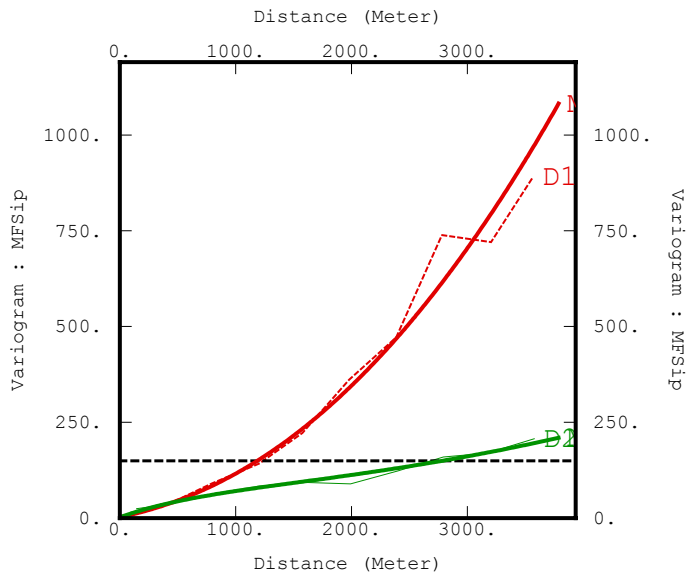

Figure 30: Experimental variogram and its model of the maximum flooding surface

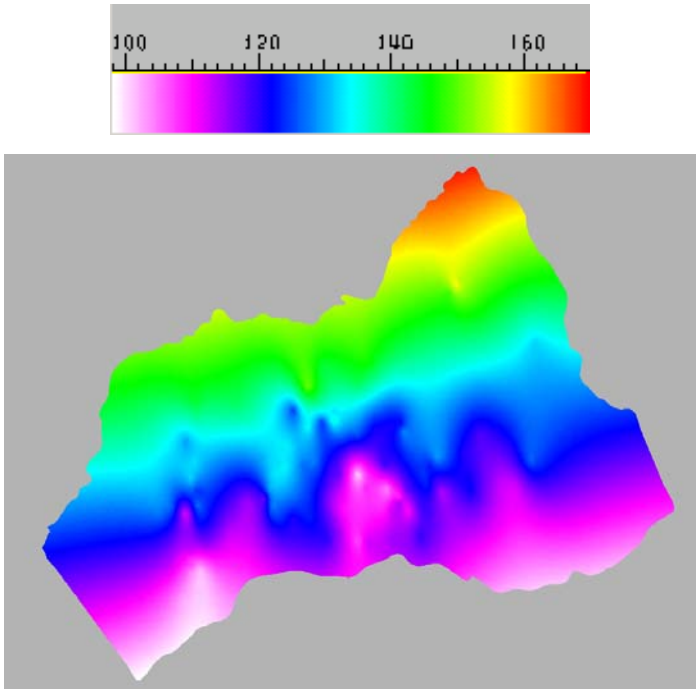

Figure 31: Elevation of the Kriged maximum flooding surface

Congaree Top

Figures 32 to 34 show the data locations, the variogram map, and the modeled direction variogram for the Congaree. The final variogram modeling parameters are:

- Structure 1: power (exp 2), az = N75, sill = 80, range N75 = 3100m, range N165 = 1100m
- Structure 2: exponential, az = N170, sill = 60, range N170 = 2300m, range N80 = 1100m
- Structure 3: spherical, sill = 10, range = 1200m
- Structure 4: nugget, sill = 2

The Kriged horizon (Fig. 35) appears to show the effect of channeling perpendicular to the coastal plain. The localized "dimples" suggests additional editing of the well top picks for the Congaree Surface.

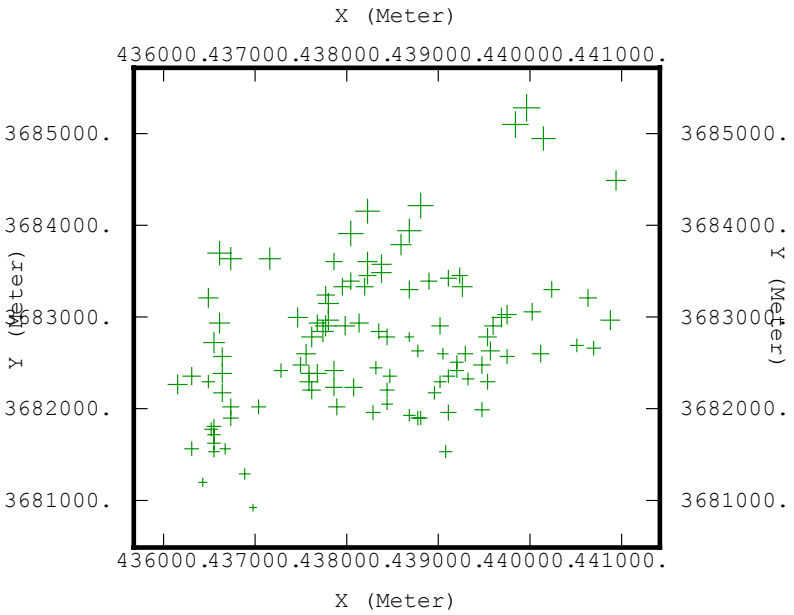

Figure 32: Congaree top well picks location

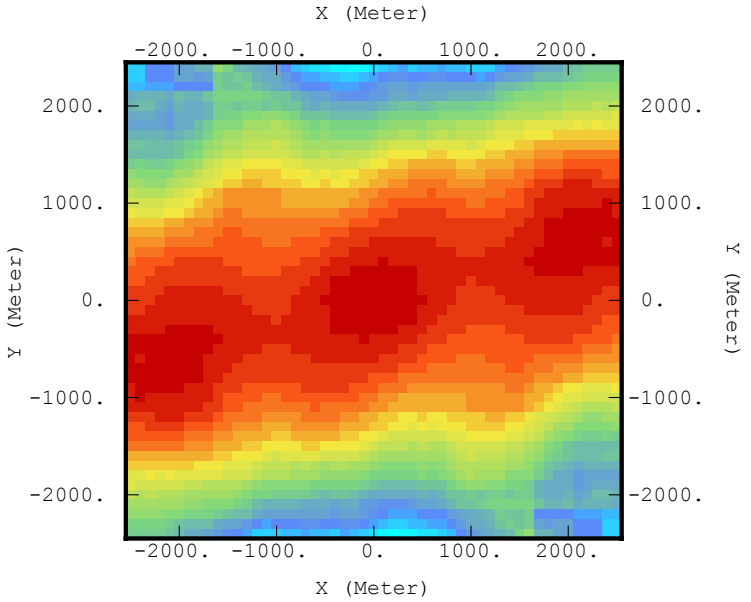

Figure 33: Variogram map of the Congaree top well picks

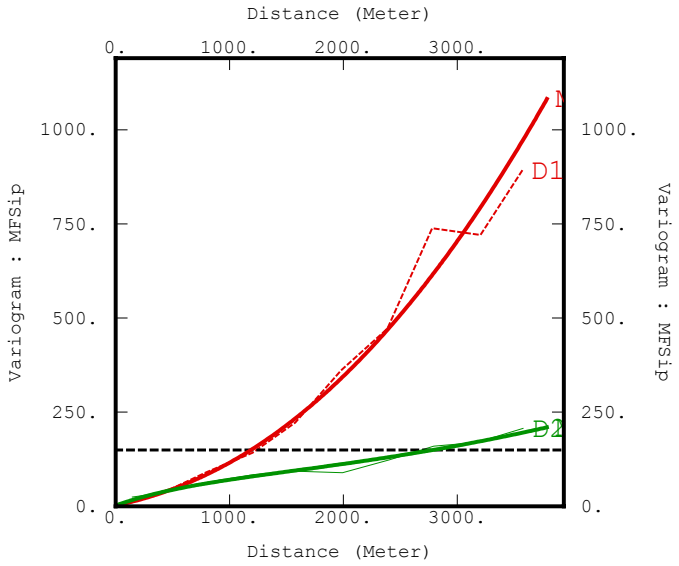

Figure 34: Experimental variogram and its model of the Congaree top

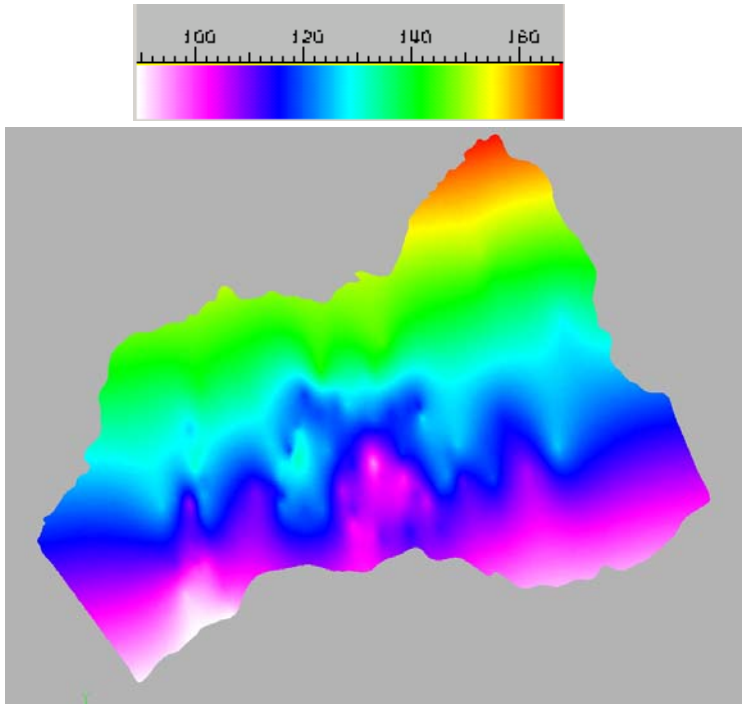

Figure 35: Elevation of the Kriged Congaree top

Ellenton Top

Figures 36 to 38 show the data locations, the variogram map, and the modeled direction variogram for the Ellenton. The final variogram modeling parameters are the same as for the Congaree surface:

- Structure 1: power (exp 2), az = N75, sill = 80, range N75 = 3100m, range N165 = 1100m

- Structure 2: exponential, az = N170, sill = 60, range N170 = 2300m, range N80 = 1100m
- Structure 3: spherical, sill = 10, range = 1200m
- Structure 4: nugget, sill = 2

The Kriged horizon (Fig. 39) appears to show the effect of channeling perpendicular to the coastal plain.

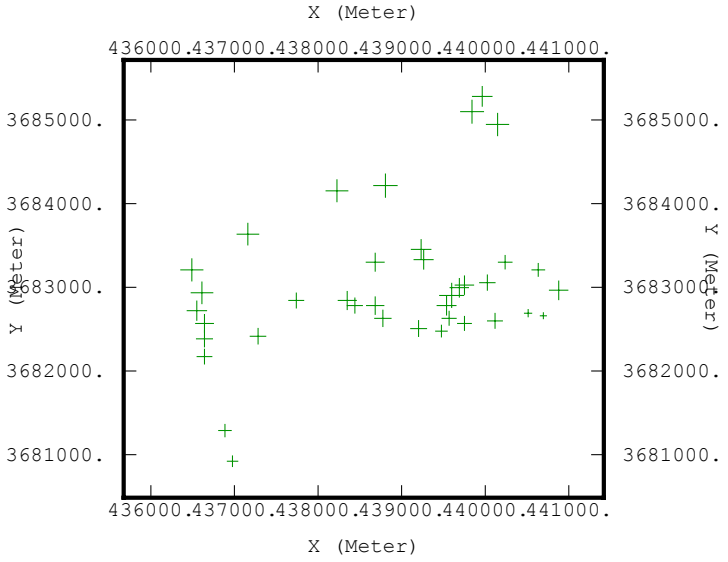

Figure 36: Ellenton top well picks location

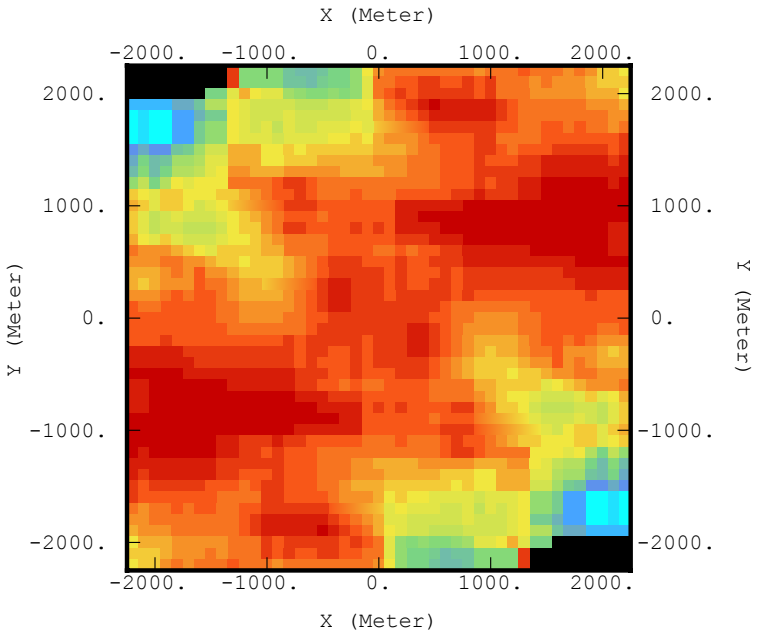

Figure 37: Variogram map of the Ellenton top well picks

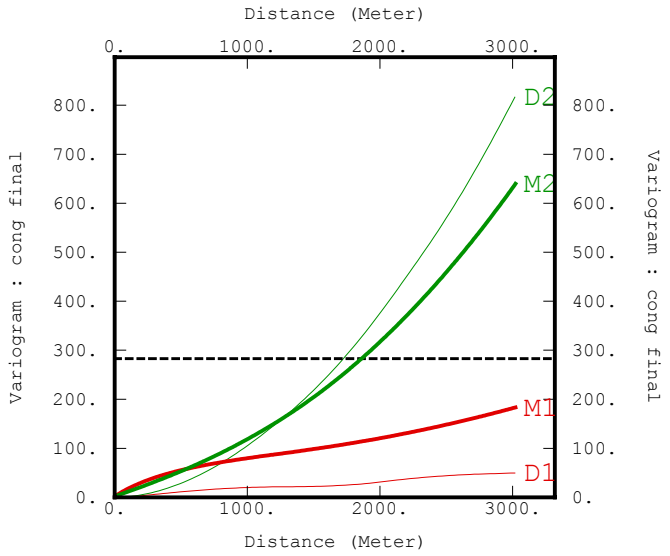

Figure 38: Experimental variogram and its model of the Ellenton top

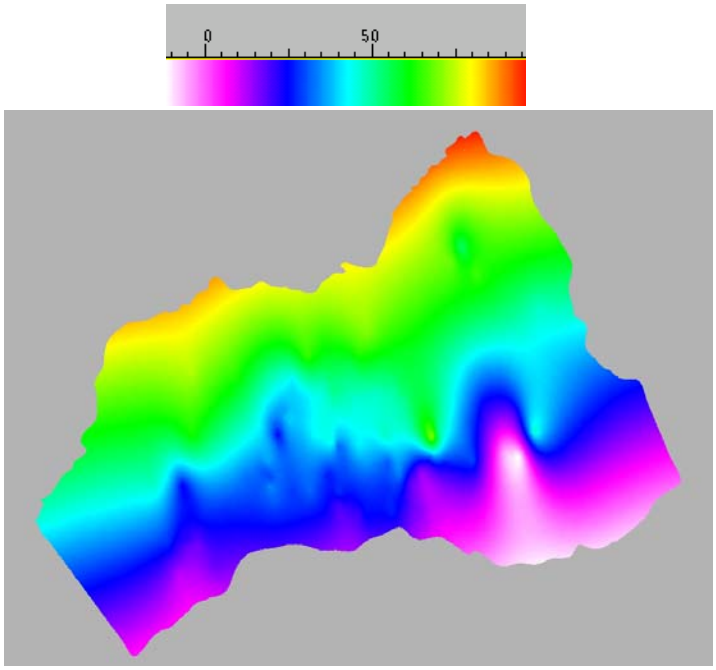

Figure 39: Elevation of the Kriged Ellenton top

The next display (Fig.40) shows all the Kriged surfaces, stacked in stratigraphic order, with the ground surface as a transparent horizon.

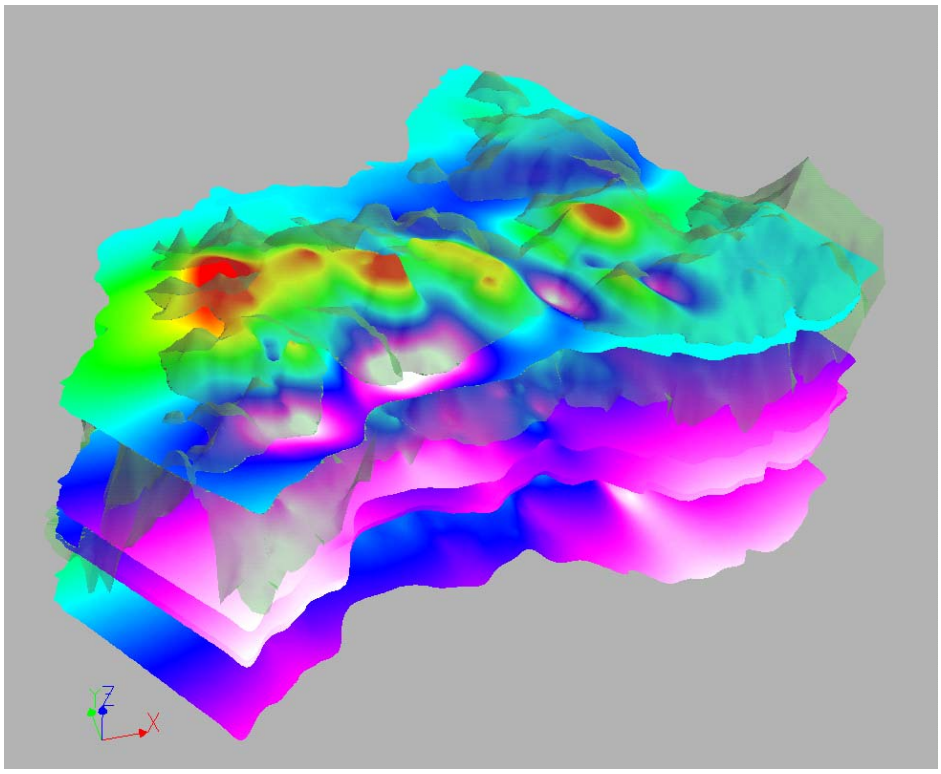

Figure 40: Complete structural model of the GSA

Depositional facies well logs analysis

Depositional facies logs derived from core data interpretation were imported into Isatis to study their variogram map and variograms. Each depositional facies (up to a total of 11 facies for the whole model) was studied separately within each formation. The facies were identified as an indicator code (integer value).

Upland Formation

The Upland Formation contains two major facies:

- Fluvial (indicator 1)
- Floodplain / Overbank Mud (indicator 2)

Indicator variogram computations are identical to continuous variables, such as depth, porosity, for example. When only two indicator values are available, as in this formation, the facies variograms are mathematically symmetric. Thus, it is only necessary to compute one variogram and one variogram map.

The formation was divided in 10 horizontal layers in order to build the 3D variogram maps, which are illustrated in Figure 41, layers 1, 3, 5, 7, and 9. The variogram model is shown in Figure 42, with the following parameters:

- Sill = 0.25
- Structures: Exponential N48 1950m (range along N48) 570m (range along N138) 55ft (vertical range) 0.05 (sill), Exponential N115 1230m 500m 22ft 0.2

Layer 1

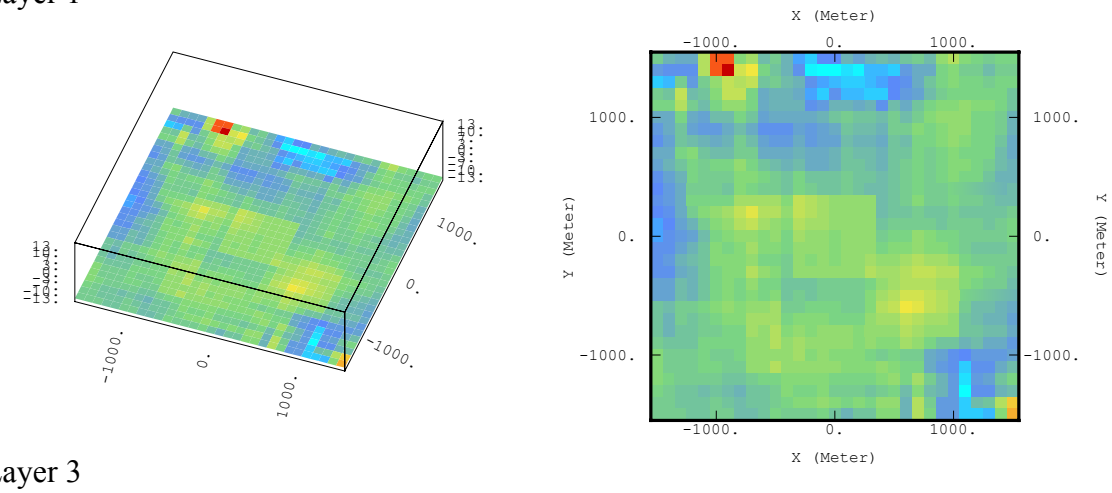

Layer 3

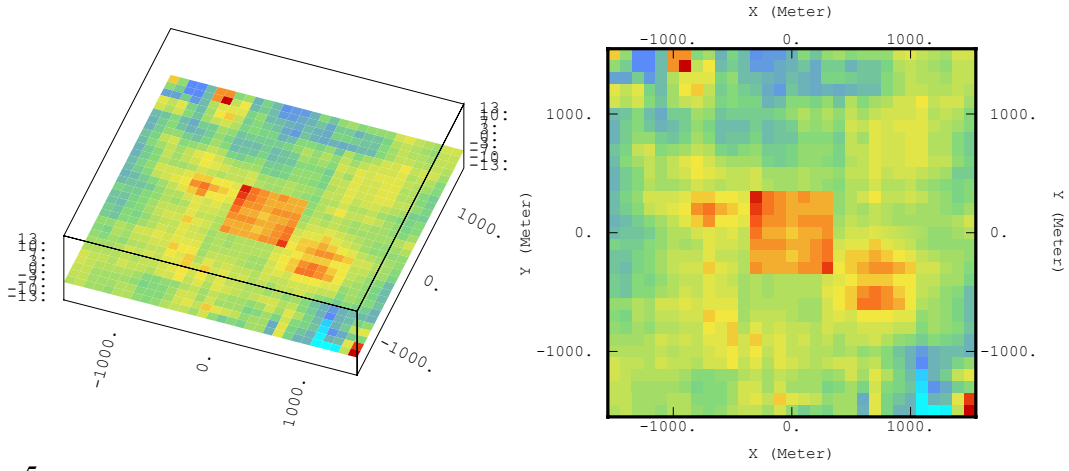

Layer 5

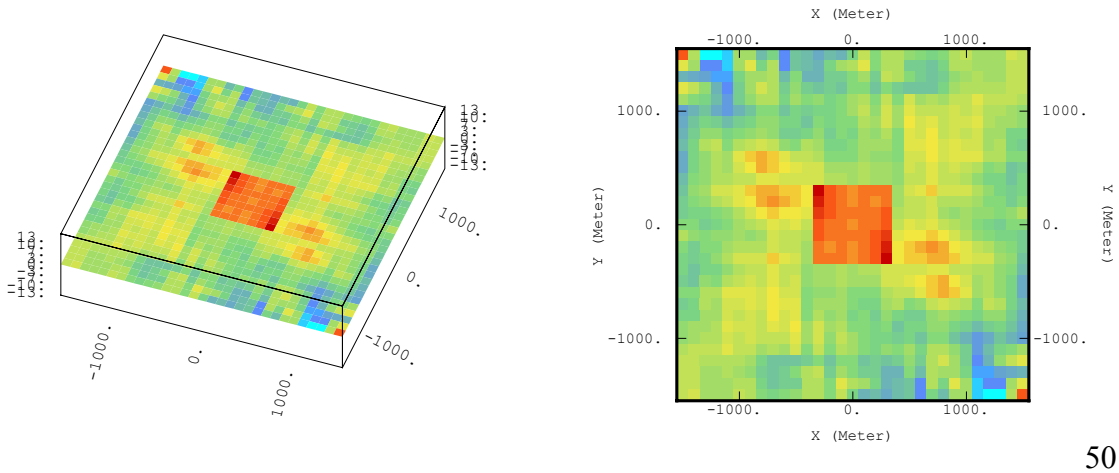

Layer 7

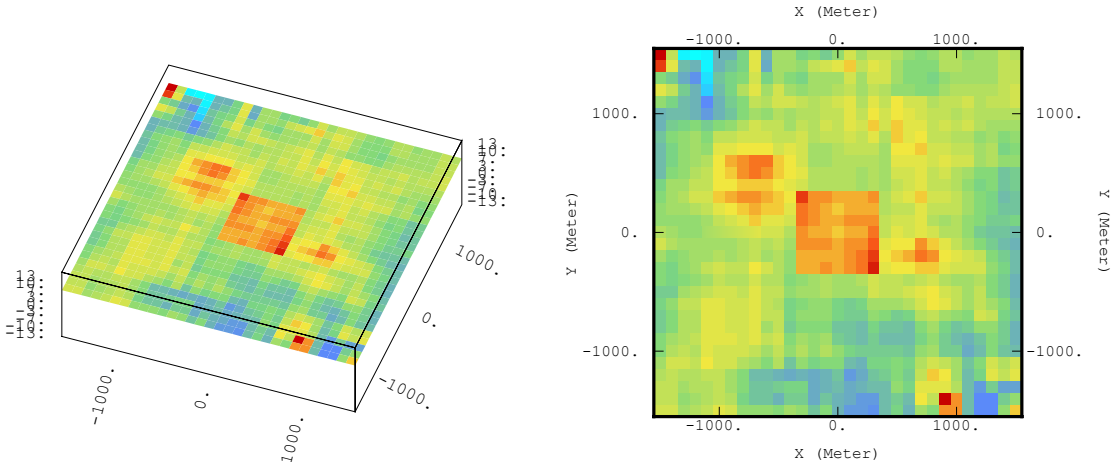

Layer 9

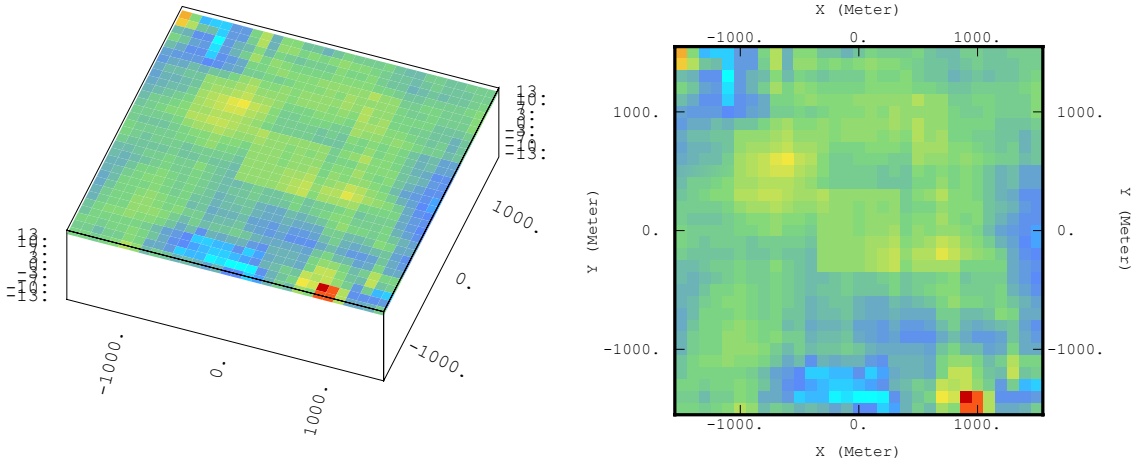

Figure 41: 3D Variogram map of the depositional facies in the Upland

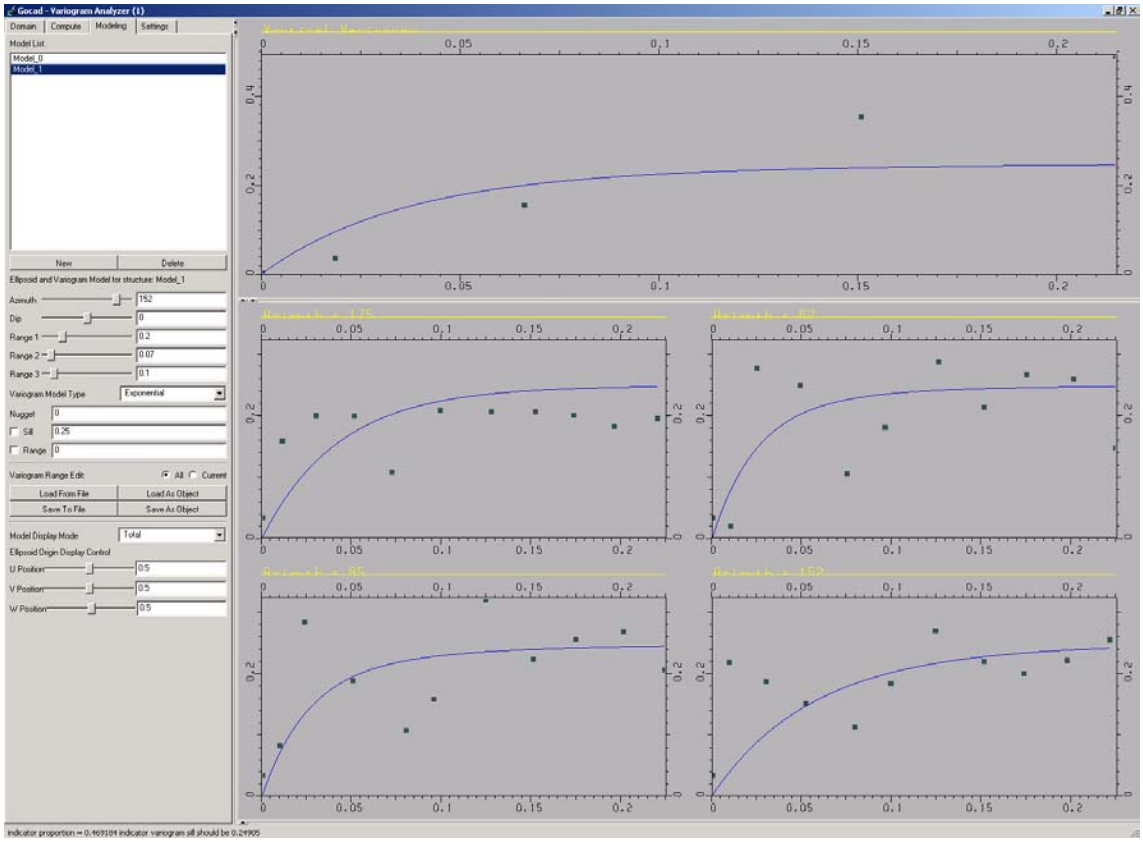

Figure 42: Experimental variogram and its model for the depositional facies in the Upland

Barnwell Group

The Barnwell Group contains two major facies:

- Tidal Flat / Lagoonal (indicator 3)
- Barrier Beach (indicator 5)

The formation was divided in 15 horizontal layers in order to build the 3D variogram maps, which are illustrated in figure 43, layers 1, 4, 10, and 15. The variogram model is shown in Figure 44, with the following parameters:

- Sill = 0.2
- Structures: Exponential N165 780m 440m 44ft 0.15, Exponential N45 1950m 350m 44ft 0.05

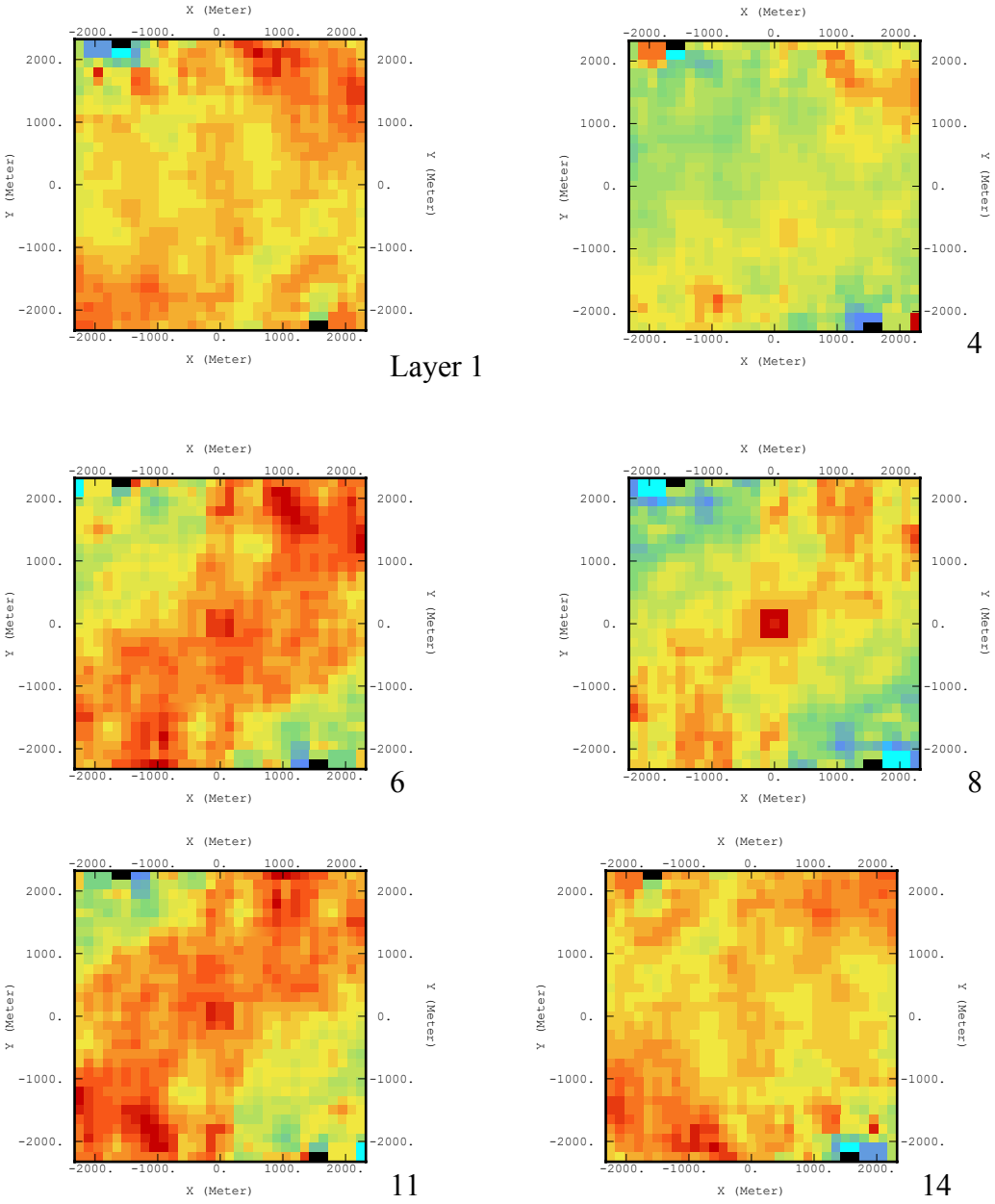

Figure 43: 3D Variogram map of the depositional facies in the Barnwell Group

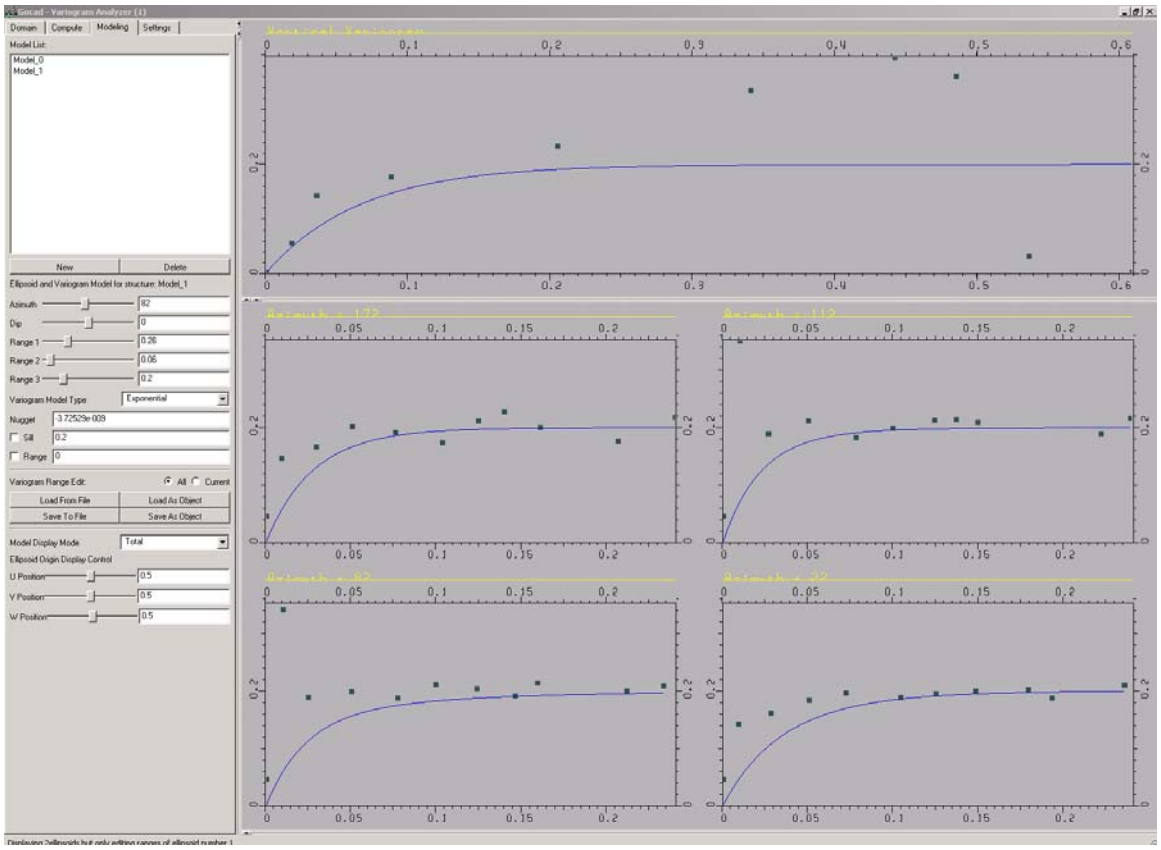

Figure 44: Experimental variogram and its model for the depositional facies in the Barnwell Group

Santee

The Santee formation contains four major facies:

- Siliciclastic Shelf (indicator 4)
- Middle Shelf (low energy) (indicator 6)
- Open/Outer Shelf (indicator 7)
- Middle Shelf (high energy) (indicator 10)

3D Variogram map for Siliciclastic Shelf

The facies was divided in 10 horizontal layers in order to build the 3D variogram maps, which are illustrated in Figure 45, Layers 1, 3, 5, 7, and 9. The variogram model is shown in Figure 46, with the following parameters:

- Sill = 0.22
- Structures = Exponential N49 500m 300m 94ft 0.11, Exponential N70 1000m 500m 94ft 0.11

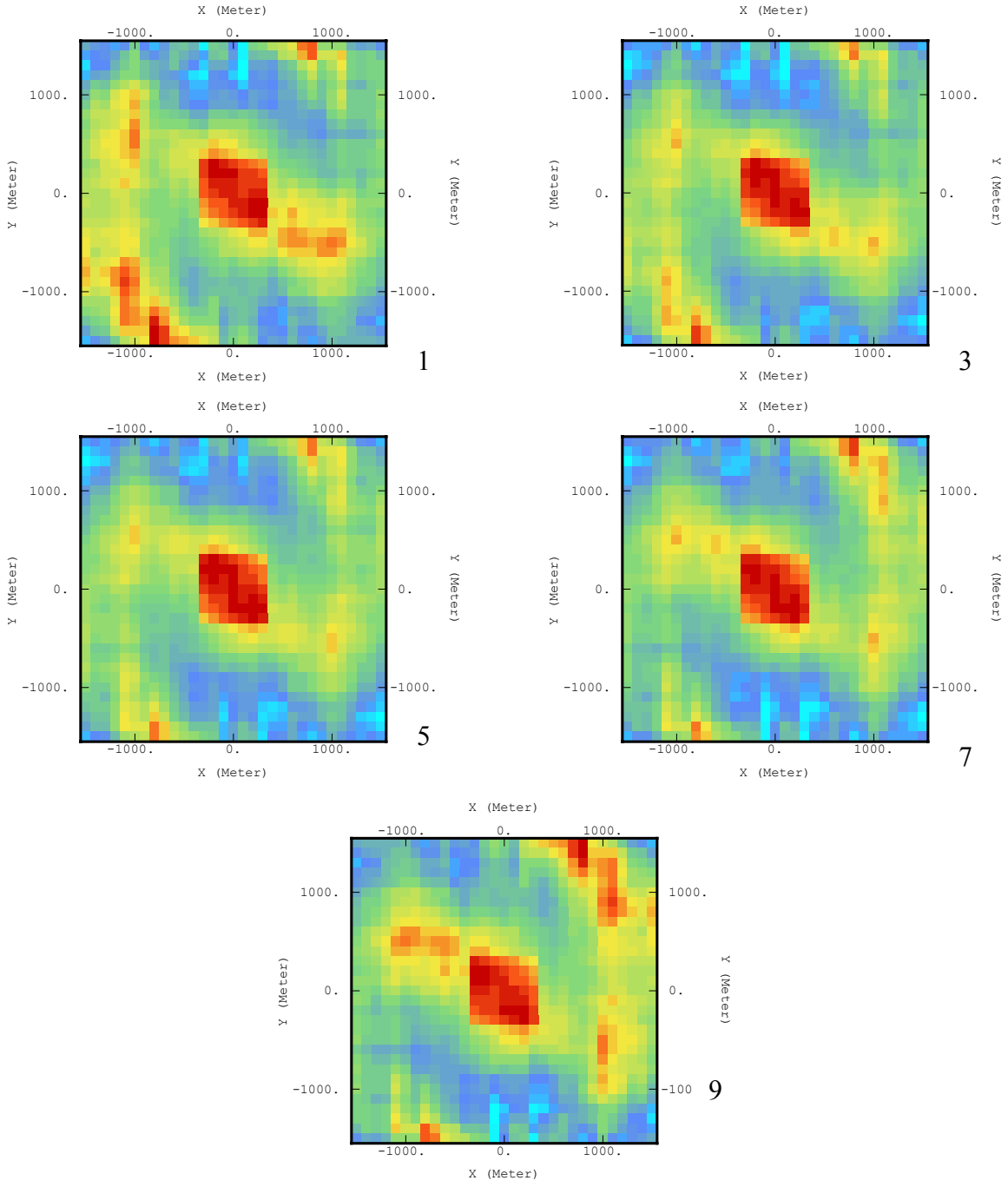

Figure 45: 3D Variogram map of the depositional facies Siliciclastic Shelf in the Santee

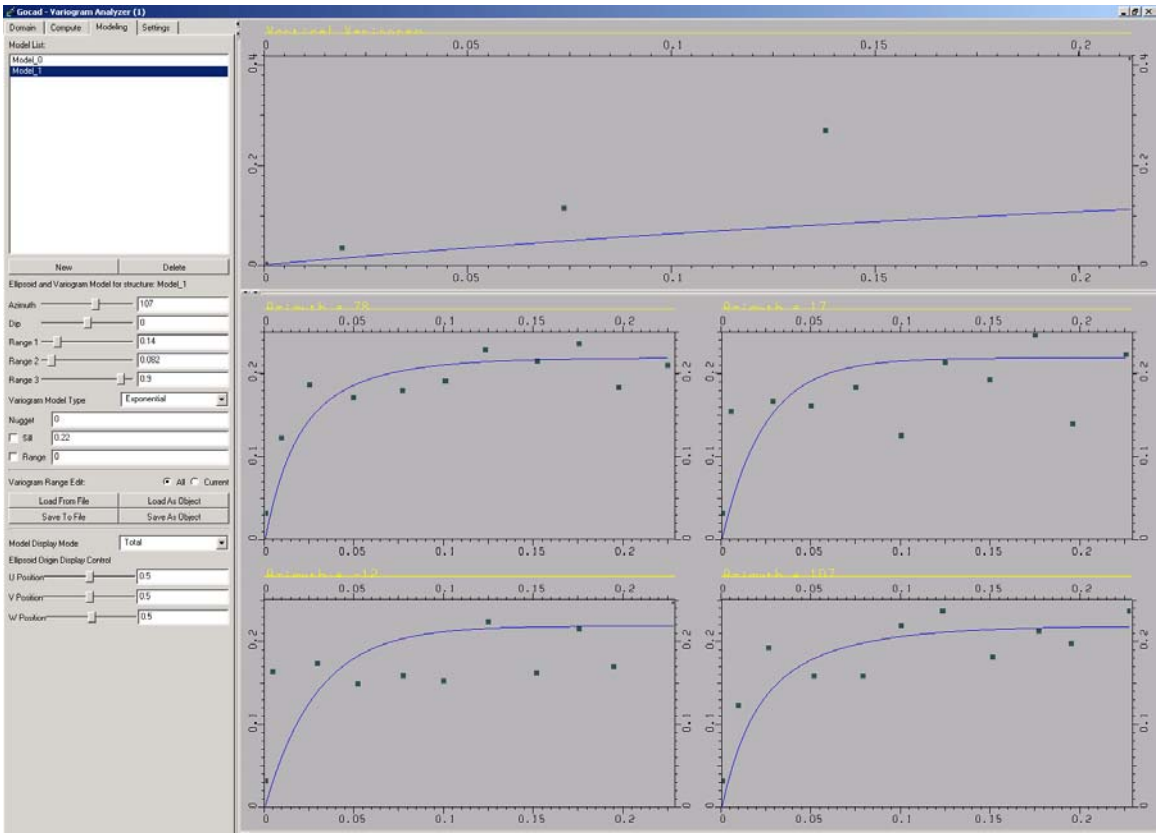

Figure 46: Experimental variogram and its model for Siliciclastic Shelf in the Santee

3D Variogram map for Middle Shelf (low energy)(done with 10 layers)

The facies was divided in 10 horizontal layers in order to build the 3D variogram maps, which are illustrated in Figure 47, Layers 1, 3, 5, 7, and 9. The variogram model is shown in Figure 48, with the following parameters:

- Sill = 0.18
- Structures = Spherical N143 1400m 1500m 83ft 0.14, Exponential N93 890m 450m 83ft 0.04

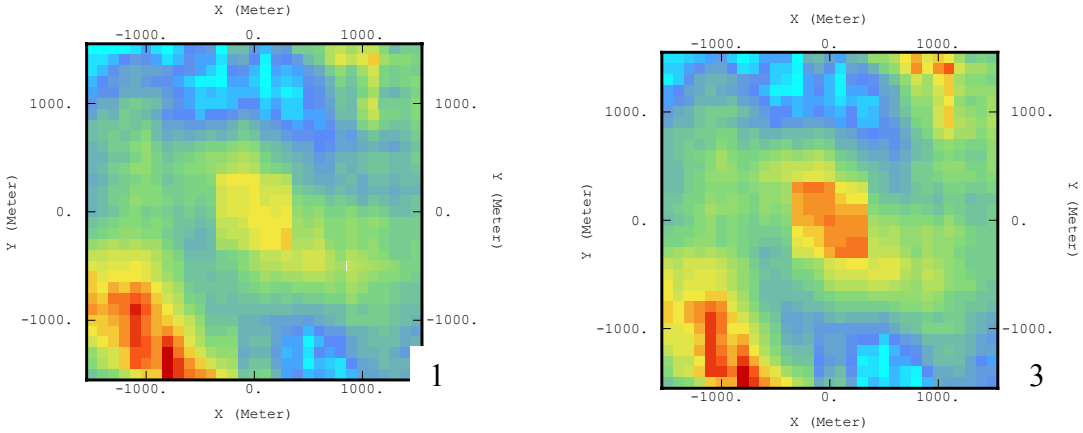

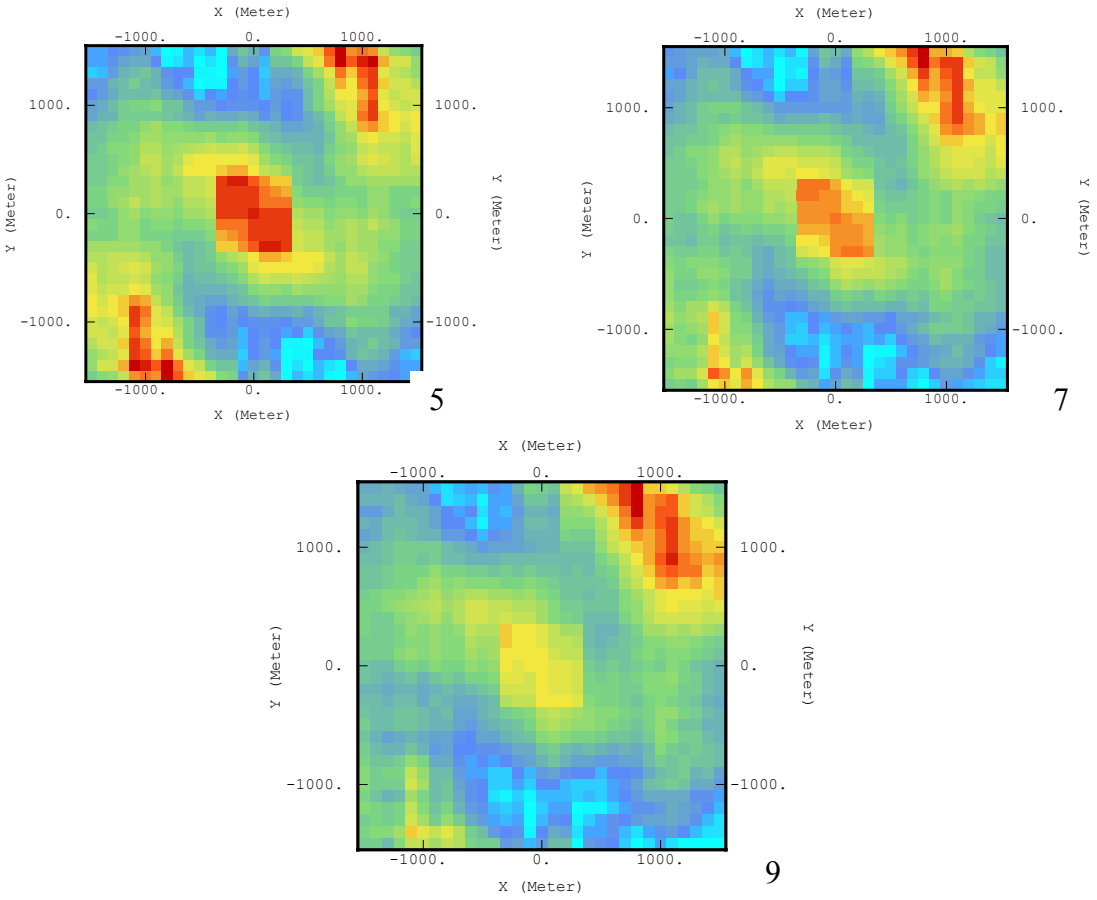

Figure 47: 3D Variogram map of the depositional facies Middle Shelf (low energy) in the Santee

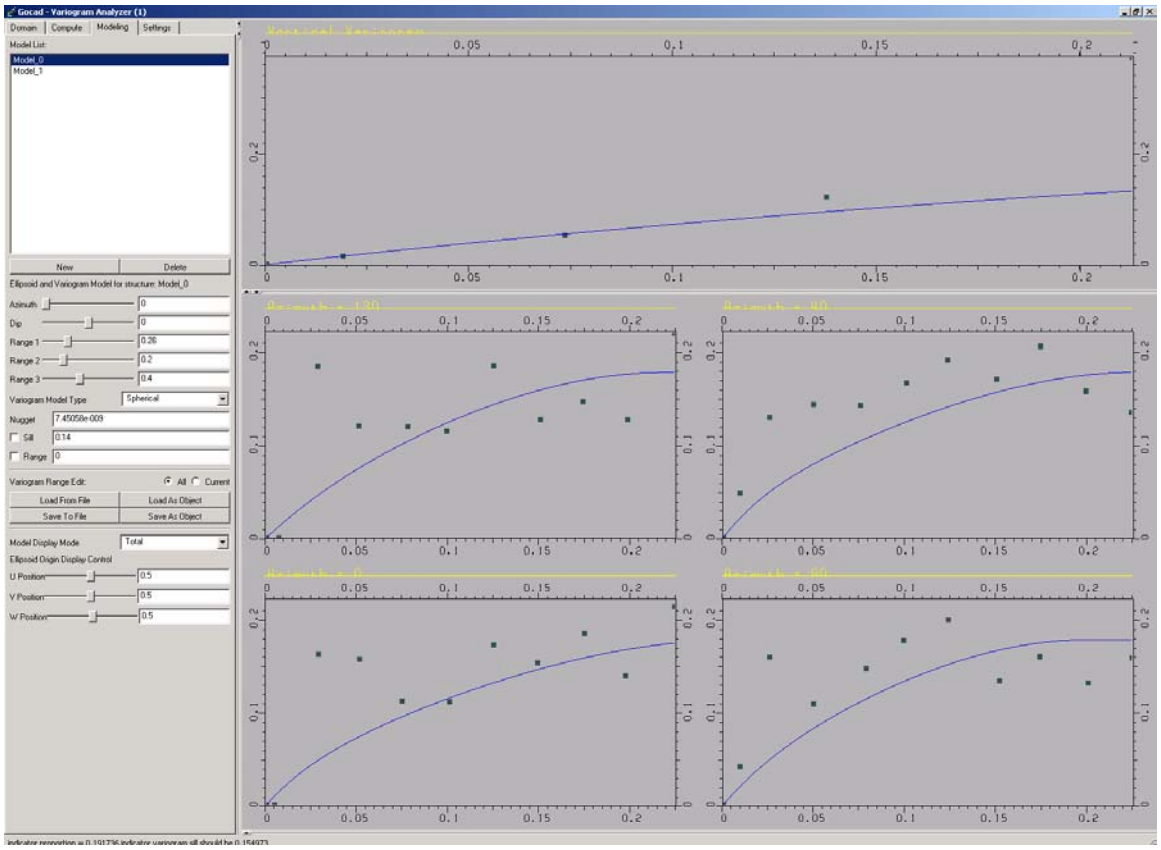

Figure 48: Experimental variogram and its model for Middle Shelf (low energy) in the Santee

3D Variogram map for Open/Outer Shelf (done with 10 layers)

The facies was divided in 10 horizontal layers in order to build the 3D variogram maps, which are illustrated in Figure 49, Layers 1, 3, 5, 7, and 9. The variogram model is shown in Figure 50, with the following parameters:

- Sill = 0.025
- Structure = Exponential N143 515m 530m 33ft 0.025

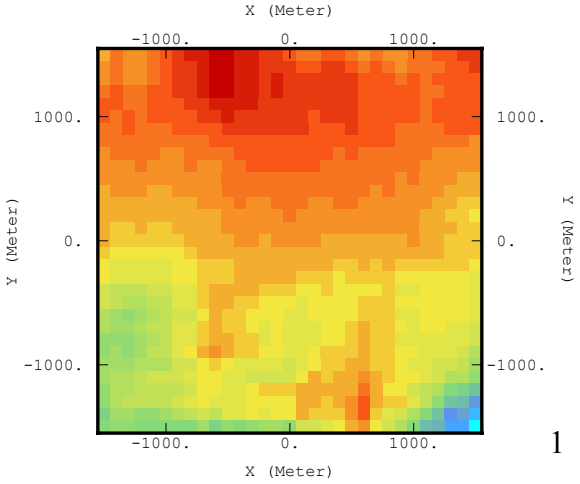

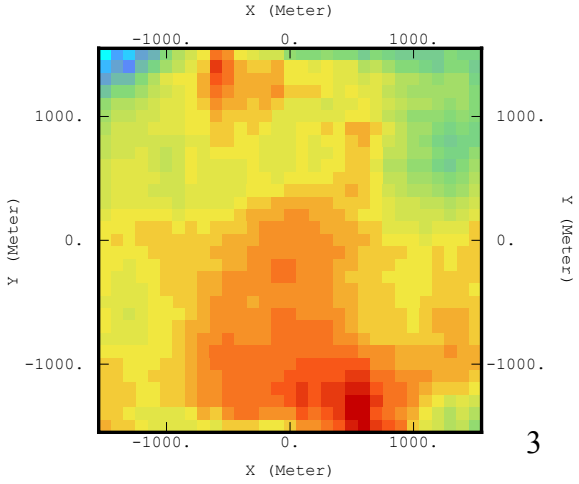

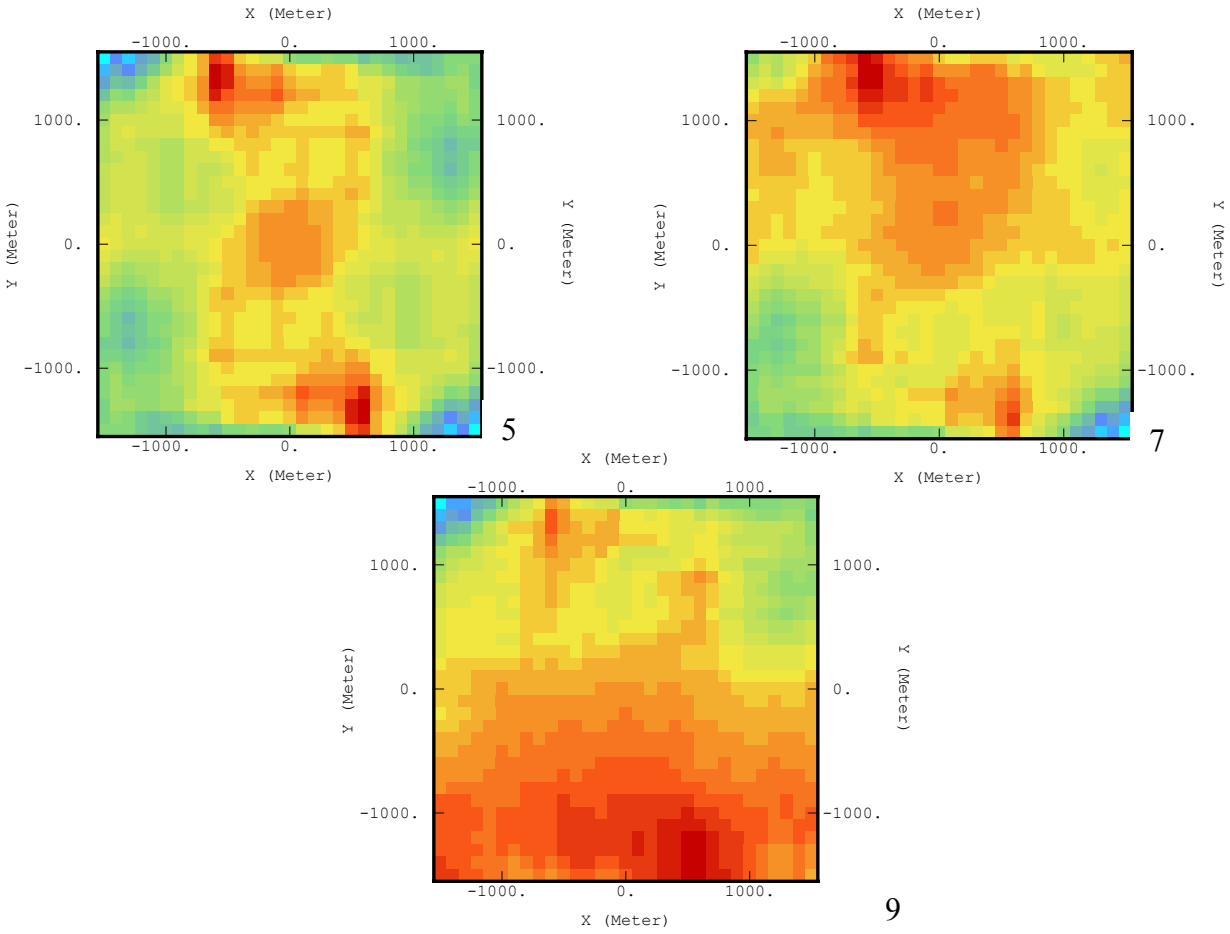

Figure 49: 3D Variogram map of the depositional facies Open/Outer Shelf in the Santee

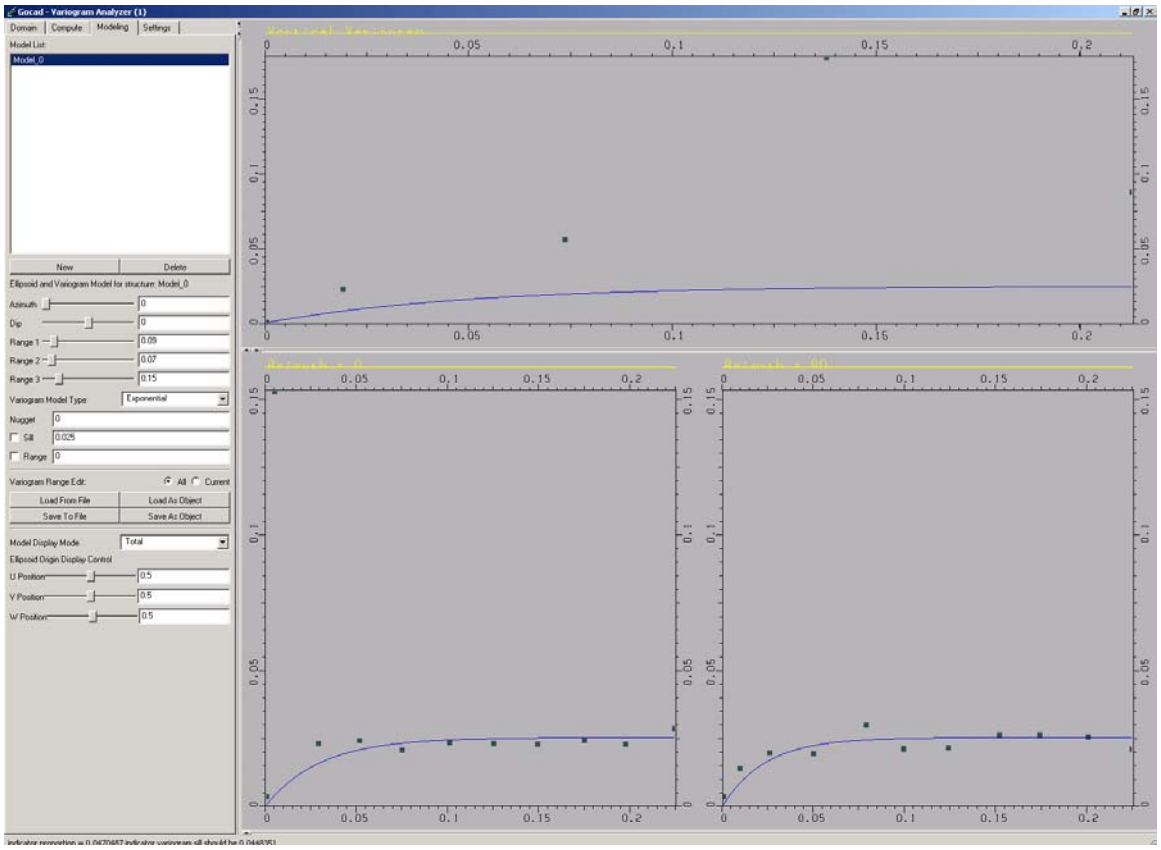

Figure 50: Experimental variogram and its model for Open/Outer Shelf in the Santee

3D Variogram map for Middle Shelf (high energy) (done with 10 layers)

The facies was divided in 10 horizontal layers in order to build the 3D variogram maps, which are illustrated in Figure 51, Layers 1, 3, 5, 7, and 9. The variogram model is shown in Figure 52, with the following parameters:

- Sill = 0.06
- Structure = Exponential N143 570m 450m 94ft

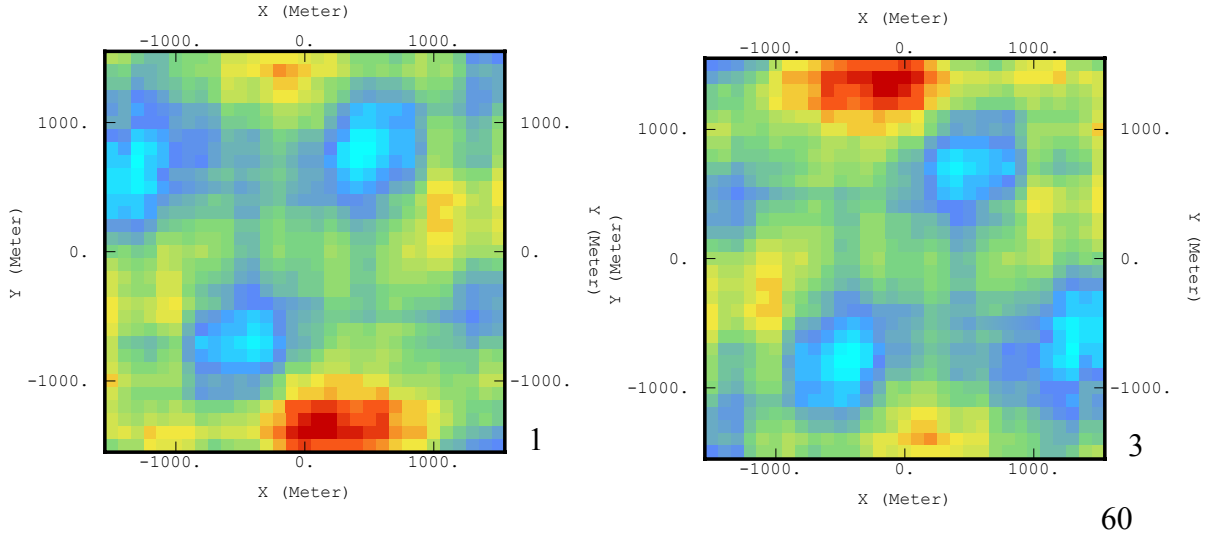

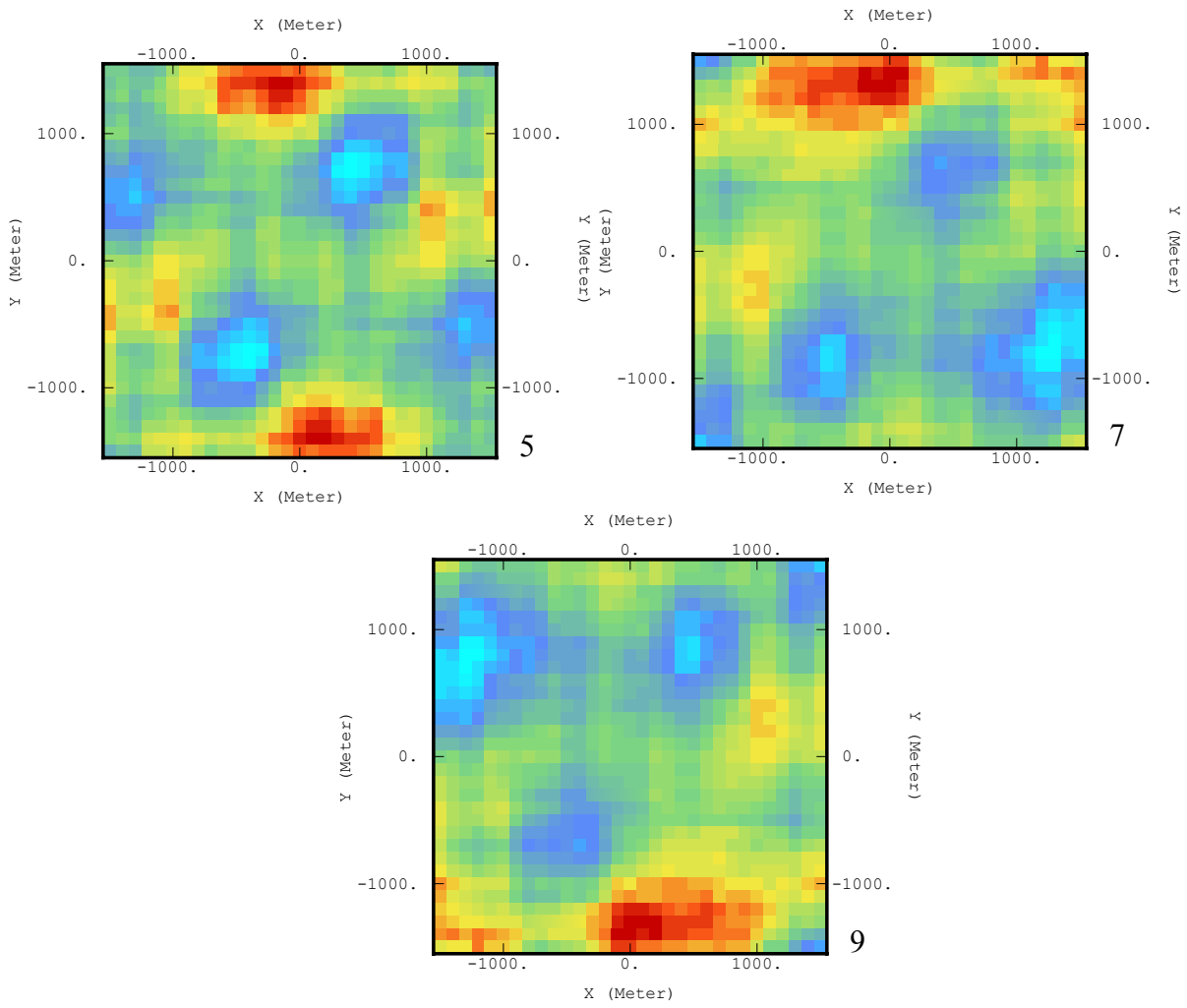

Figure 51: 3D Variogram map of the depositional facies Middle Shelf (high energy) in the Santee

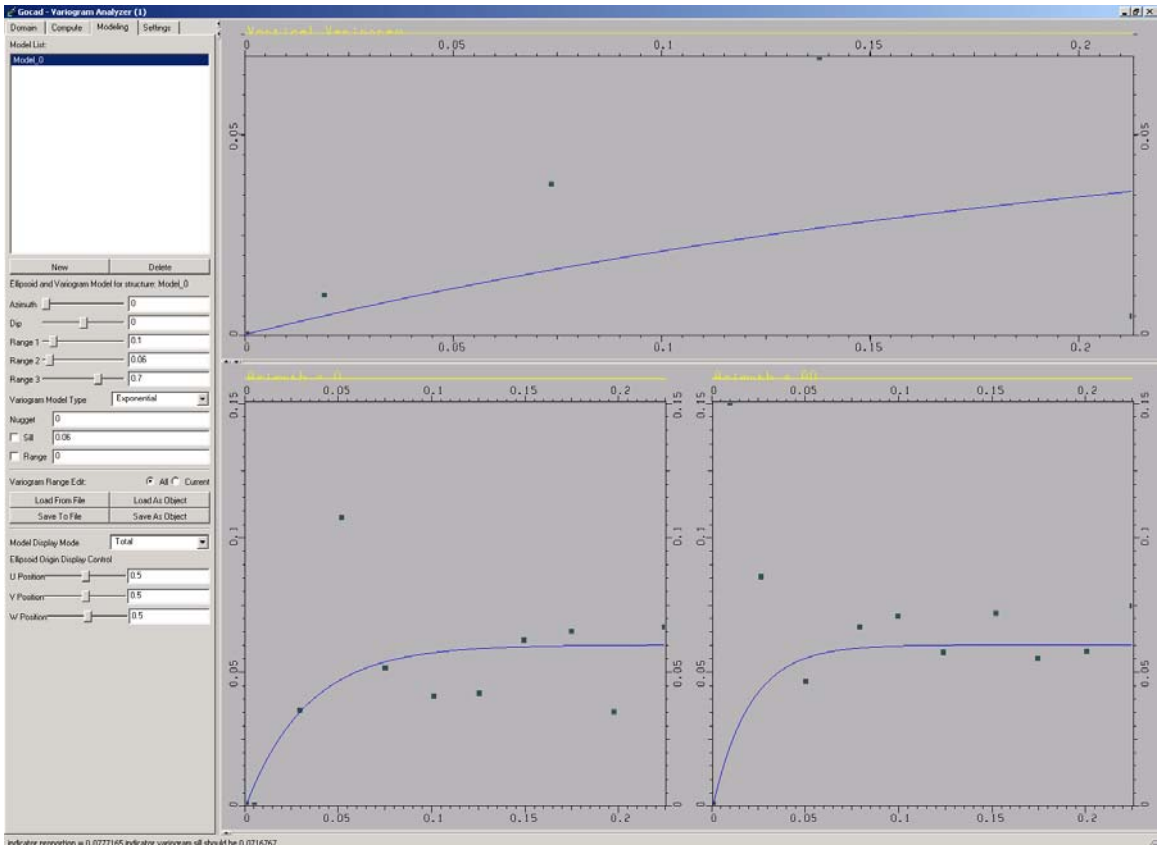

Figure 52: Experimental variogram and its model for Middle Shelf (high energy) in the Santee

Green Clay Formation

The Green Clay Formation is a very thin and is consisting of only clay. It was decided not to simulate any facies for this formation. Petrophysical properties will be assigned to the entire formation.

Congaree

The Congaree formation contains two major facies:

- Lower Shoreface (indicator 8)
- Inner Bay / Lagoonal (indicator 11)

The facies was divided in 15 horizontal layers in order to build the 3D variogram maps, which are illustrated in Figure 53, Layers 1, 4, 7, 8, 10, and 13. The variogram model is shown in Figure 54, with the following parameters:

- Sill = 0.14
- Structure = Exponential N10 1340m 600m 21ft 0.07, Exponential N70 1110m 600m 21ft 0.07

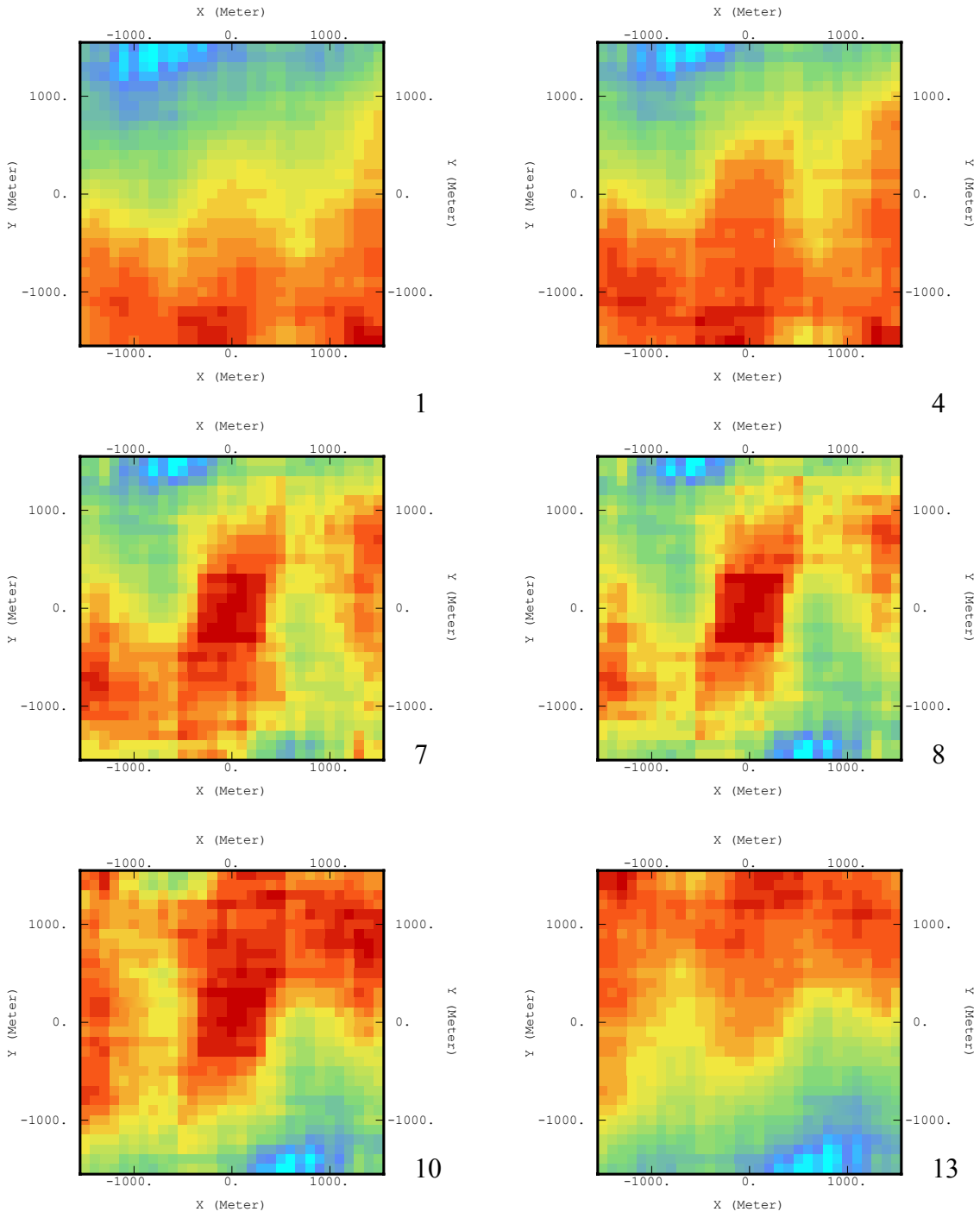

Figure 53: 3D Variogram map of the depositional facies in the Congaree

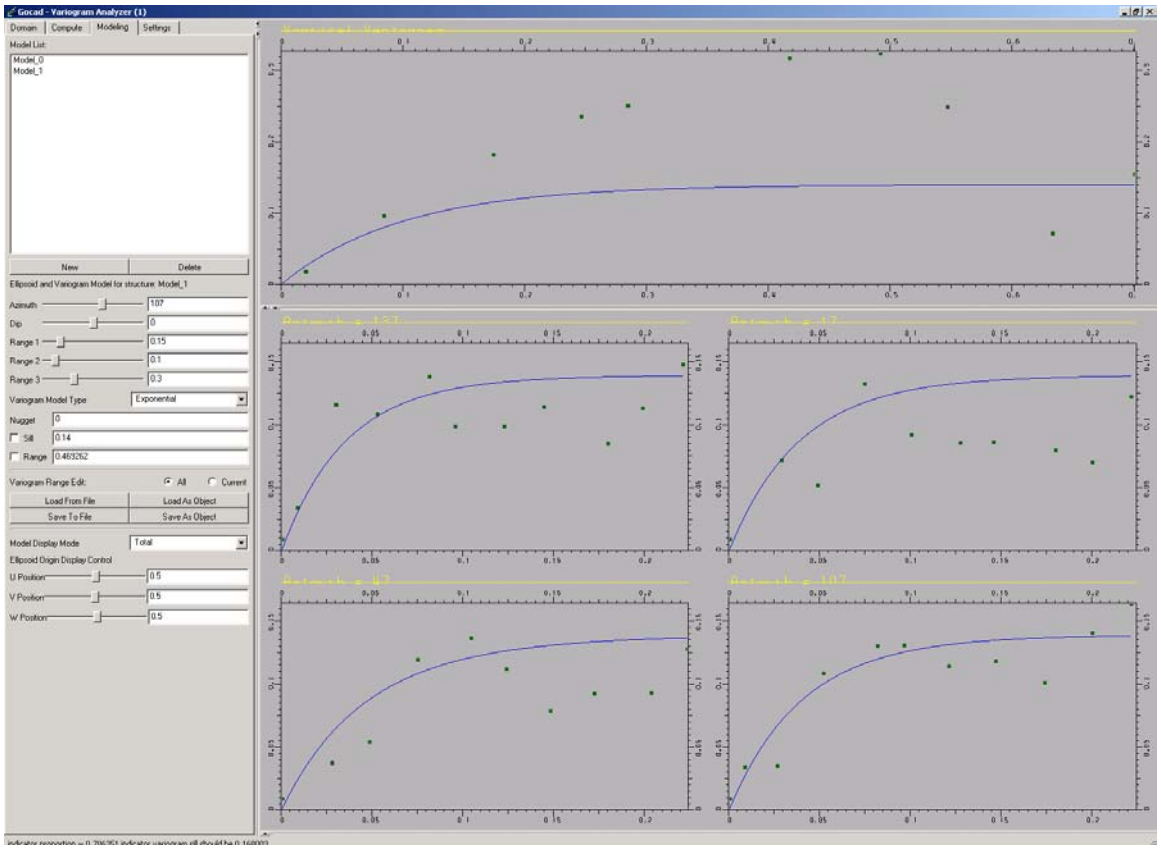

Figure 54: Experimental variogram and its model for depositional facies in the Congaree

The 3D variogram maps provide a visual confirmation of the correlation ellipse or ellipse when multiple anisotropic directions are contained in the data, as is the case with the SRS data. Based on the variogram maps, experimental variograms were computed and modeled for each facies within each formation. Sequential Indicator Simulation uses the variogram models to distribute the facies within their specific formation. Two hundred simulations were computed for each facies within each formation.

Sequential Indicator Simulation of the depositional facies

Upland

The following series of Figures (55-57) illustrates one simulation from among the 200 (left) and the most common facies computed per cell from the 200 (right). Red is Floodplain/Overbank muds and yellow is Fluvial.

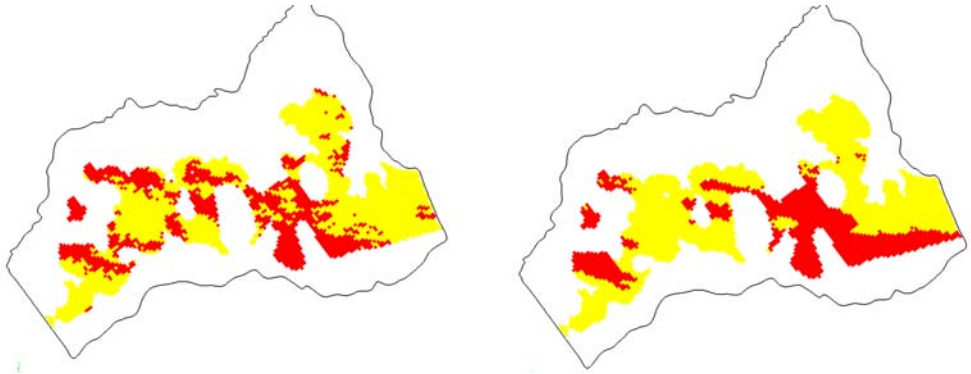

Figure 55: grid layer at the Upland formation bottom

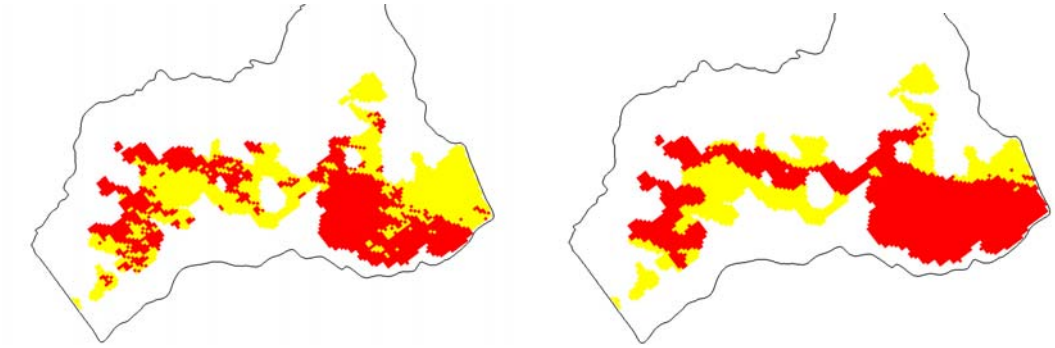

Figure 56: grid layer at the Upland formation middle

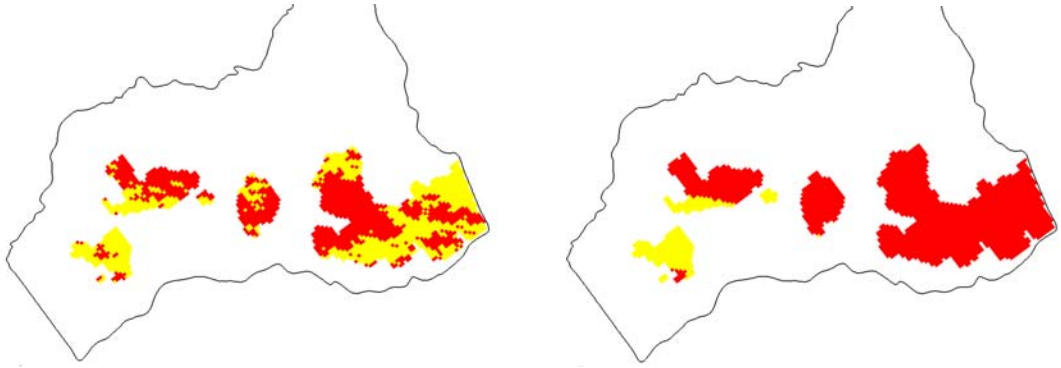

Figure 57: grid layer at the Upland formation top

Barnwell Group (Tobacco Road)

The following series of Figures (58-60) illustrates one simulation from among the 200 (left) and the most common facies computed per cell from the 200 (right). Red is Tidal Flat/Lagoonal and Yellow is Barrier Beach

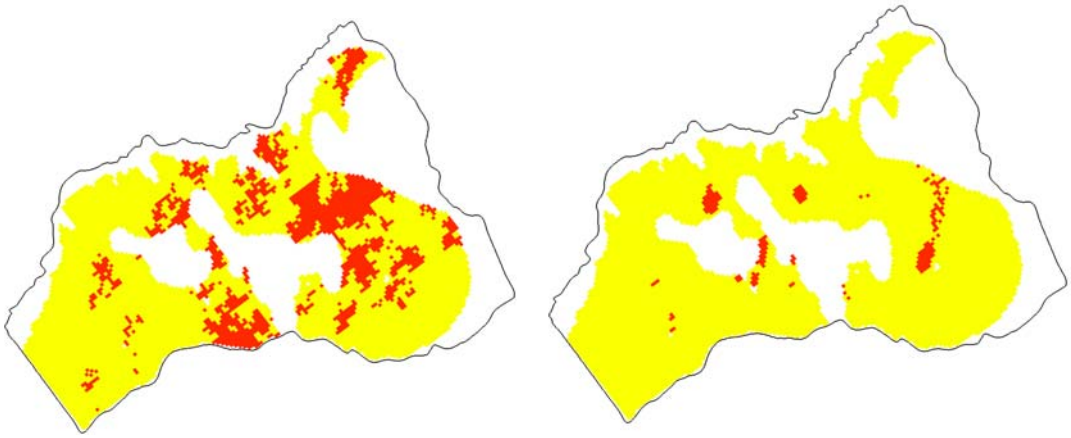

Figure 58: grid layer at the Barnwell Group formation bottom

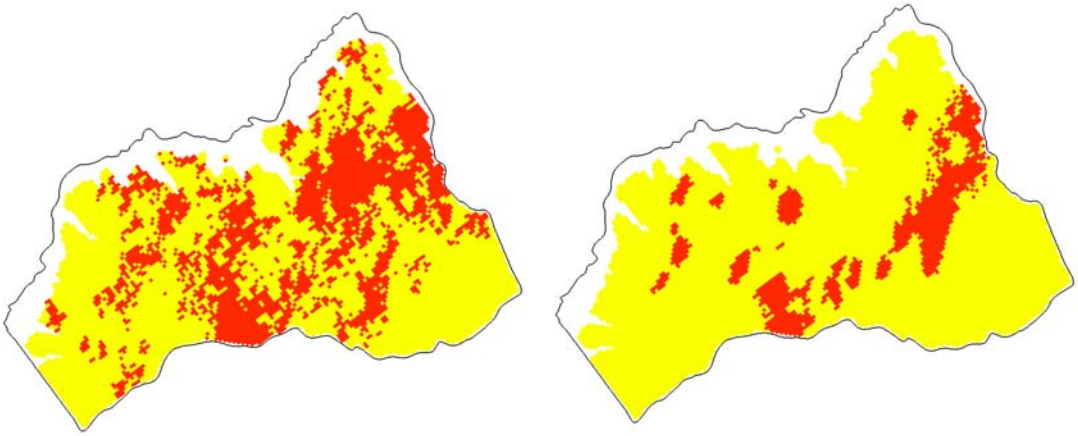

Figure 59: grid layer at the Barnwell Group formation middle

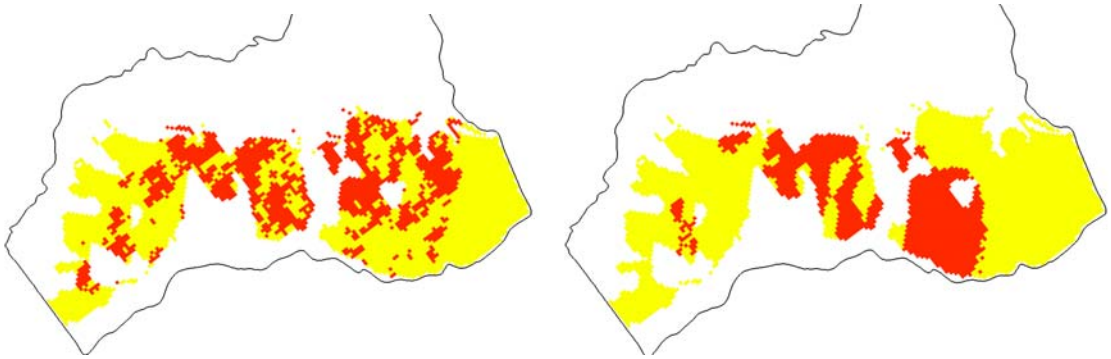

Figure 60: grid layer at the Barnwell Group formation top

Santee

The following series of Figures (61-63) illustrates one simulation from among the 200 (left) and the most common facies computed per cell from the 200 (right). Orange is Siliciclastic Shelf, Yellow is middle shelf low energy, Green is open/outer shelf, and Black middle shelf high energy.

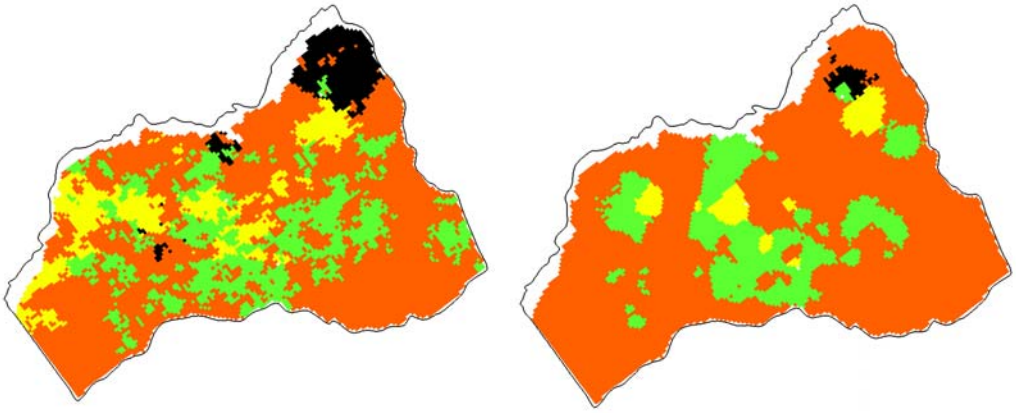

Figure 61: grid layer at the Santee formation bottom

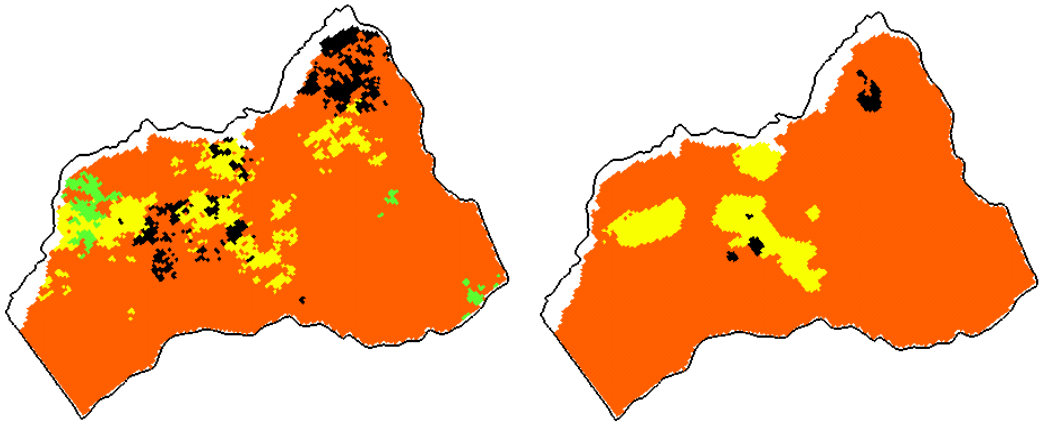

Figure 62: grid layer at the Santee formation bottom

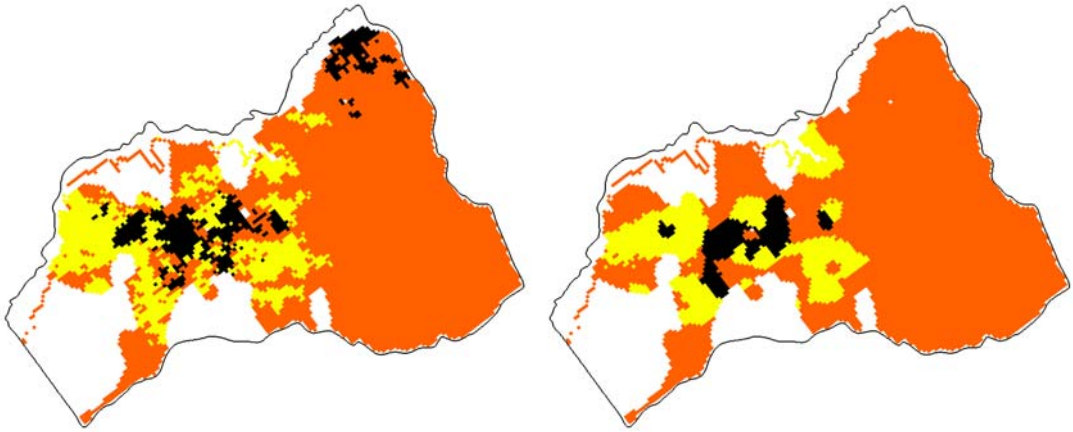

Figure 63: grid layer at the Santee formation bottom

Congaree

The following series of Figures (64-66) illustrates one simulation from among the 200 (left) and the most common facies computed per cell from the 200 (right). Yellow is Lower Shoreface, and Green is Inner Bay/Lagoonal.

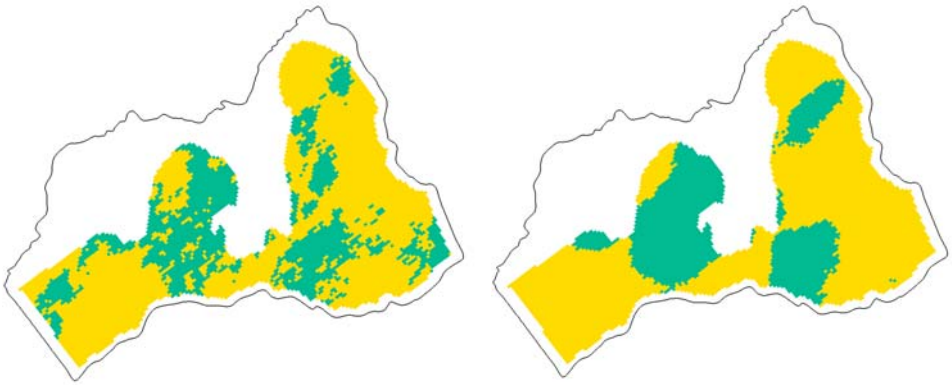

Figure 64: grid layer at the Congaree formation bottom

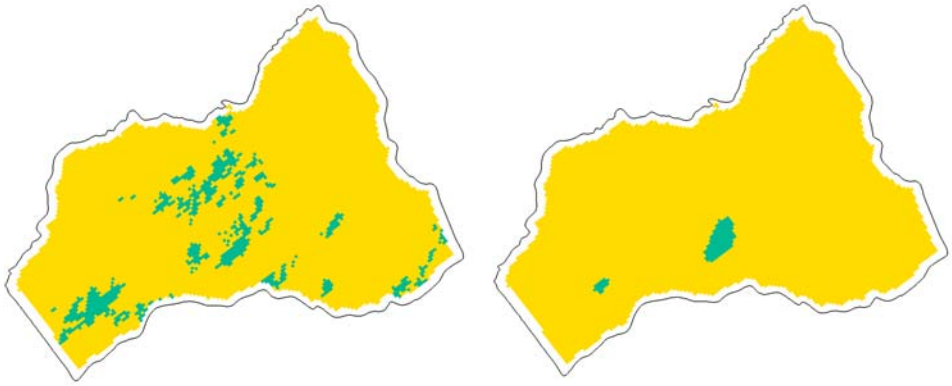

Figure 65: grid layer at the Congaree formation middle

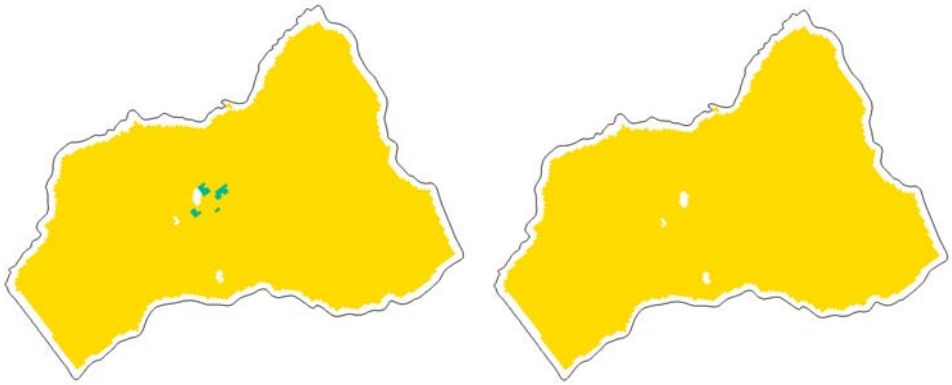

Figure 66: grid layer at the Congaree formation top

Petrophysics well logs analysis

Before creating the simulations, the petrophysical logs (Fig. 67) were upscaled to the resolution of the vertical grid cells by transferring the properties of well type to the grid cells penetrated by a well. This process implies upscaling procedure because the resolution of well log is finer than the grid cell thickness. The penetrated cell value is the average of all the log-scale values within the cell. Once this process was completed, variogram maps and variograms were computed for the petrophysical properties for each facies within each formation.

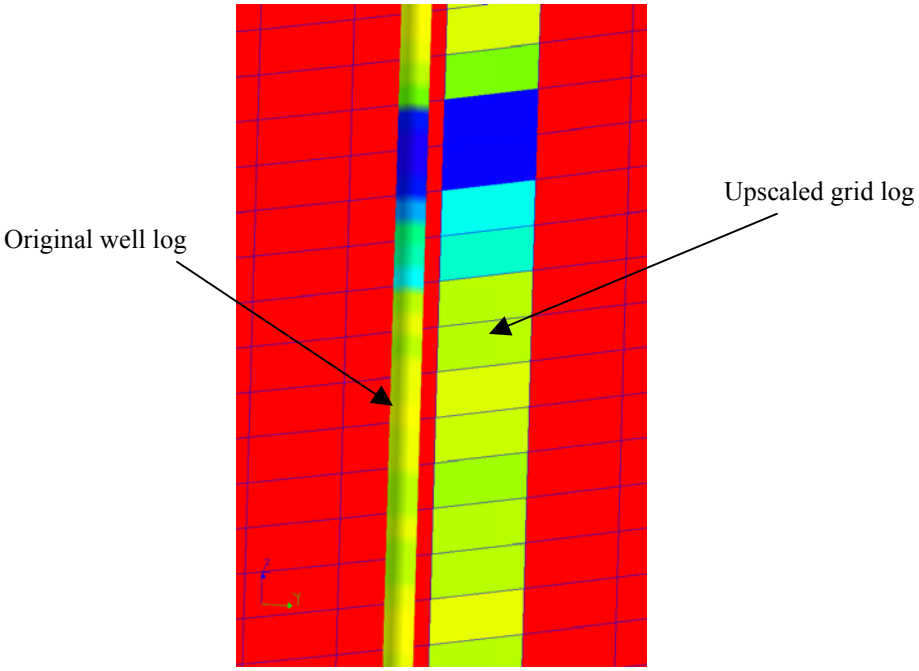

Figure 67: Well log versus upscaled grid log

Upland

- Percent mud in "Fluvial" (variogram map done with 10 layers)
  - Sill = 1
  - Structure = Exponential N135 460m 375m 26ft 0.9, nugget 0.1

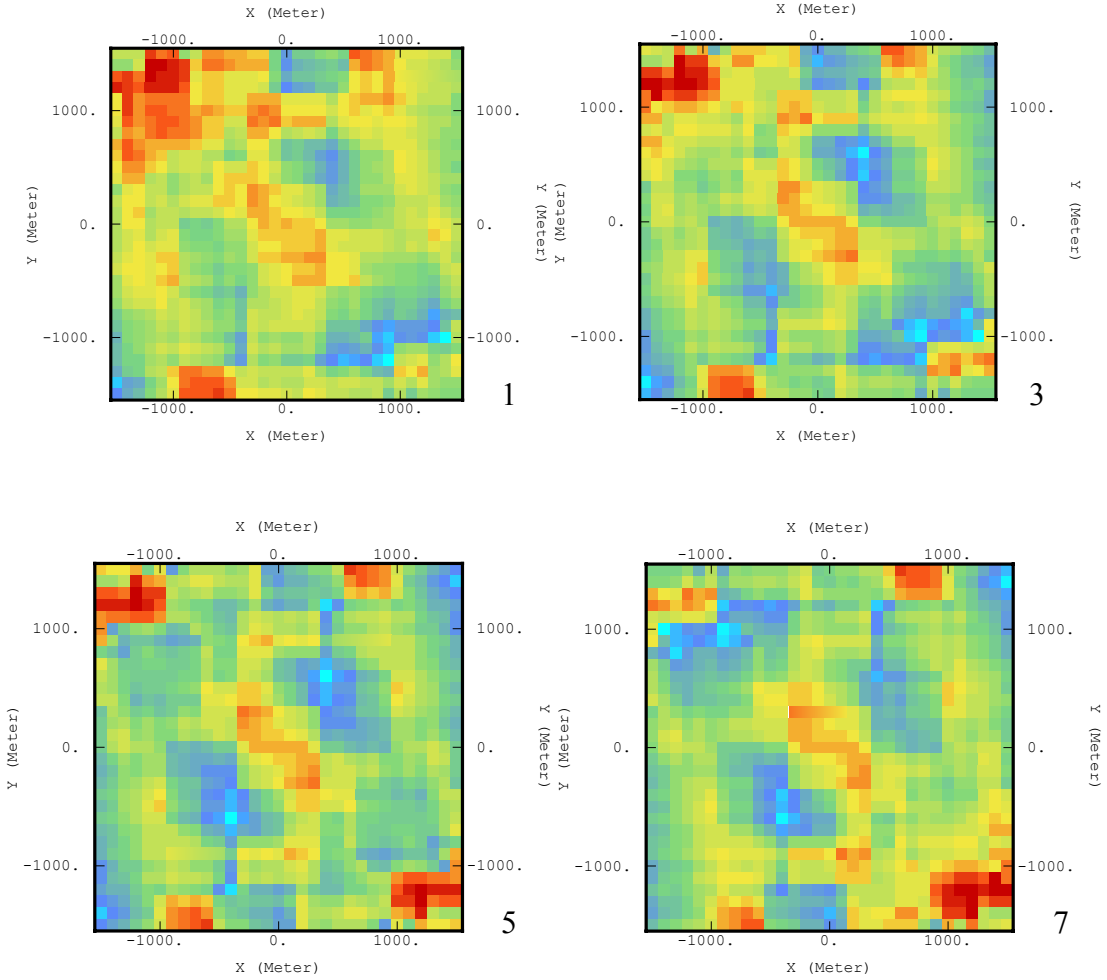

Figure 68: 3D Variogram map of percent mud in "Fluvial" in the Upland

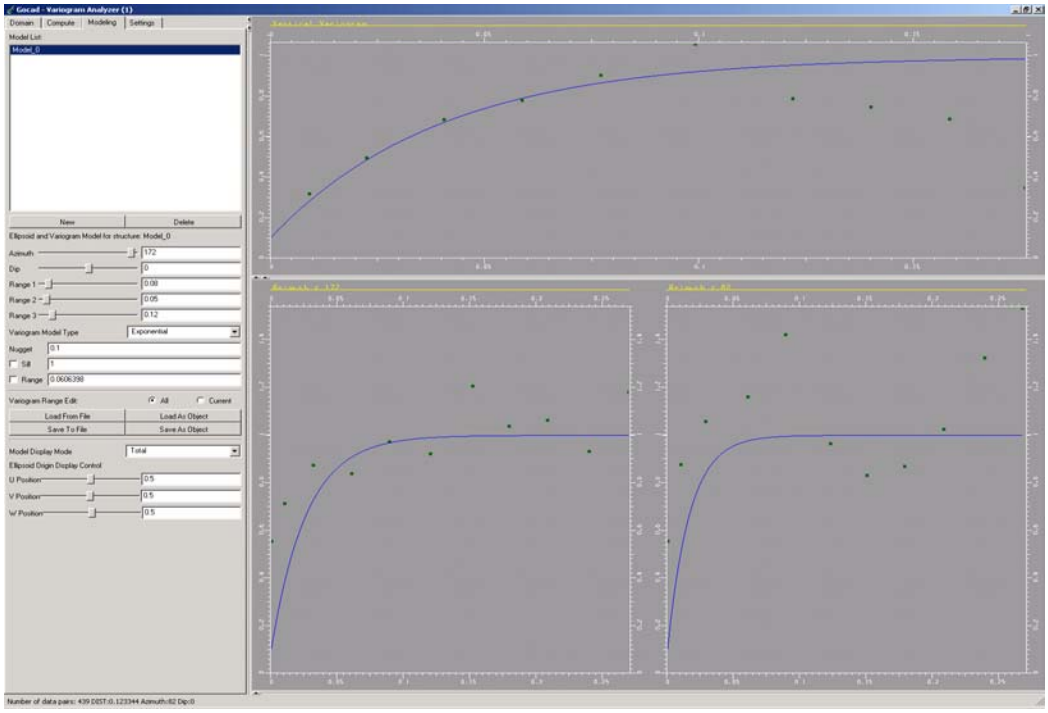

Figure 69: Experimental variogram and its model for percent mud in "Fluvial" (Upland)

- Percent mud in "Floodplain/Overbank Muds" (variogram map done with 10 layers)

  - Sill = 1
  - Structure = Exponential N155 160m 110m 22ft 0.8, nugget 0.2

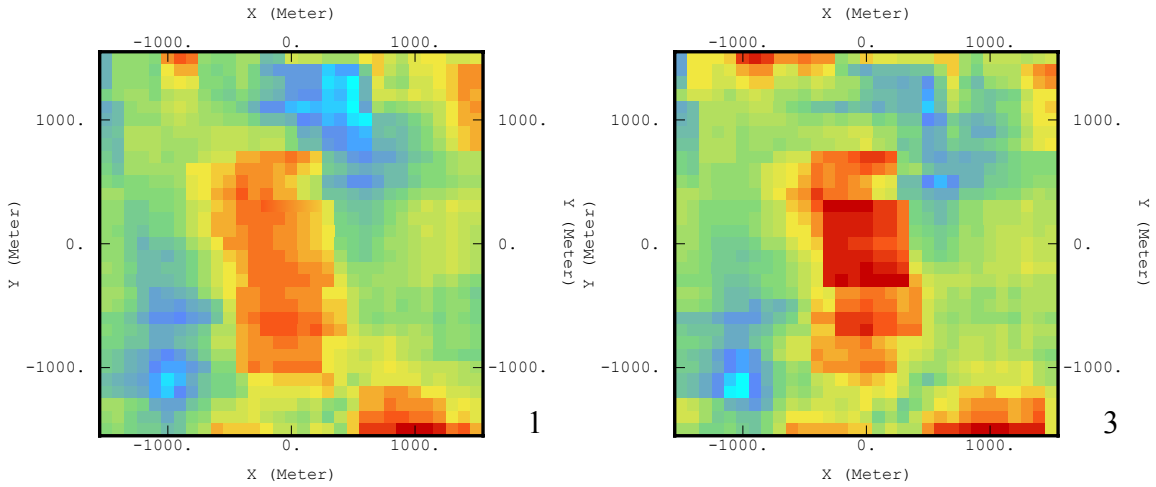

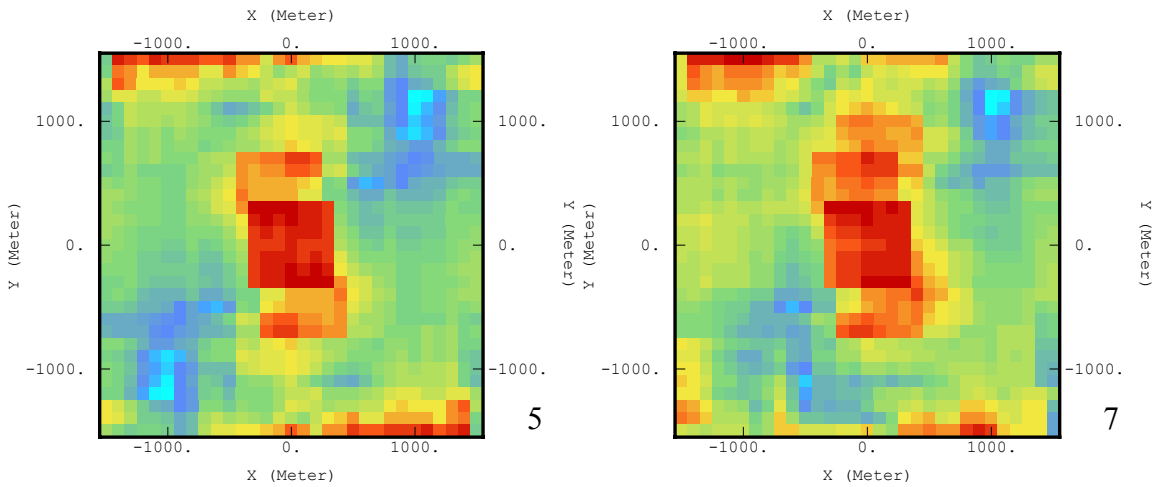

Figure 70: 3D Variogram map of percent mud in "Flood Plain/Overbank Muds" in the Upland

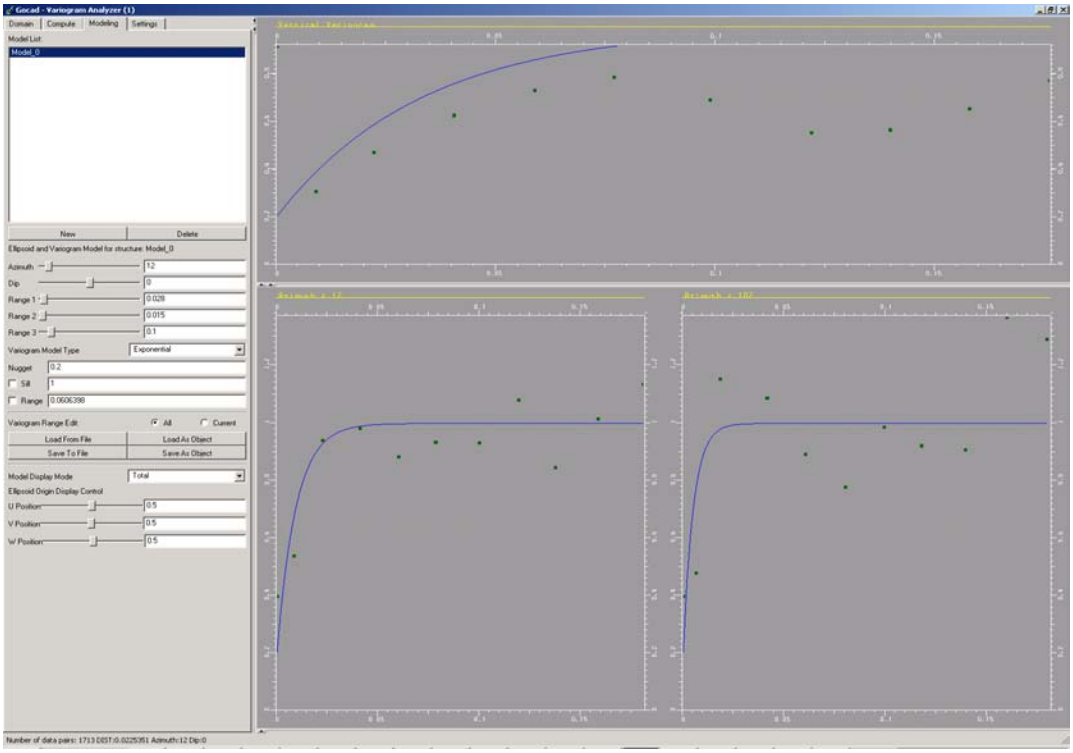

Figure 71: Experimental variogram and its model for percent mud in "Floodplain/Overbank Muds" (Upland)

Barnwell Group

- Percent mud in "Tidal Flat/Lagoonal" (variogram map done with 15 layers)
  - Sill = 1
  - Structures = Exponential N155 58m 75m 7ft 0.3, Exponential N75 145 90 44 0.5, nugget 0.2

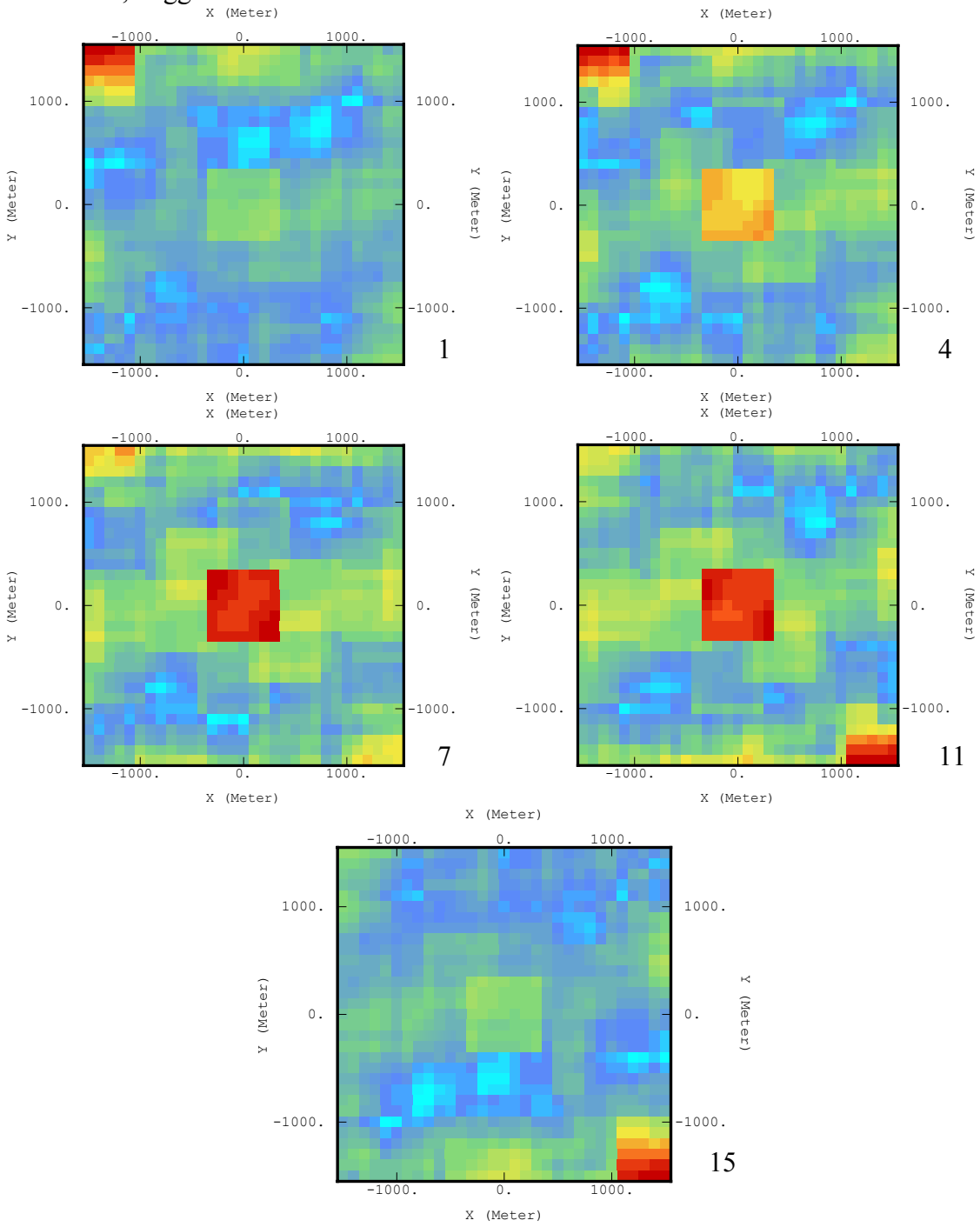

Figure 72: 3D Variogram map of percent mud in "Tidal Flat/Lagoonal" in the Barnwell Group

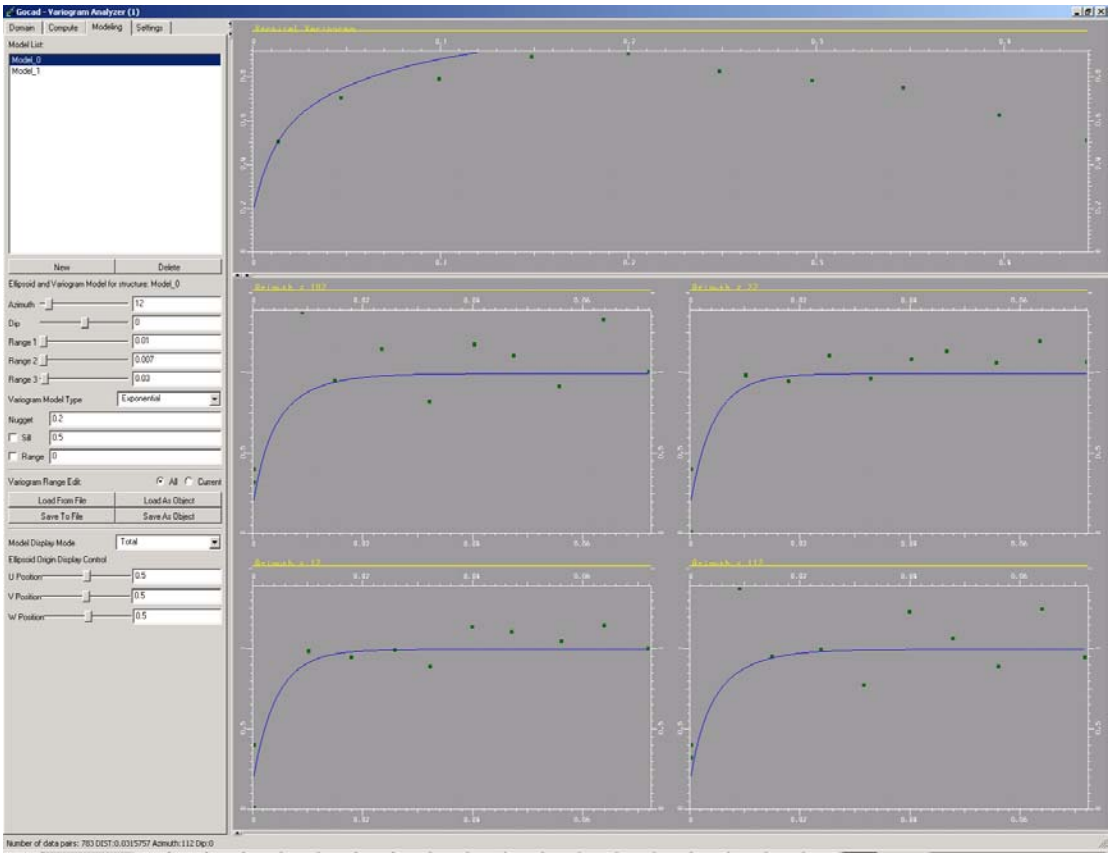

Figure 73: Experimental variogram and its model for percent mud in "Tidal flat/Lagoonal" (Barnwell Group)

- Percent mud in "Barrier Beach" (variogram map done with 15 layers)
  - Sill = 1
  - Structure = Exponential N45 190m 125m 22ft 0.8, nugget 0.2

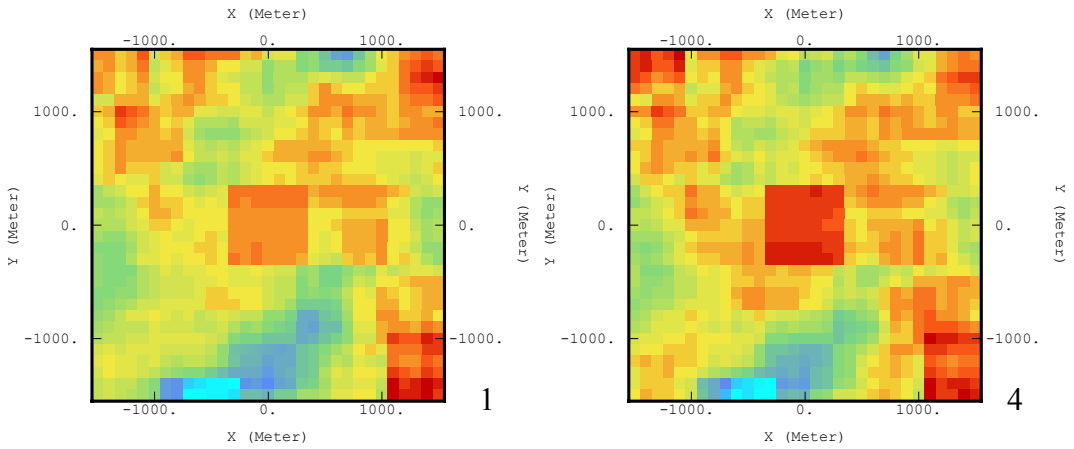

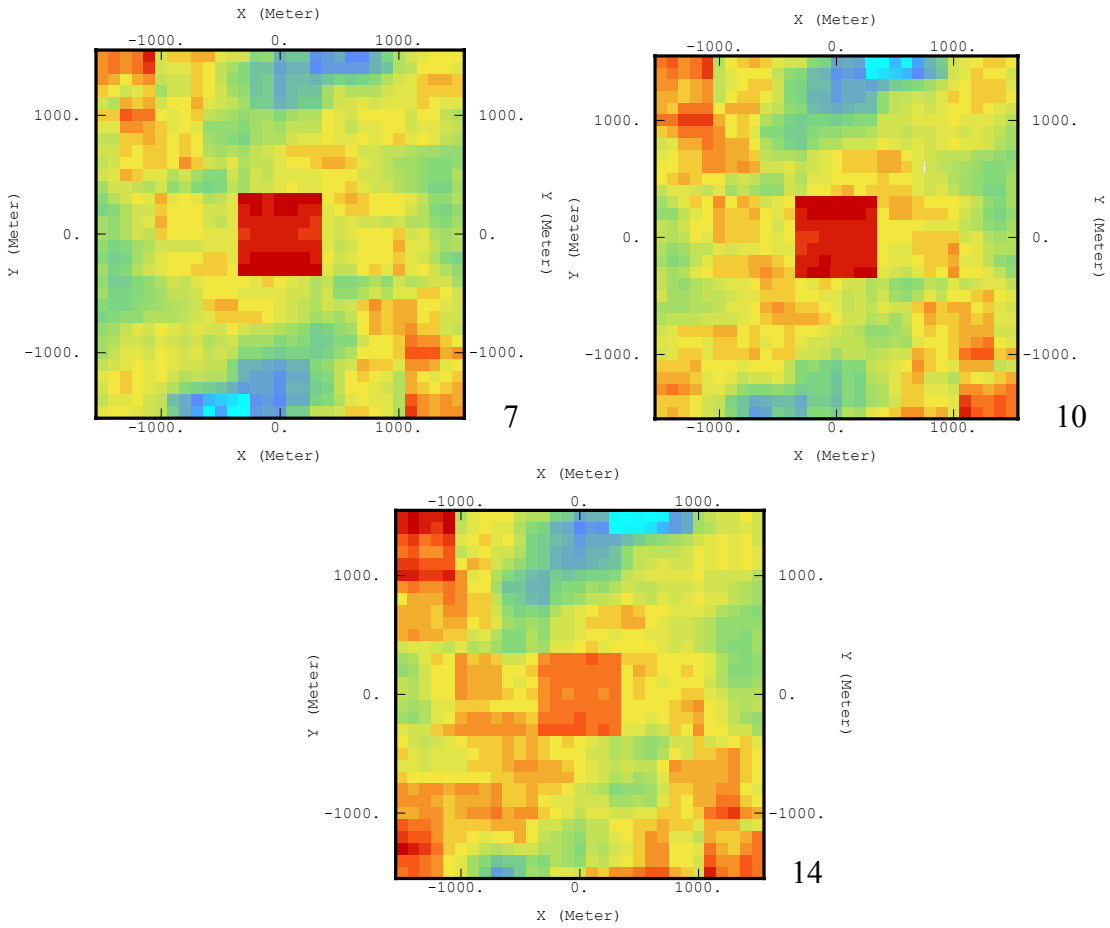

Figure 74: 3D Variogram map of percent mud in "Barrier Beach" in the Barnwell Group

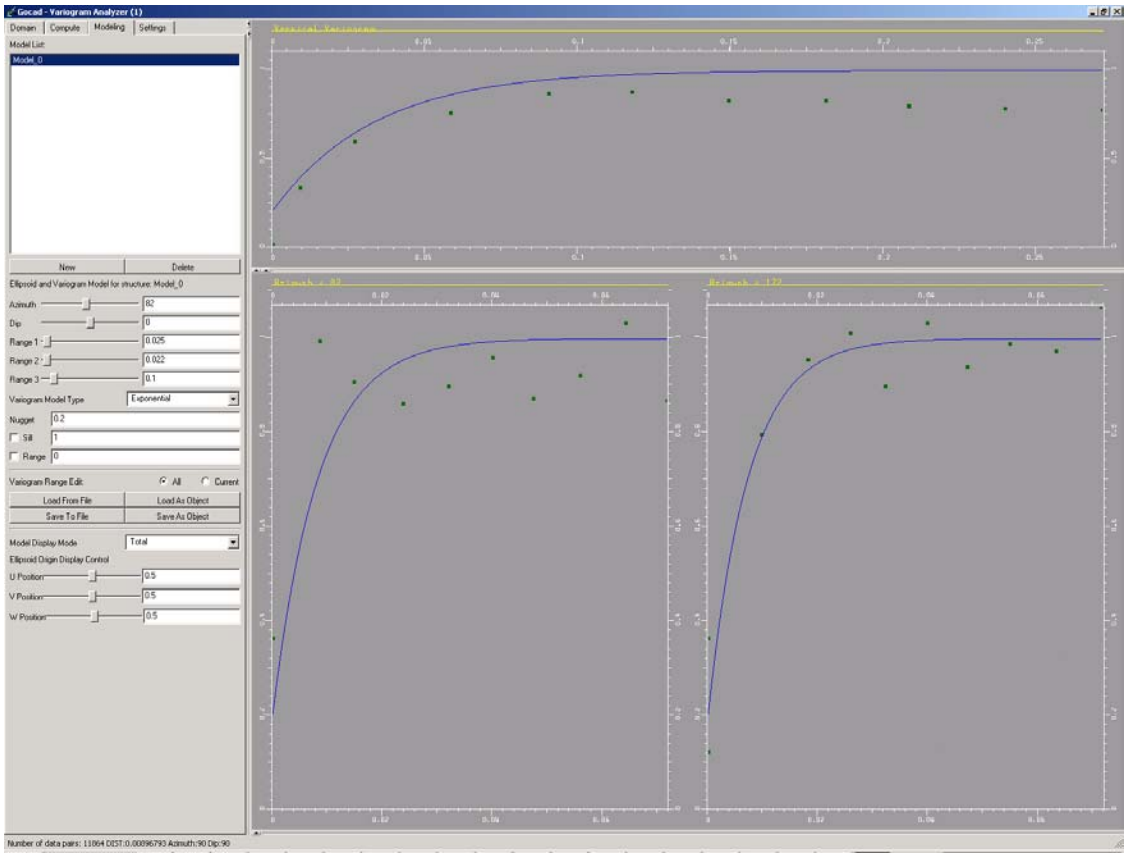

Figure 75: Experimental variogram and its model for percent mud in "Barrier Beach" (Barnwell Group)

Santee

The variogram maps for the Santee were computed using the data already assigned to the grid to increase the computational time, that why some of them could seem odd.

- Percent mud in "Middle Shelf (high energy)" (variogram map done with 1 layers)
  - Sill = 1
  - Structures = Exponential N143 515m 300m 13ft 0.85, nugget 0.15

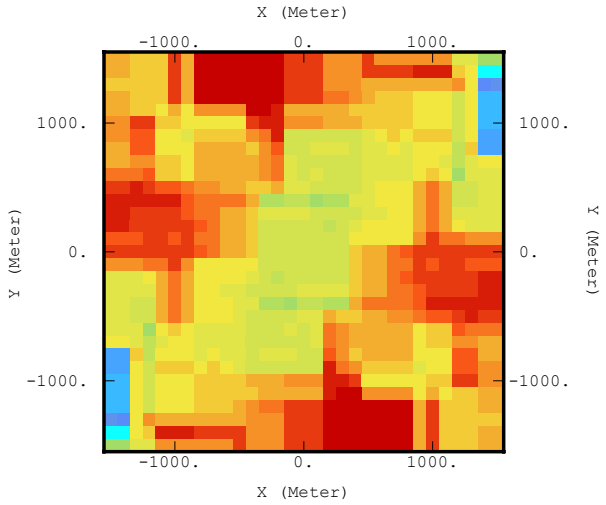

Figure 76: 3D Variogram map of percent mud in "Middle Shelf (high energy)" in the Santee

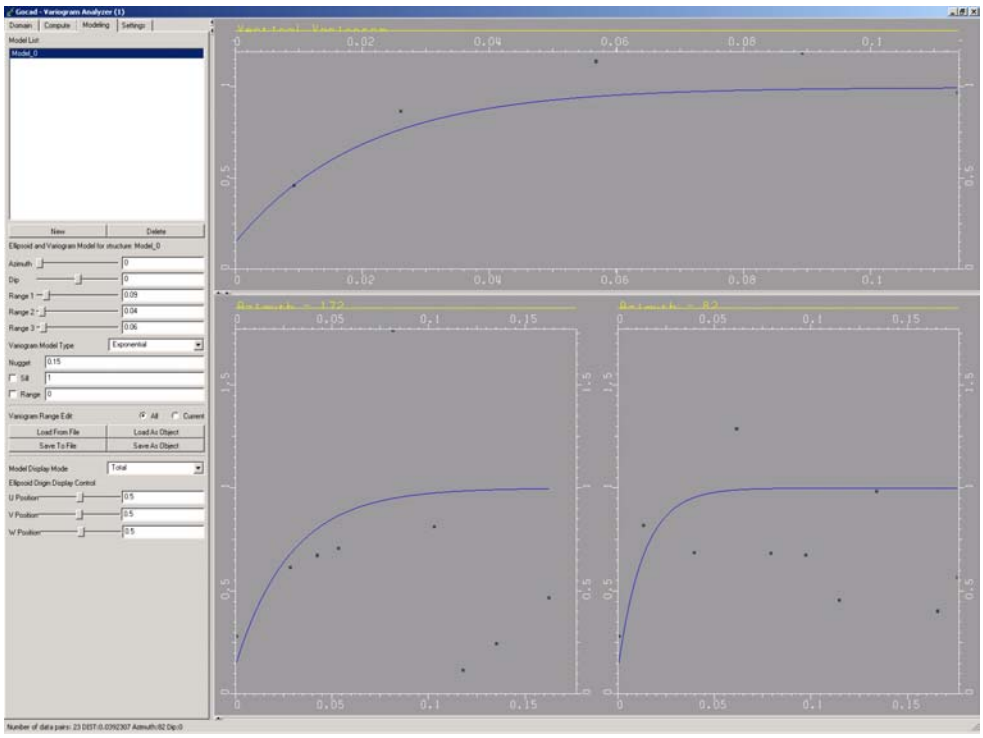

Figure 77: Experimental variogram and its model for percent mud in "Middle Shelf (high energy)" (Santee)

- Percent mud in "Siliciclastic Shelf" (variogram map done with 1 layers)
  - Sill = 1
  - Structures = Exponential N135 630m 525m 26ft 0.7, nugget 0.3

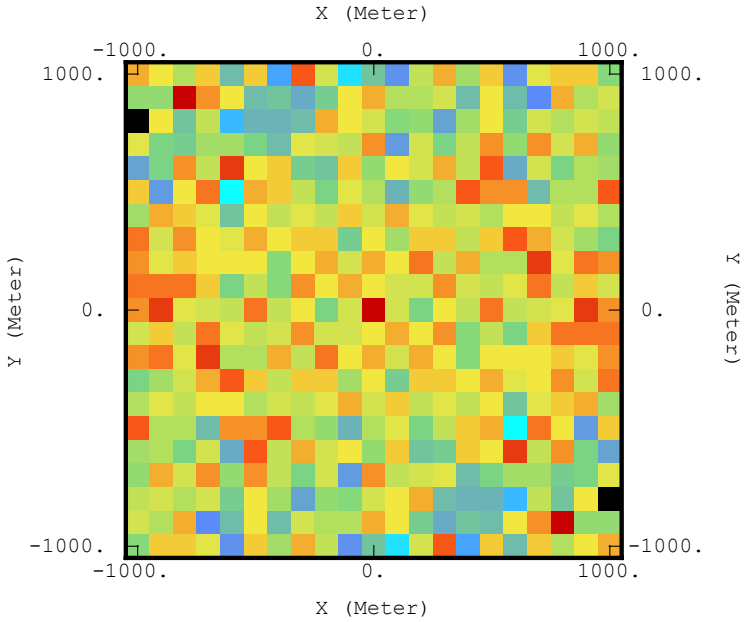

Figure 78: 3D Variogram map of percent mud in "Siliciclastic Shelf" in the Santee

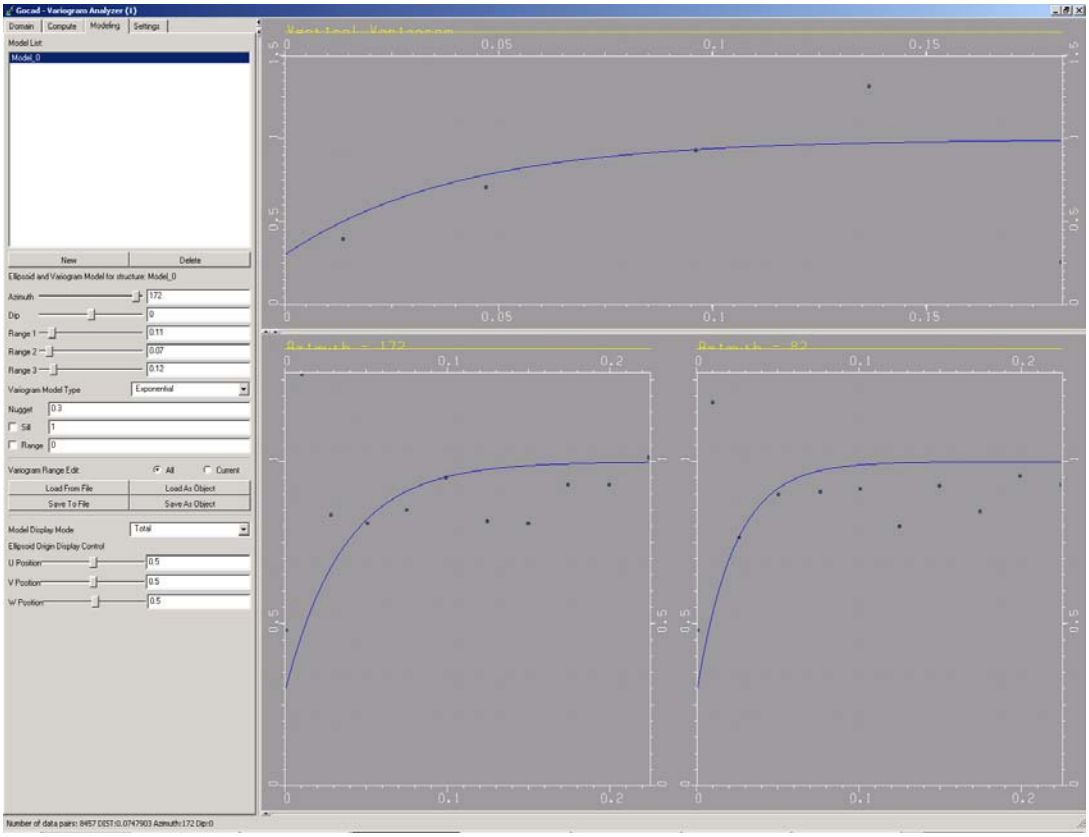

Figure 79: Experimental variogram and its model for percent mud in "Siliciclastic Shelf" (Santee)

- Percent mud in "Middle shelf (low energy)" (variogram map done with 1 layers)
  - Sill = 1
  - Structures = Exponential N135 400m 225m 26ft 0.8, nugget 0.2

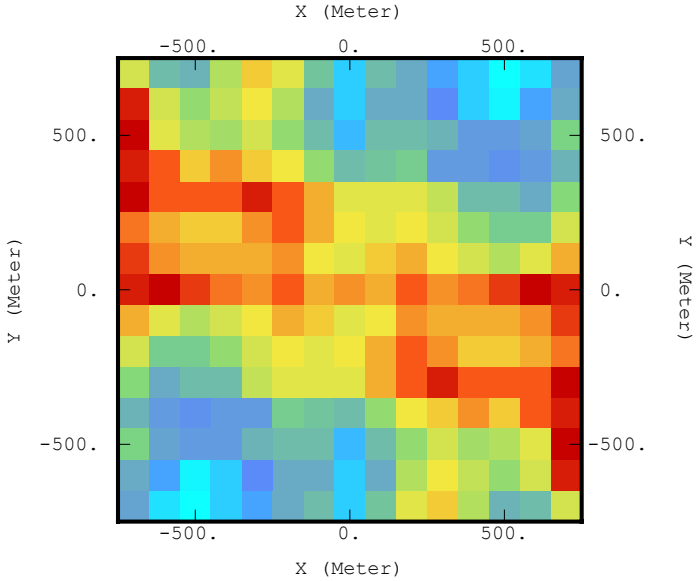

Figure 80: 3D Variogram map of %mud in "Middle Shelf (low energy)" in the Santee

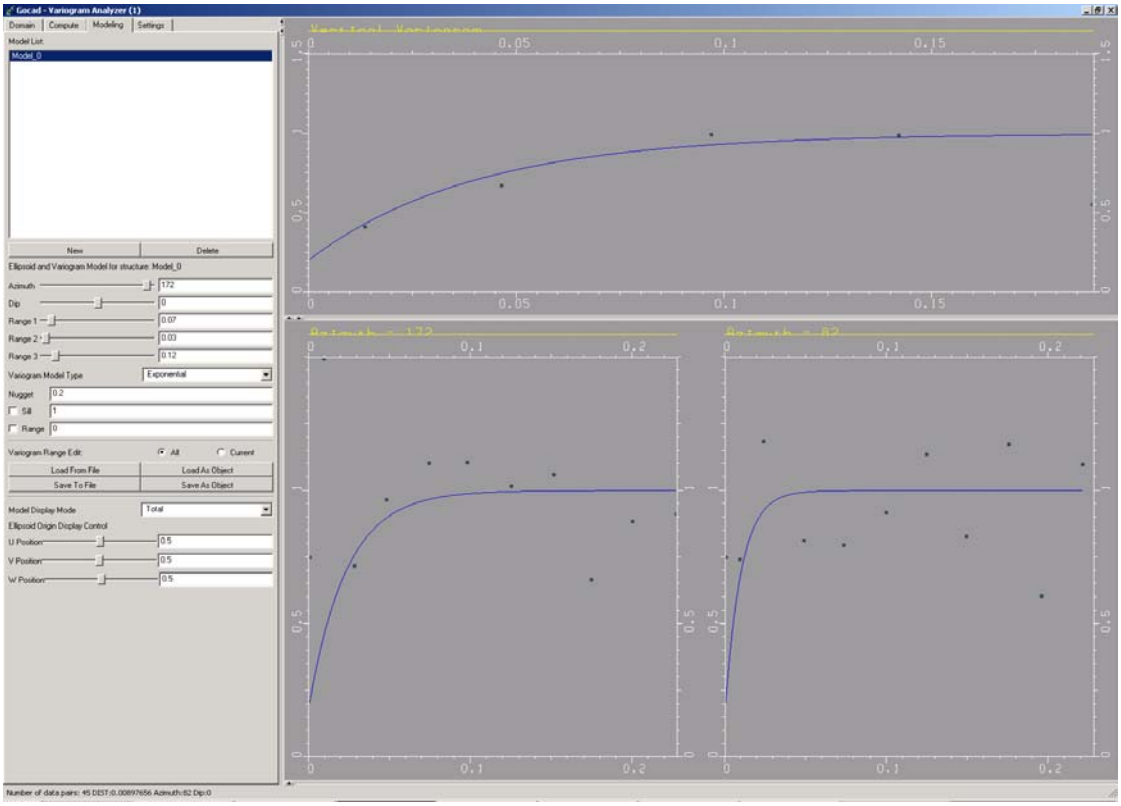

Figure 81: Experimental variogram and its model for percent mud in "Middle shelf (low energy)" (Santee)

- Percent mud in "Open/Outer Shelf" (variogram map done with 1 layers)

- Sill = 1
- Structures = Exponential N135 400m 225m 4ft 0.8, nugget 0.2

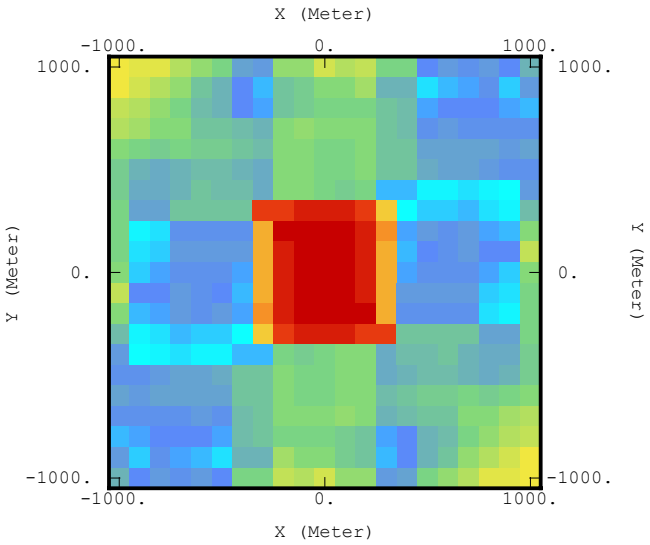

Figure 82: 3D Variogram map of percent mud in "Open/Outer Shelf" in the Santee

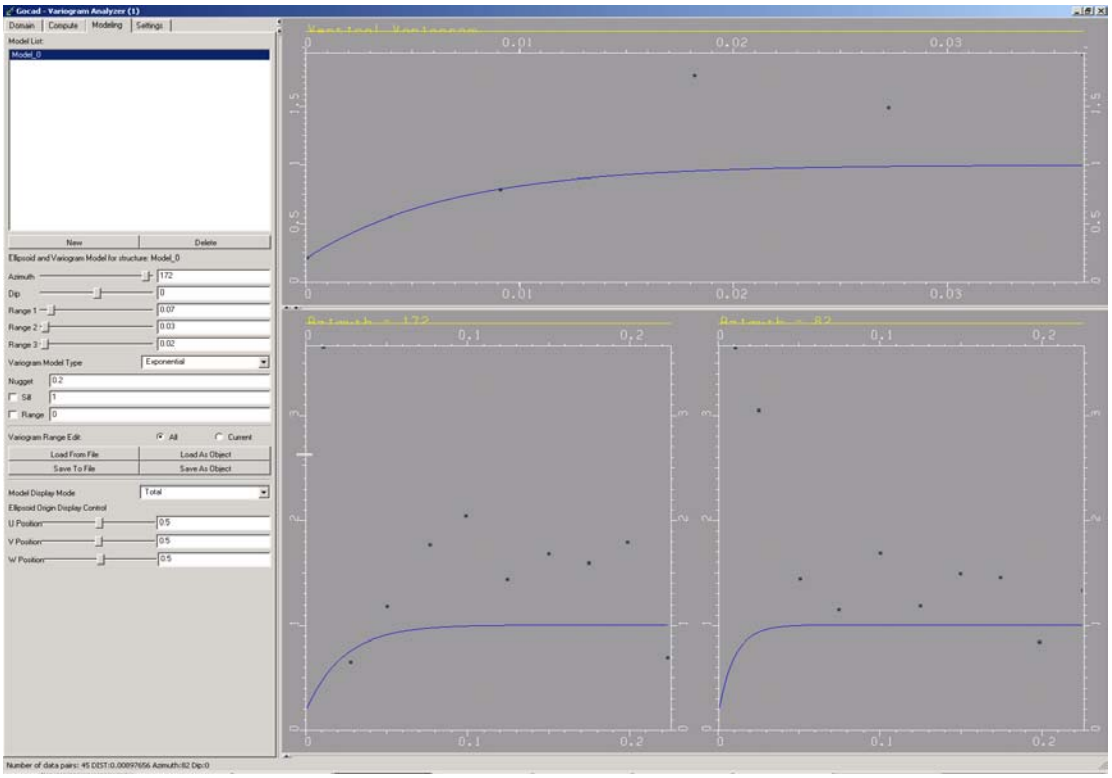

Figure 83: Experimental variogram and its model for percent mud in "Open/Outer shelf" (Barnwell Group)

Green Clay

- Percent mud (variogram map done with 1 layers)
  - Sill = 1
  - Structures = Exponential N55 380m 295m 6.5ft 0.8, nugget 0.2

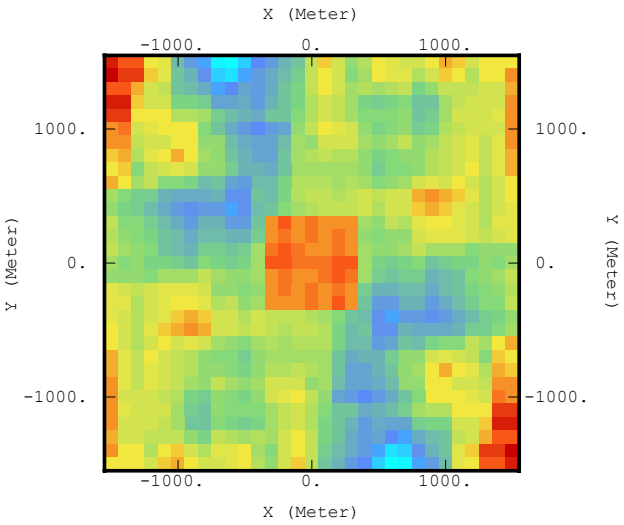

Figure 84: 3D Variogram map of percent mud in the Green CLay

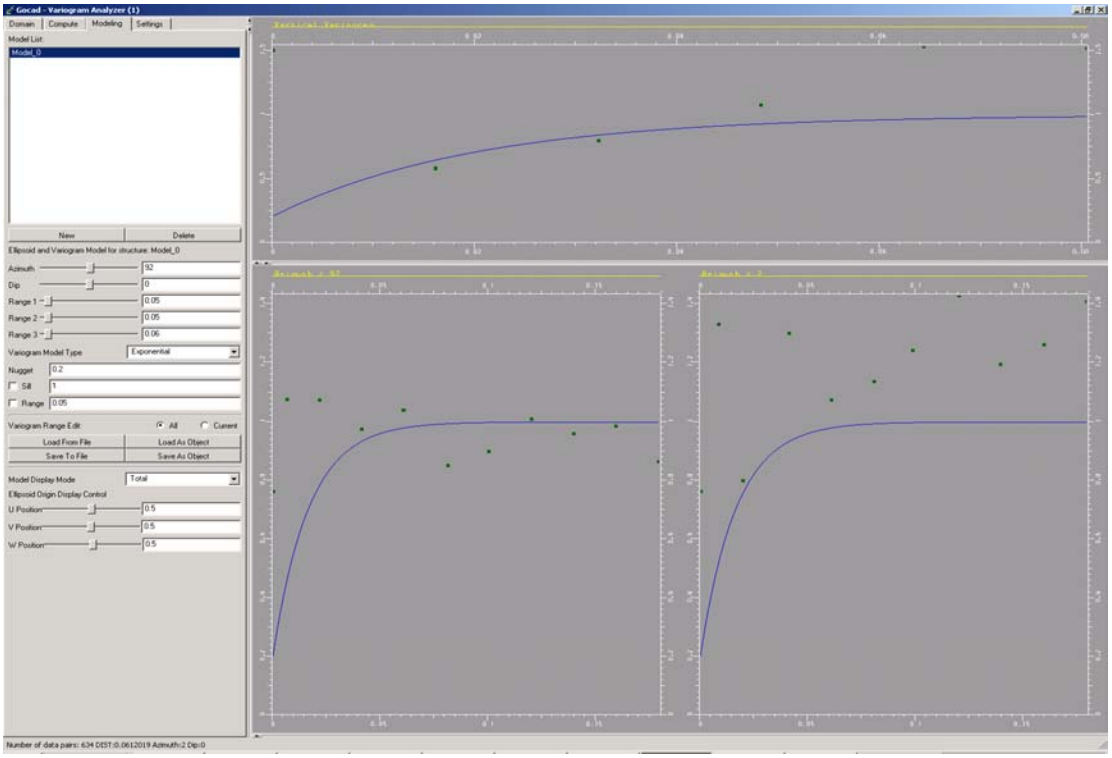

Figure 85: Experimental variogram and its model for percent mud in the Green Clay

Congaree

- Percent mud in "Innerbay/Lagoonal" (variogram map done with 15 layers)
  - Sill = 1
  - Structures = Exponential N0 650m 600m 12ft 0.8, nugget 0.2

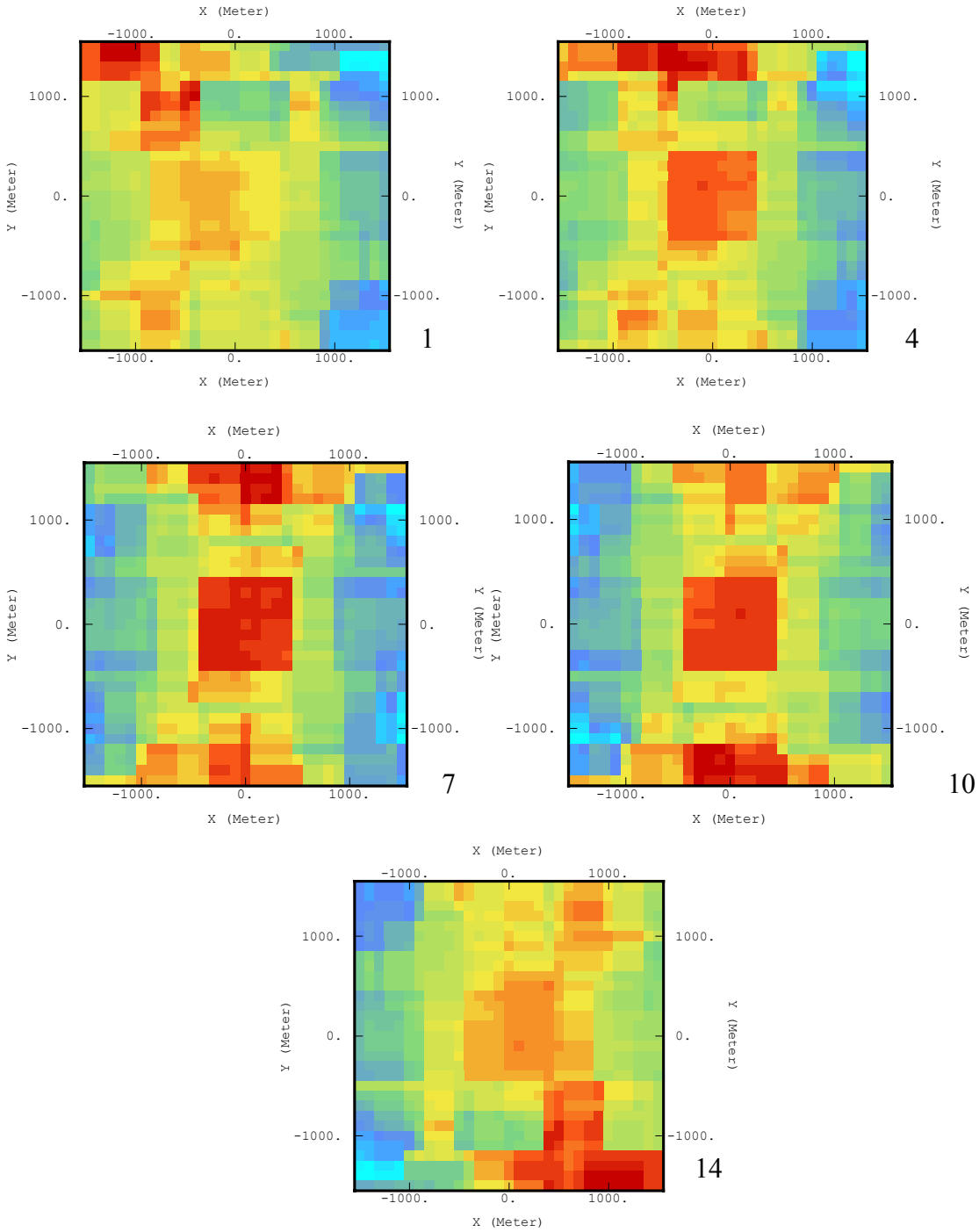

Figure 86: 3D Variogram map of percent mud in "Inner Bay/Lagoonal" in the Congaree

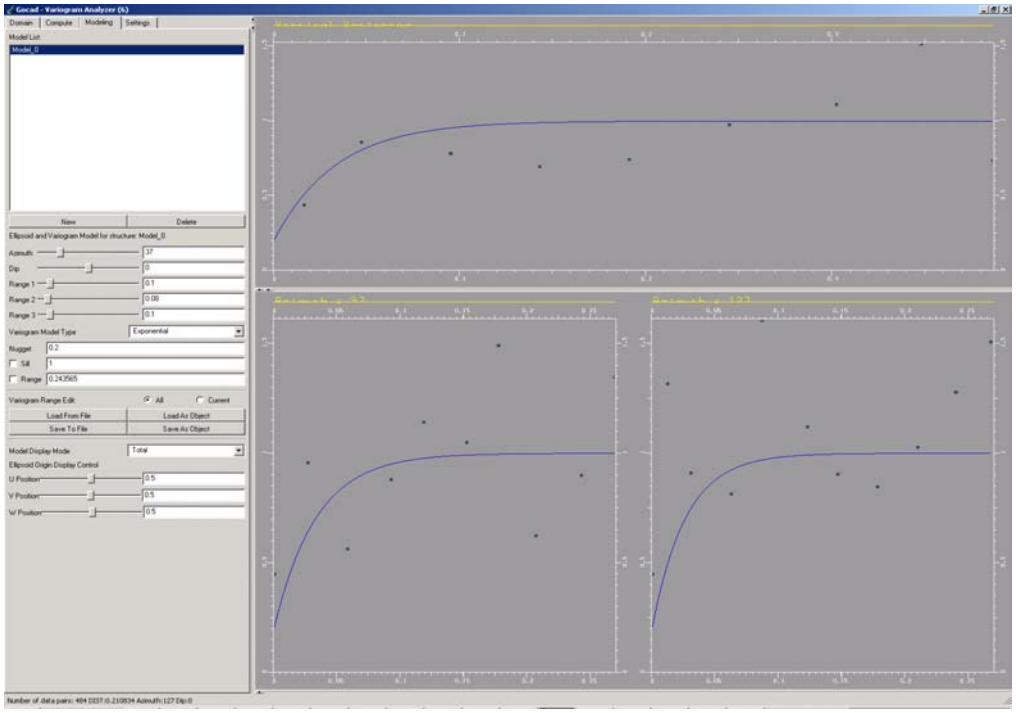

Figure 87: Experimental variogram and its model for percent mud in "Innerbay/Lagoonal" (Congaree)

- Percent mud in "Lower shoreface" (variogram map done with 15 layers)
  - Sill = 1
  - Structures = Exponential N135 235m 230m 14ft 0.75, N135 4200m 3700m 12.5ft 0.25

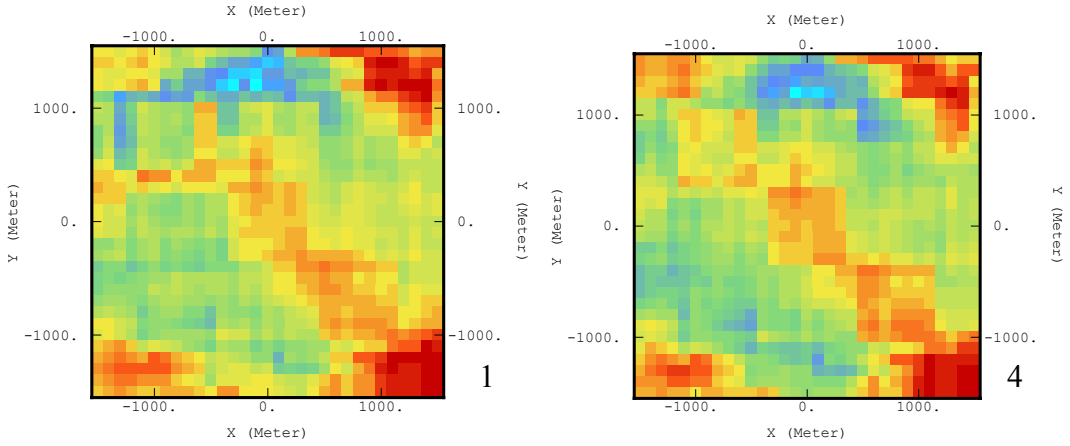

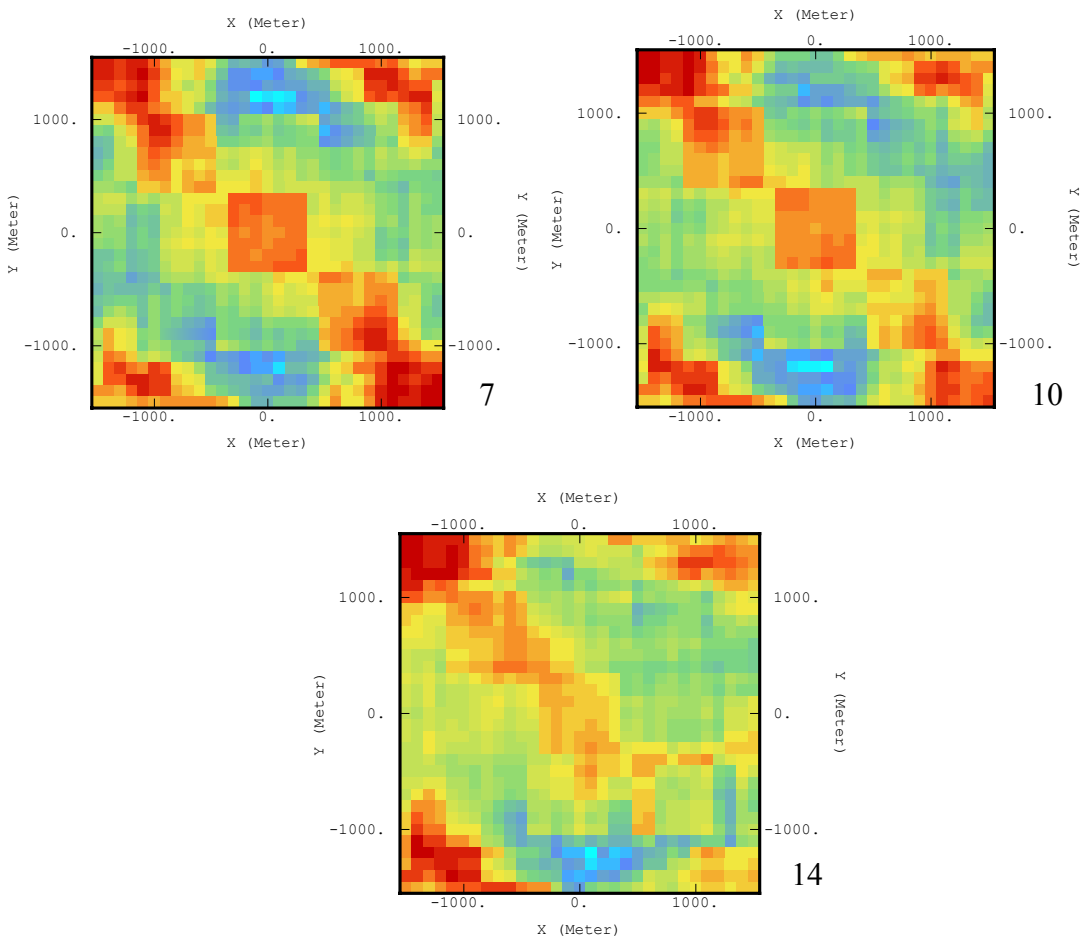

Figure 88: 3D Variogram map of percent mud in "Lower Shoreface" in the Congaree

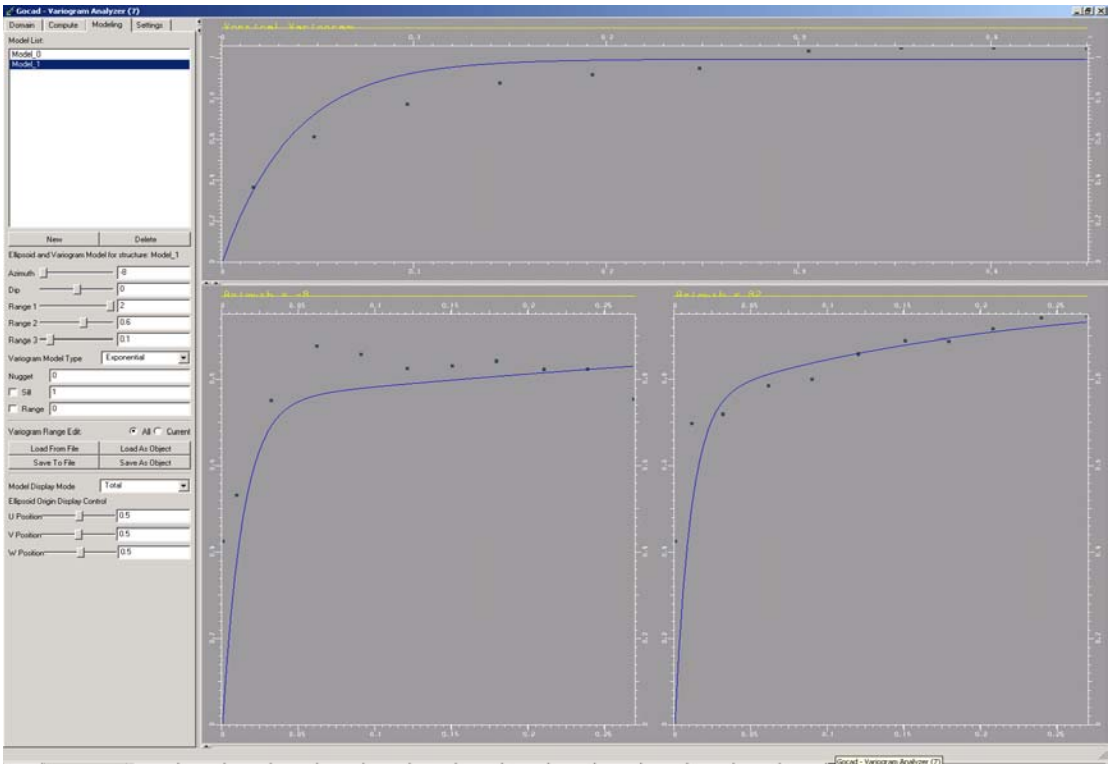

Figure 89: Experimental variogram and its model for percent mud in "Lower Shoreface" (Congaree)

Sequential Gaussian Simulations of Percent mud in the different facies of each formation with post-processing

Upland

- *Percent Mud modeling*

Corresponding depositional facies map (most common facies per cell map) for the maps shown below

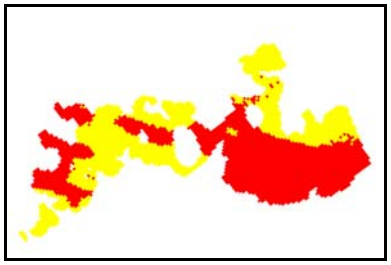

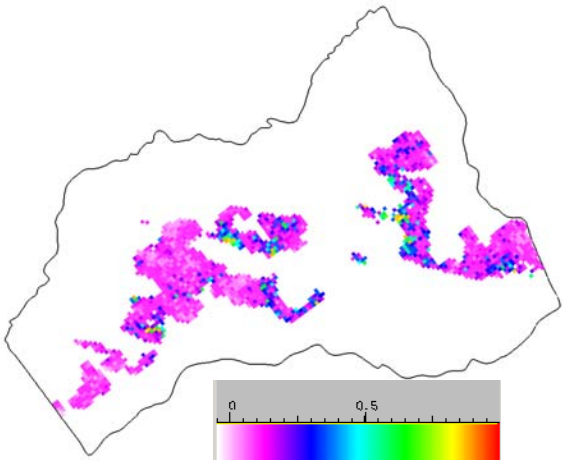

one SGS in "Fluvial" depositional facies

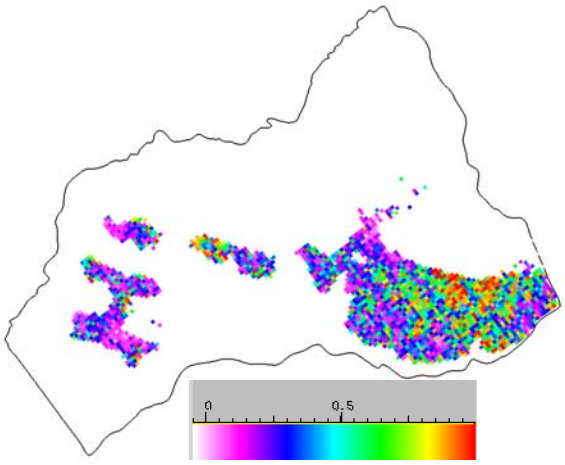

one SGS in "Floodplain/Overbank muds" depositional facies

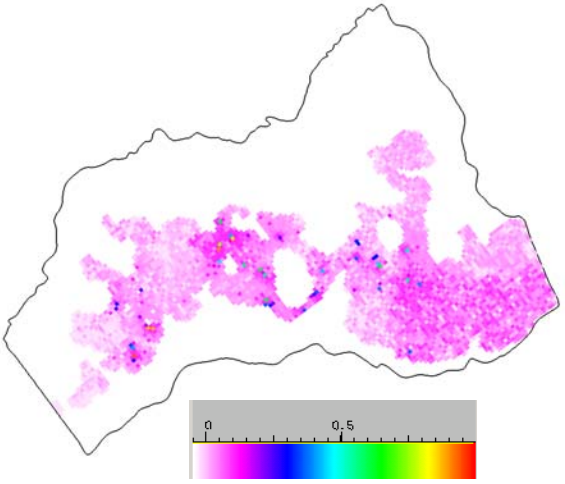

Minimum value per cell of the 200 SGS in both facies

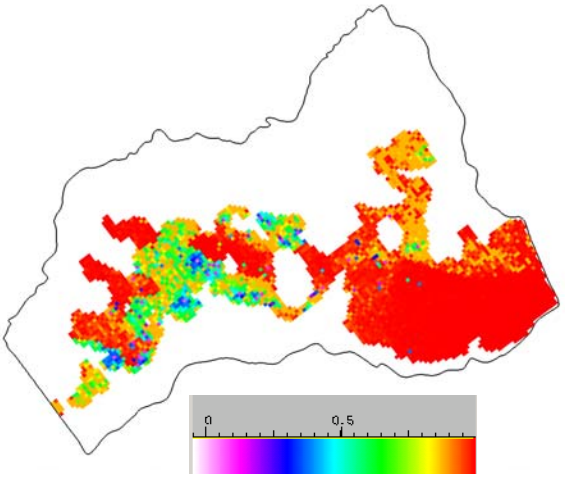

Maximum per cell

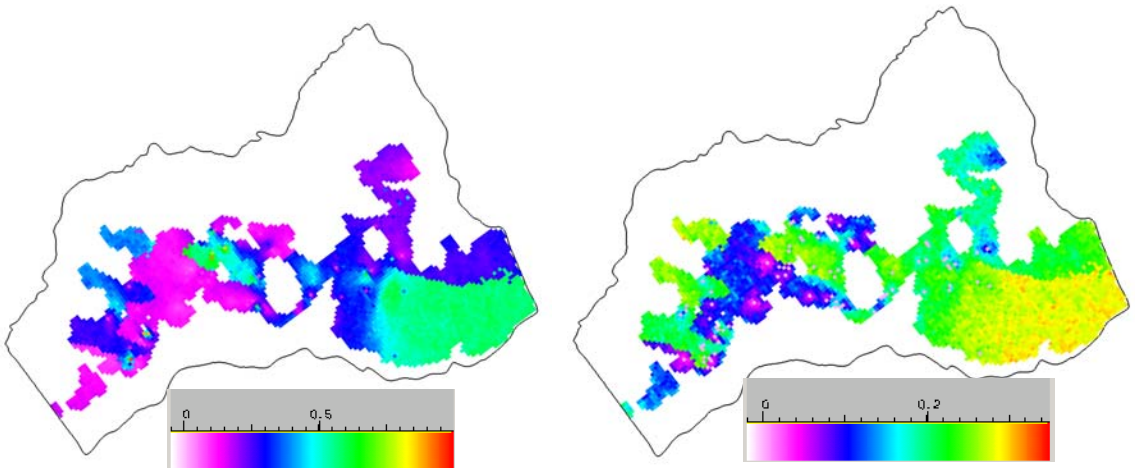

Mean per cell

Standard deviation per cell

Figure 90: %mud modeling in the Upland

- *CPT Friction Ratio modeling*

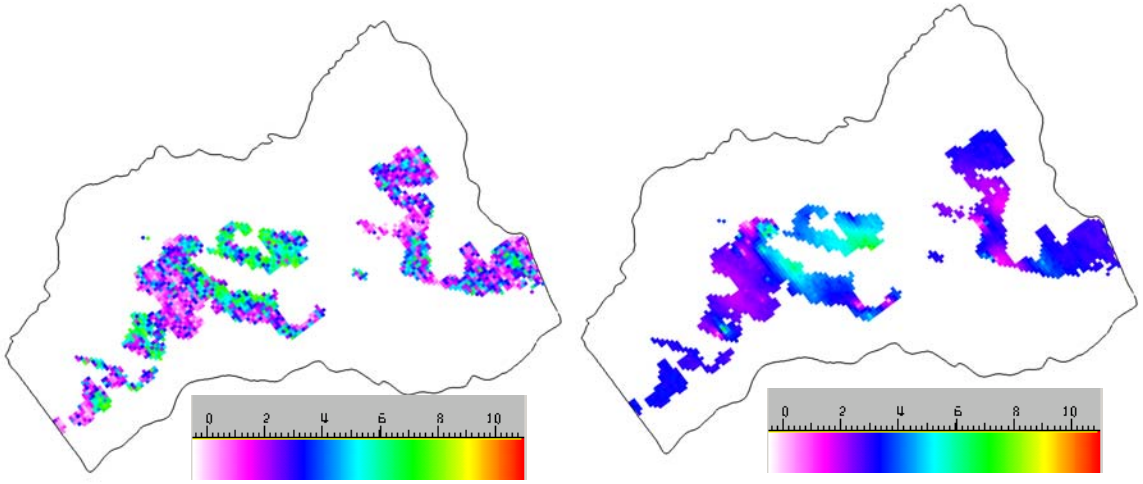

a simulation of Friction Ratio in "Fluvial" depositional facies

mean of friction ratio in "Fluvial" depositional facies

Figure 91: Friction Ratio modeling in the Upland

The mean value calculated for each cell from the 200 SGS of Percent mud was cross-plotted against the Friction Ratio logs at the Friction Ratio logs location. The cross-plot was made separately in each modeled facies (Figures 92 & 93). The correlation coefficient in the "Fluvial" facies was greater than 0.2. As described in the workflow, the Friction Ratio was modeled so that percent mud can be remodeled for that particular facies using collocated cosimulation where the hard data = Percent mud data, and the soft data = mean value of friction ratio calculated in a cell from the 200 SGS.

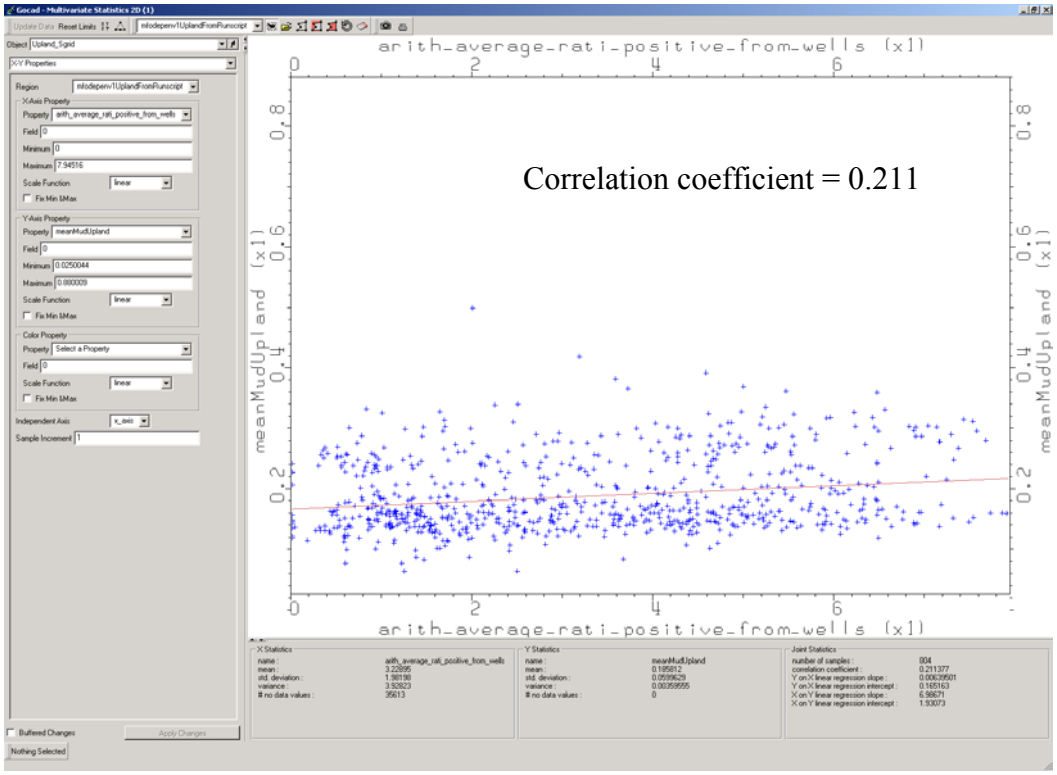

Figure 92: Cross-plot of the mean per cell of percent mud against Friction Ratio from well logs at the logs location for the facies "Fluvial" in the Upland

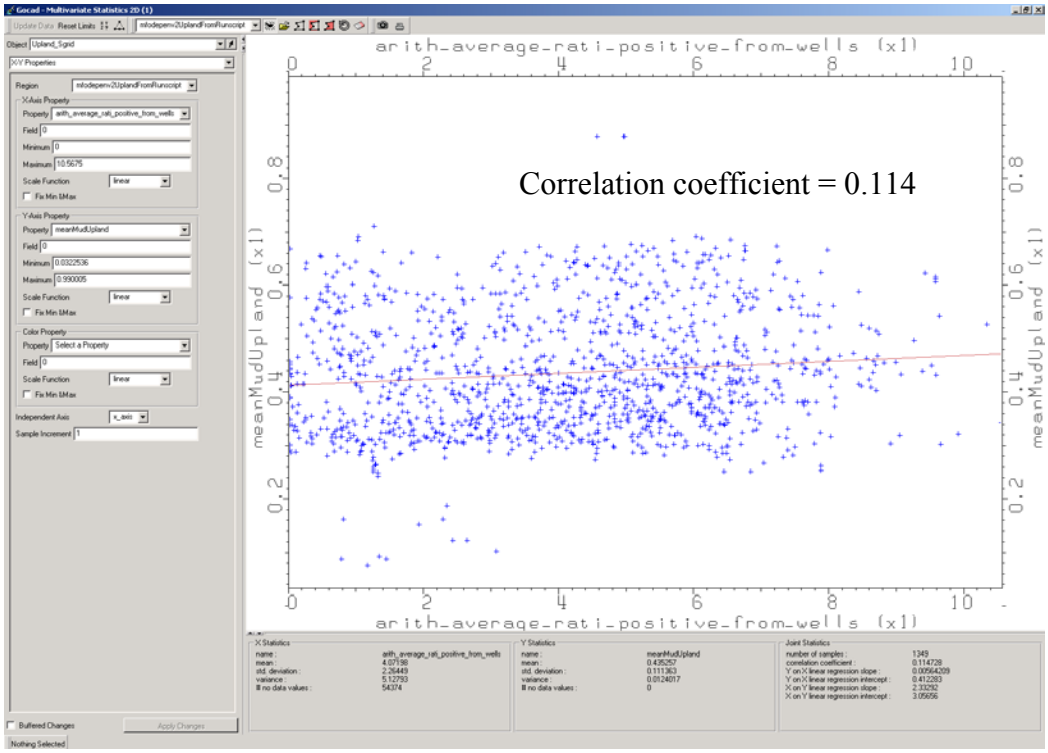

Figure 93: Cross-plot of the mean per cell of percent mud against Friction Ratio from well logs at the logs location for the facies "Floodplain/Overbank Muds" in the Upland

- *Percent Mud modeling using CPT Friction Ratio modeling*

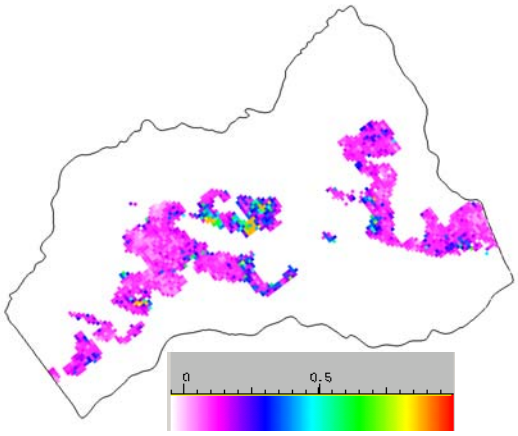

collocated cosimulation of %mud with the mean per cell of friction ratio in "Fluvial"

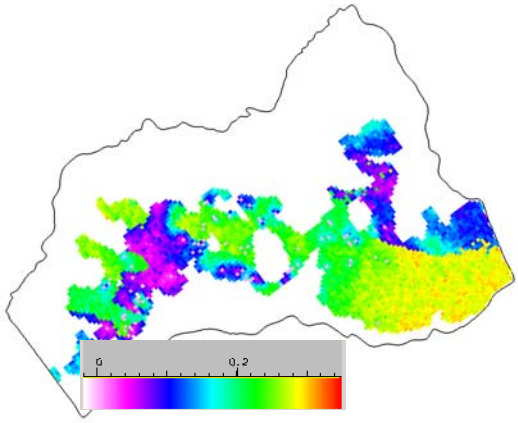

standard deviation of %mud in all the facies (in "Fluvial" the result is from collocated cosimulation)

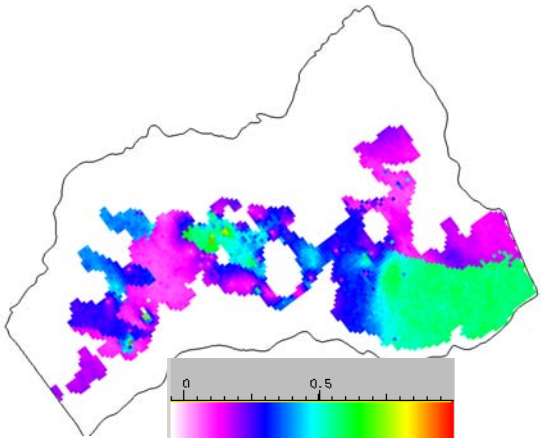

mean per cell of %mud in all the facies (in "Fluvial" the result is from collocated cosimulation)

Figure 94: Percent mud modeling in the Upland using Friction Ratio

Barnwell Group

- *Percent Mud modeling*

Corresponding deposional facies map (most common facies per cell map) for the maps shown below

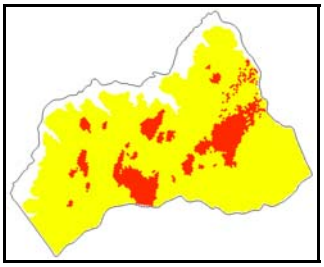

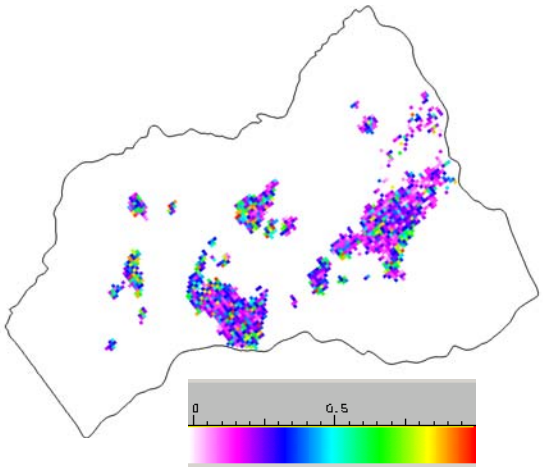

one SGS in "Tidal Flat Lagoonal" depositional facies

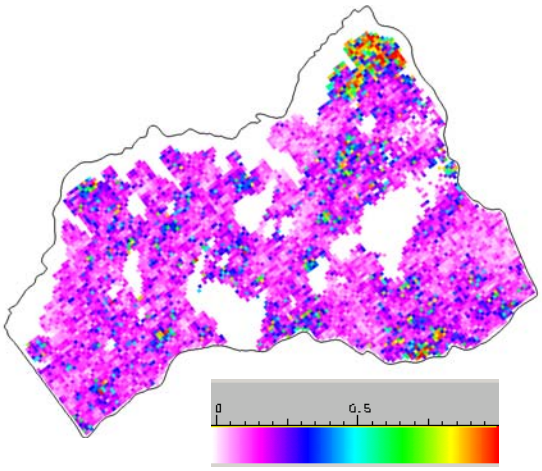

one SGS in "Barrier Beach" depositional facies

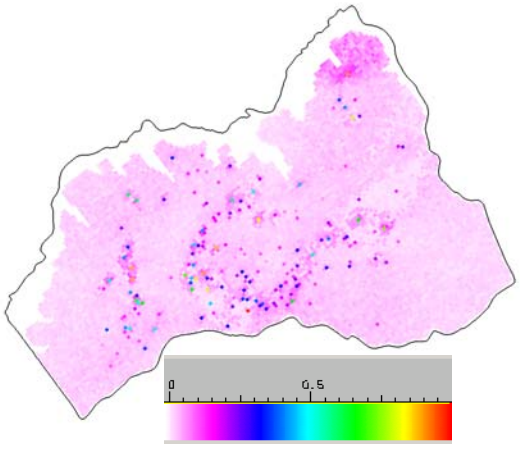

Minimum value per cell of the 200 SGS in both facies

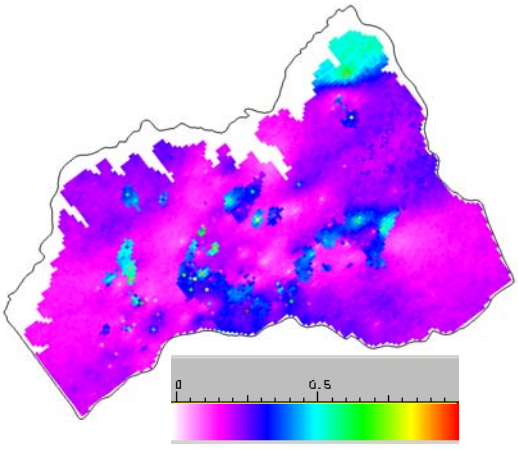

Mean per cell

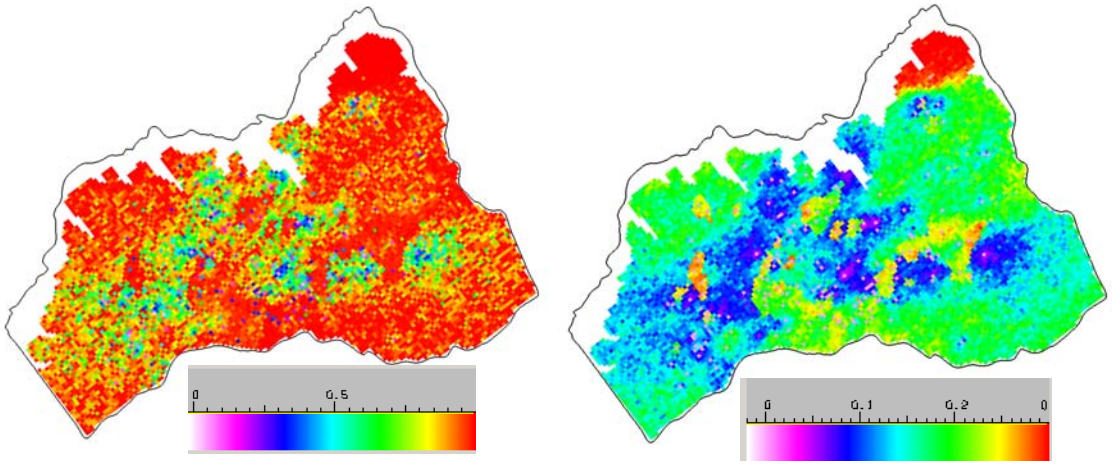

Figure 95: Percent mud modeling in the Barnwell Group

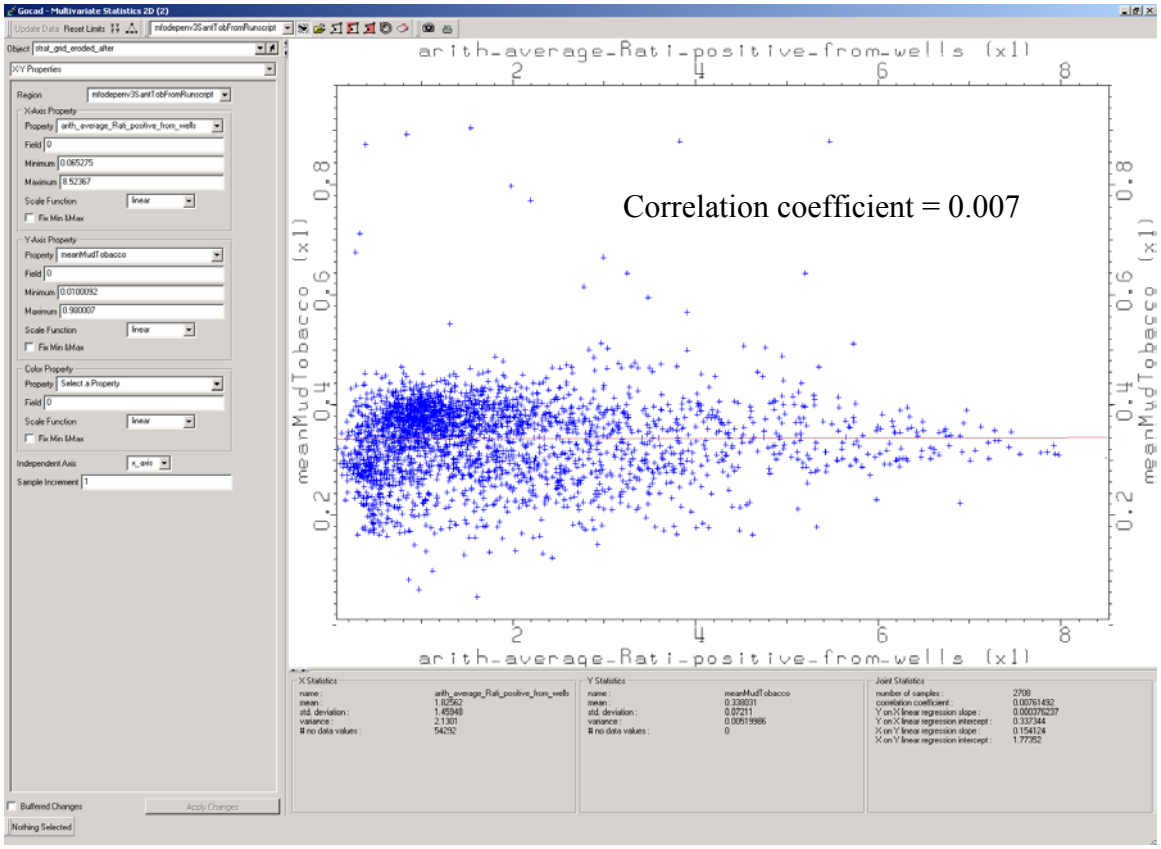

Figure 96: Cross-plot of the mean per cell of percent mud against Friction Ratio from well logs at the logs location for the "Tidal Flat/Lagoonal" facies in the Barnwell Group

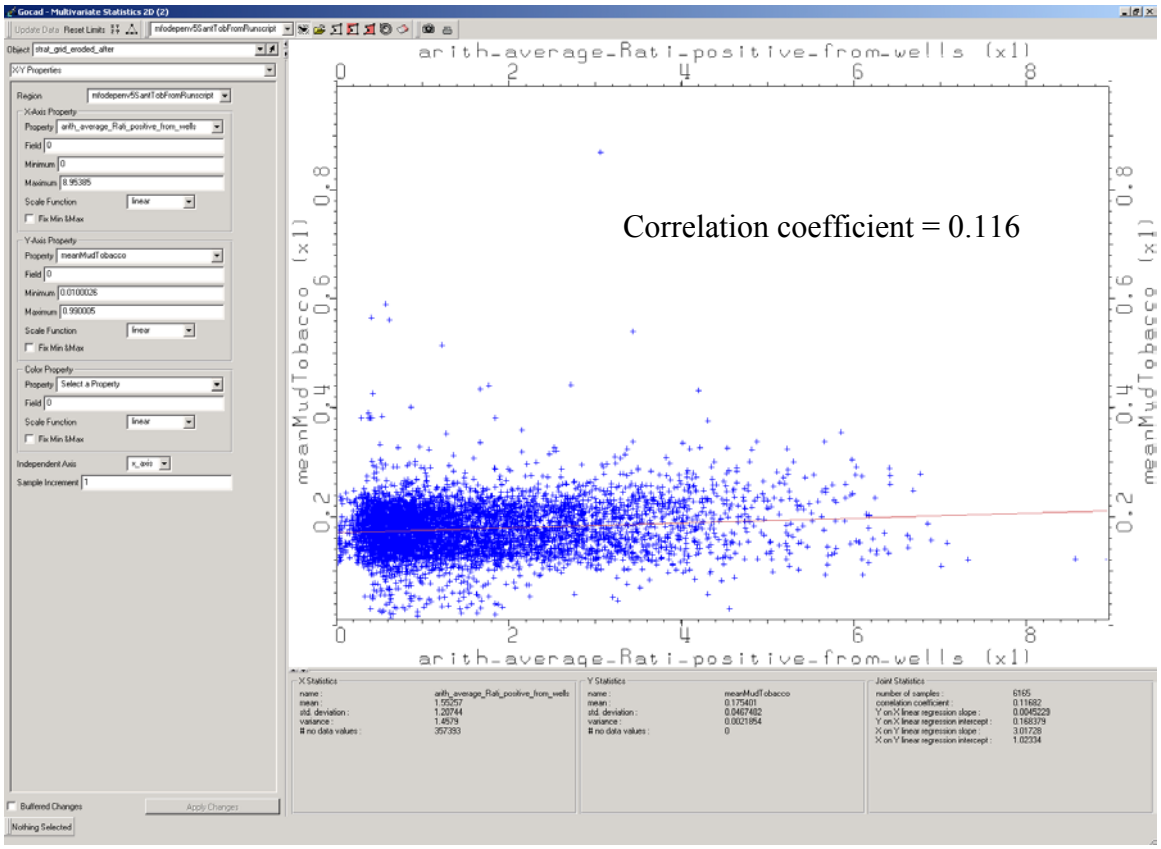

Figure 97: Cross-plot of the mean per cell of percent mud against Friction Ratio from well logs at the logs location for the "Barrier Beach" facies in the Barnwell Group

Santee

- *Percent Mud modeling*

Corresponding deposional facies map (most common facies per cell map) for the maps shown below

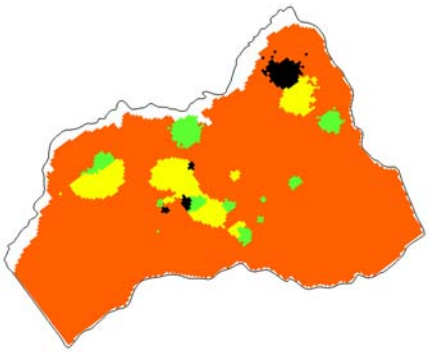

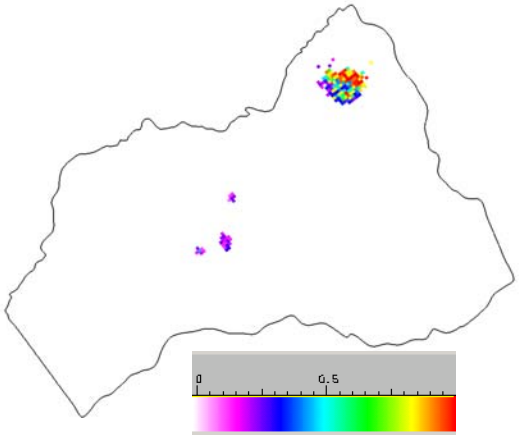

one SGS in "Middle Shelf (high energy)" depositional facies

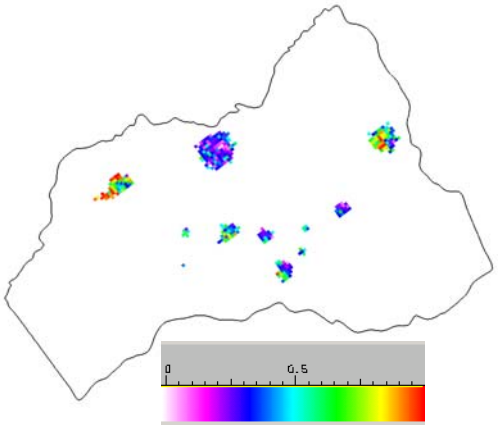

one SGS in "Open/Outer Shelf" depositional facies

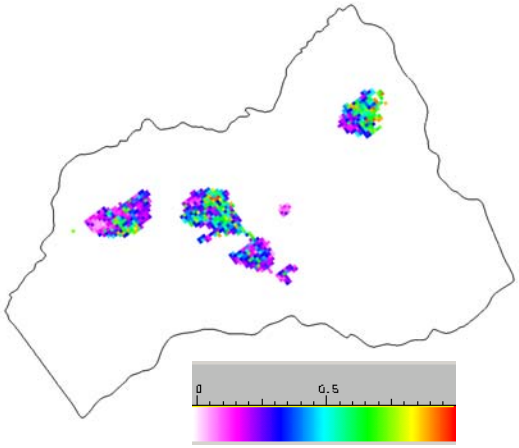

one SGS in "Middle Shelf (high energy)" depositional facies

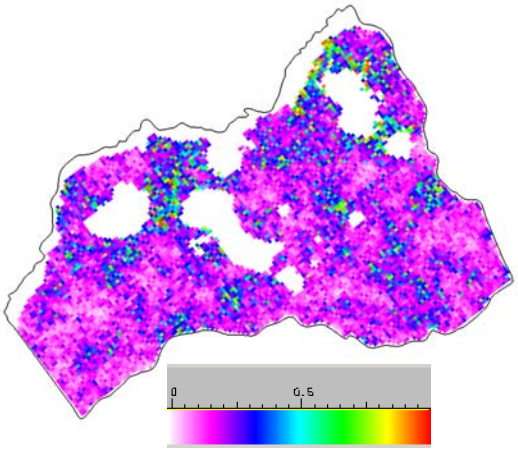

one SGS in "Open/Outer Shelf" depositional facies

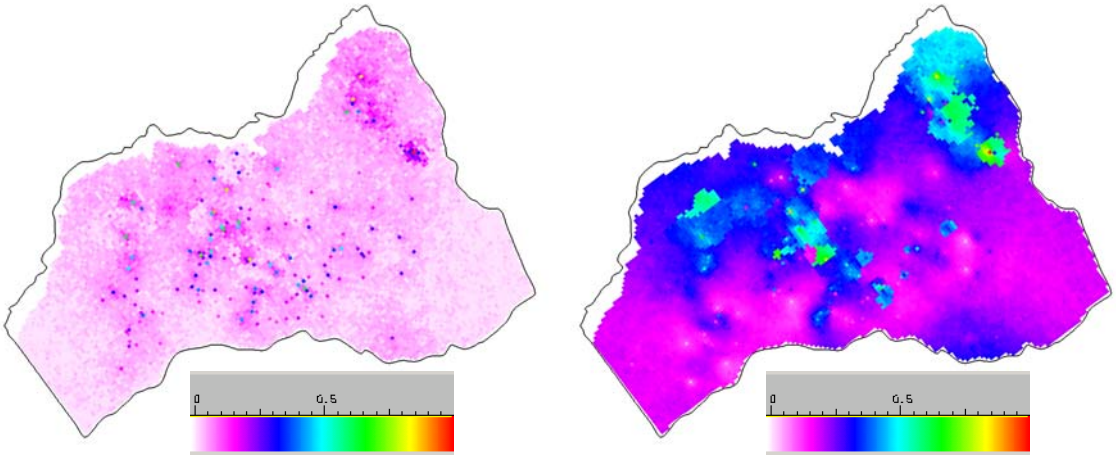

Minimum value per cell of the 200 SGS in both facies

Mean per cell

max

stdd

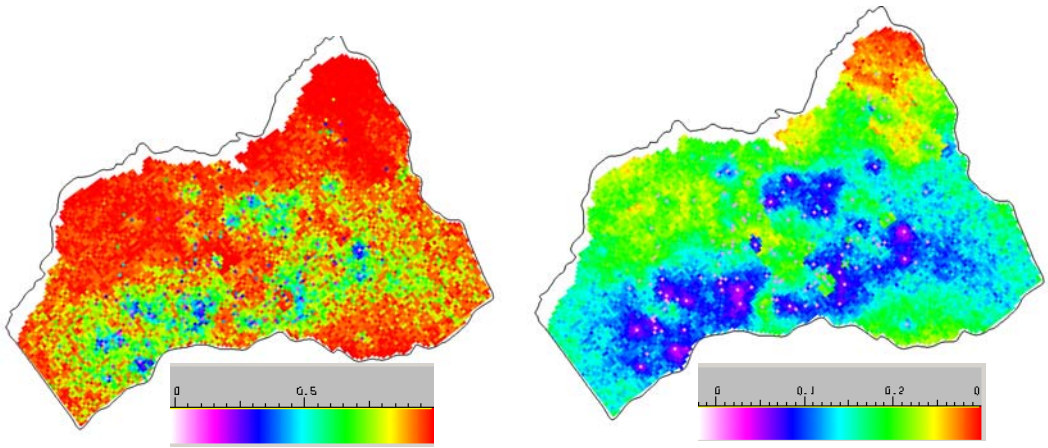

Maximum per cell

Standard deviation per cell

Figure 98: Percent mud modeling in the Santee

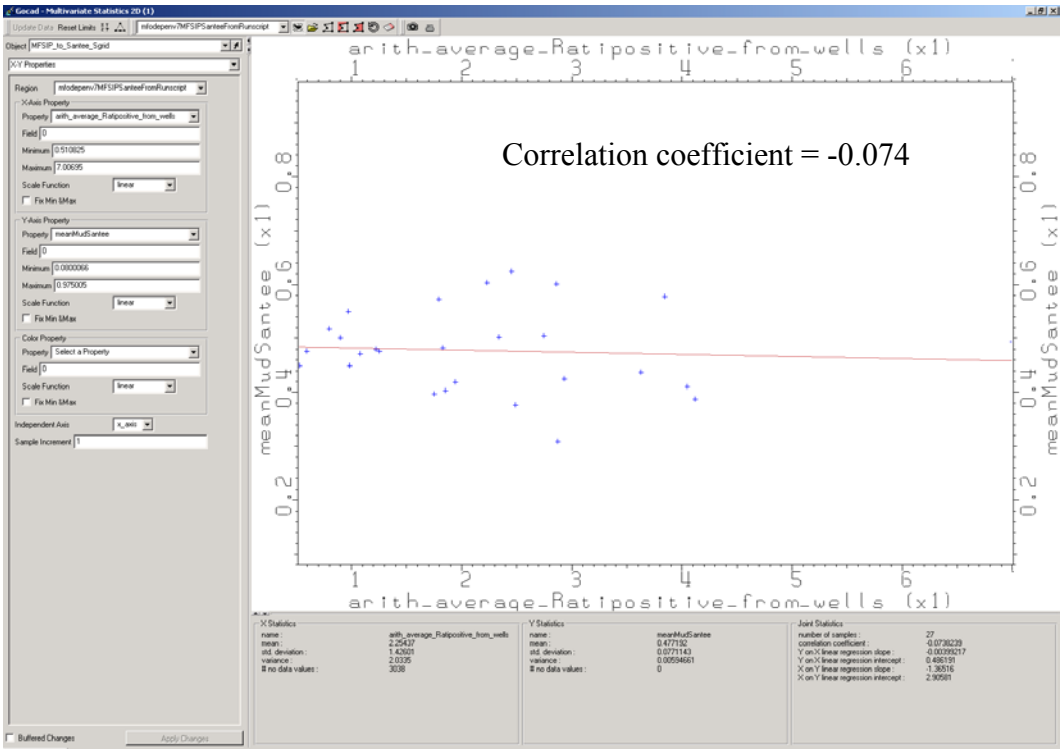

Figure 99: Cross-plot of the mean per cell of percent mud against Friction Ratio from well logs at the logs location for the "Open/Outer Shelf" facies in the Santee

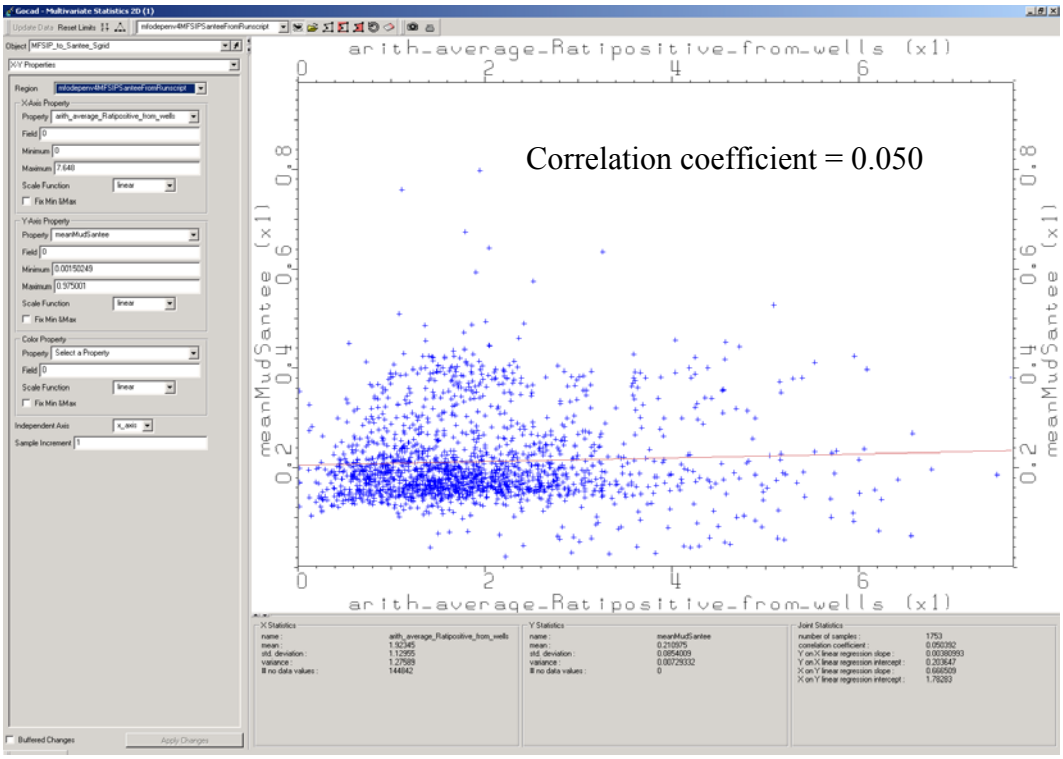

Figure 100: Cross-plot of the mean per cell of percent mud against Friction Ratio from well logs at the logs location for the "Siliciclastic Shelf" facies in the Santee

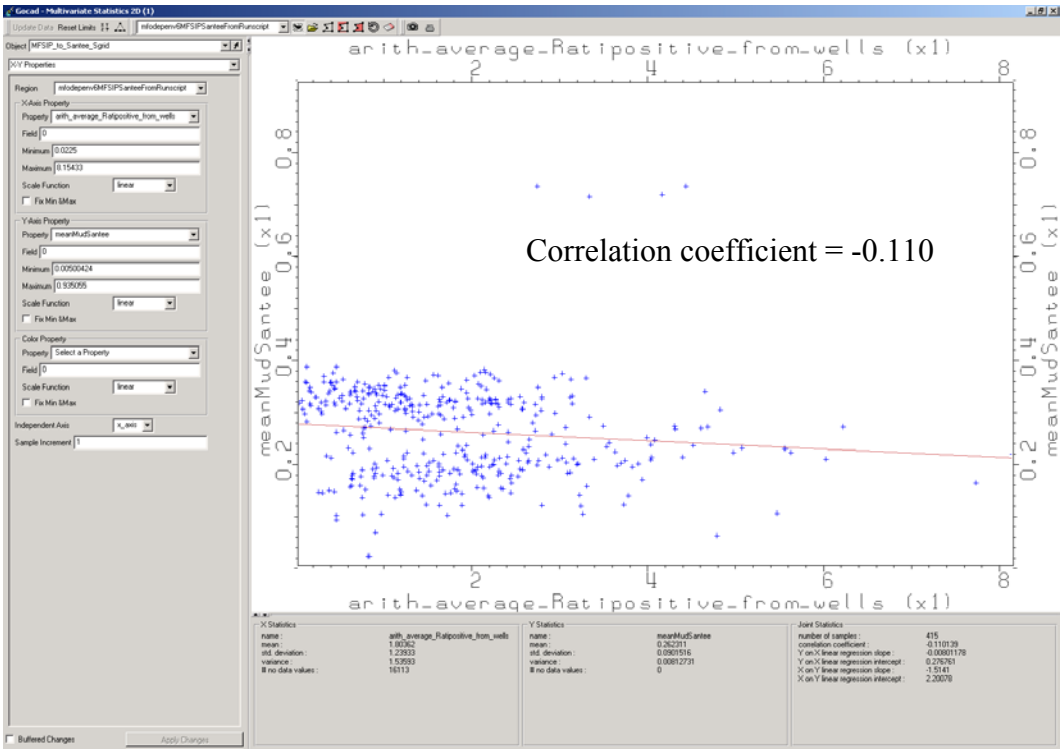

Figure 101: Cross-plot of the mean per cell of percent mud against Friction Ratio from well logs at the logs location for the "Middle Shelf (low energy)" facies in the Santee

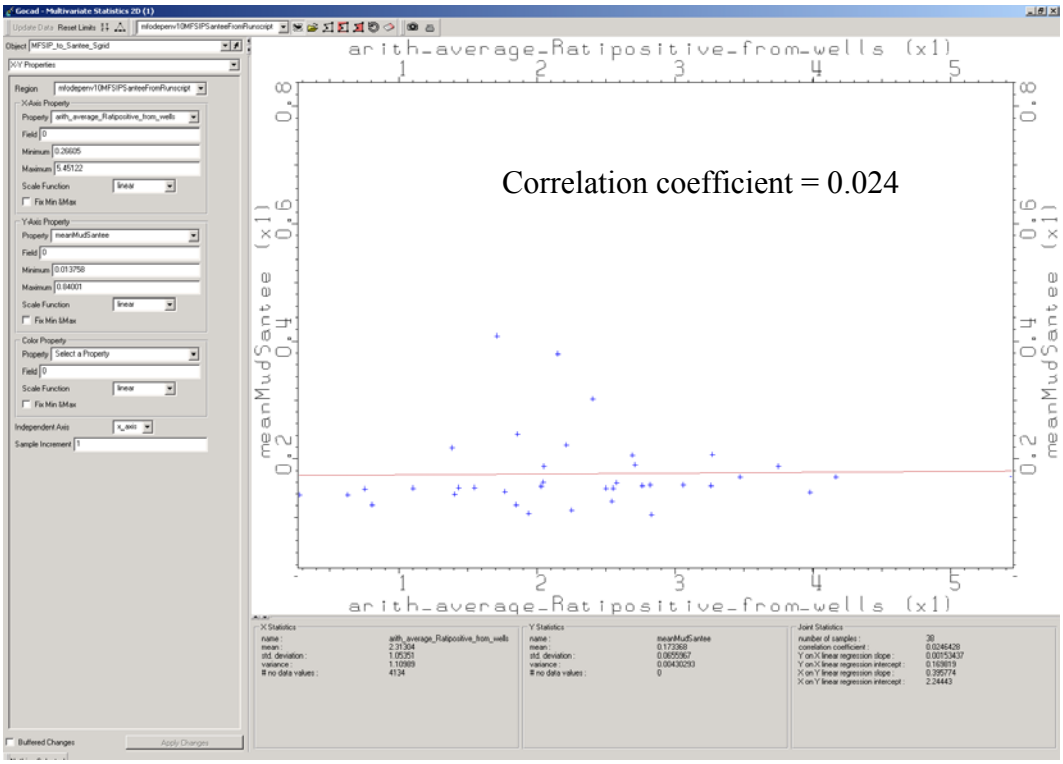

Figure 102: Cross-plot of the mean per cell of percent mud against Friction Ratio from well logs at the logs location for the "Middle Shelf (high energy)" facies in the Santee

Green Clay

- *Percent Mud modeling*

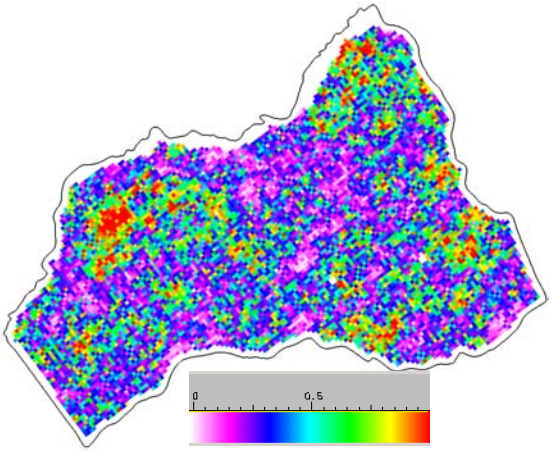

one SGS in the whole Green Clay

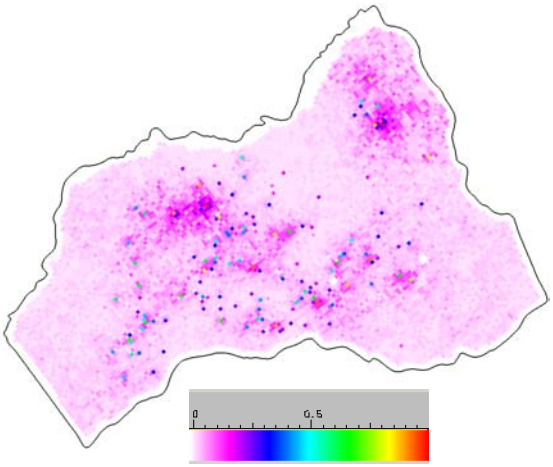

Minimum value per cell of the 200 SGS

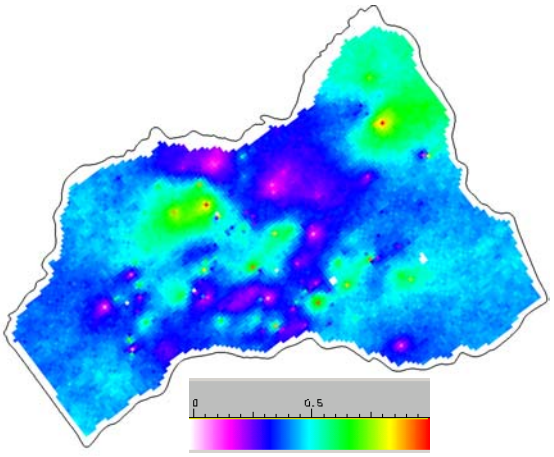

Mean per cell

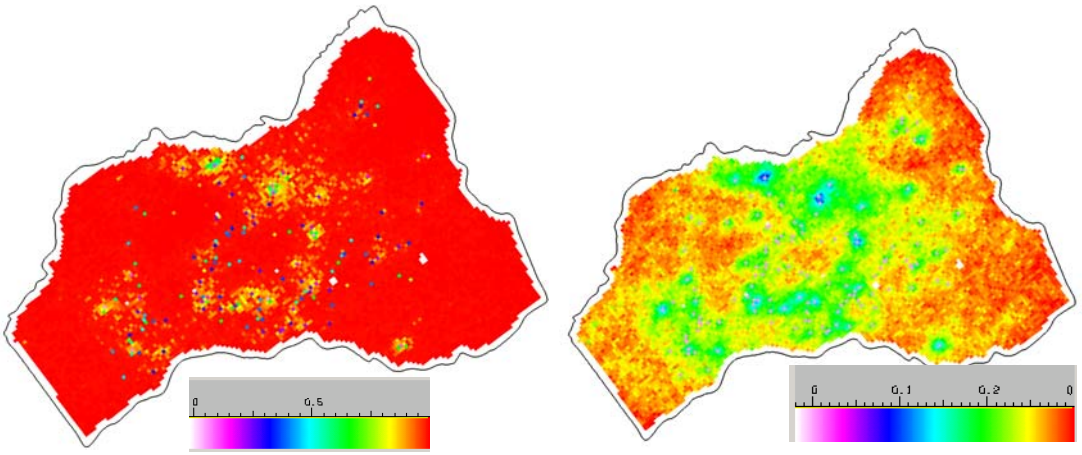

Maximum value per cell of the 200 SGS Standard deviation per cell

Figure 103: Percent mud modeling in the Green Clay

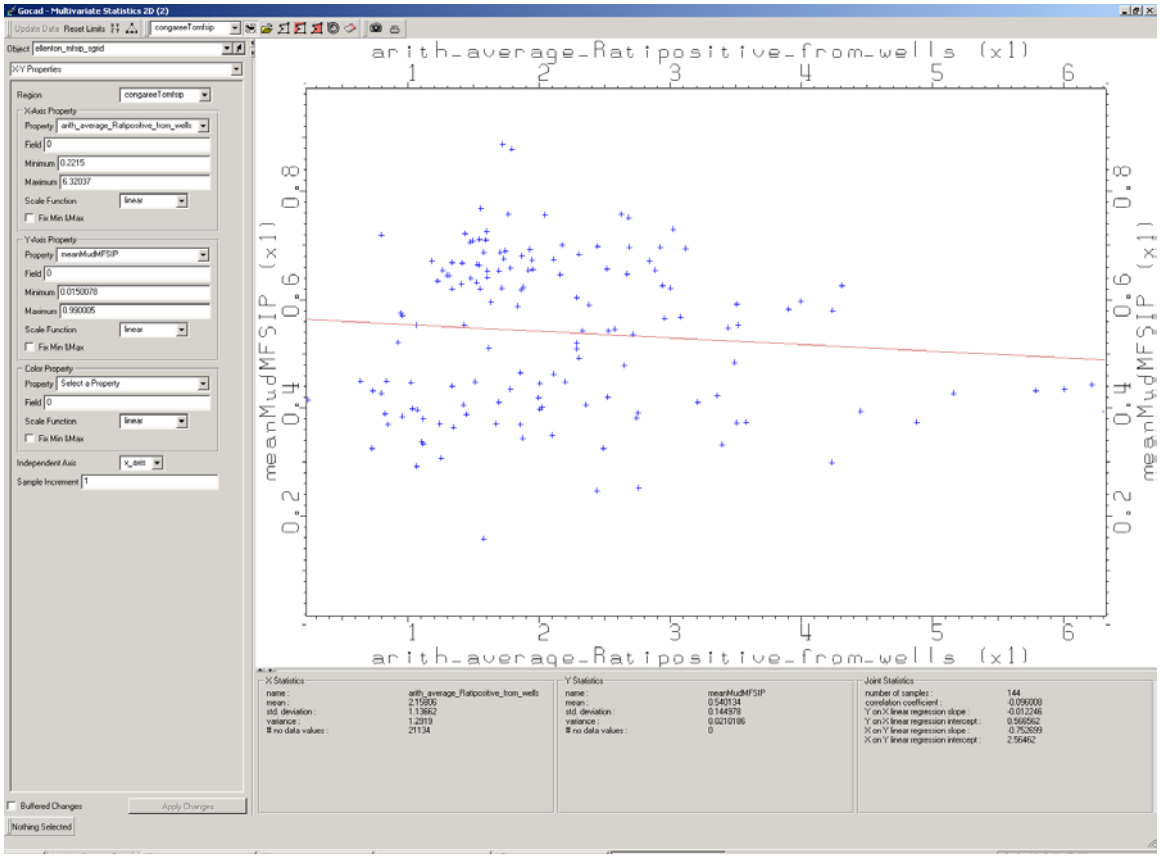

Figure 104: Cross-plot of the mean per cell of percent mud against Friction Ratio from well logs at the logs location in the Green Clay

Congaree

- *Percent Mud modeling*

Corresponding depositional facies map (most common facies per cell map) for the maps shown below

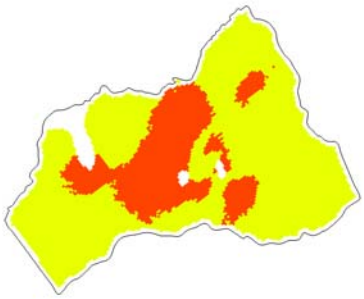

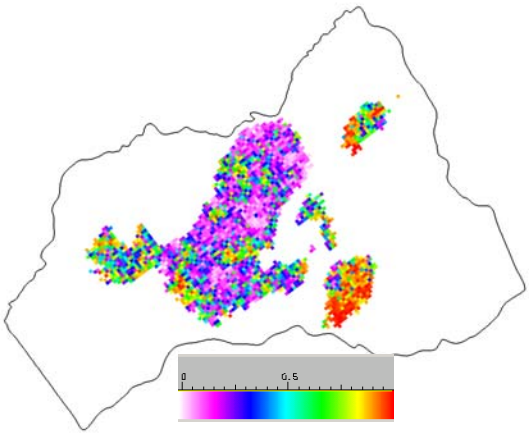

one SGS in "Inner Bay/Lagoonal" depositional facies

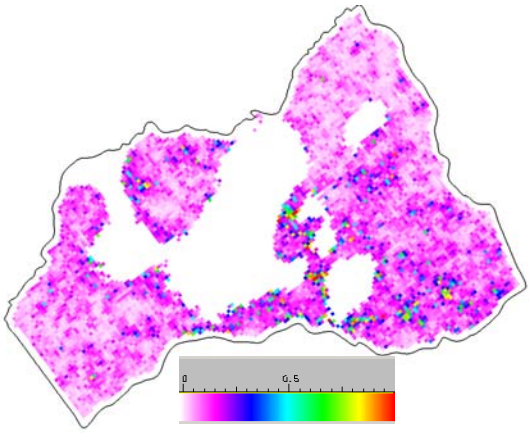

one SGS in "Lower Shoreface" depositional facies

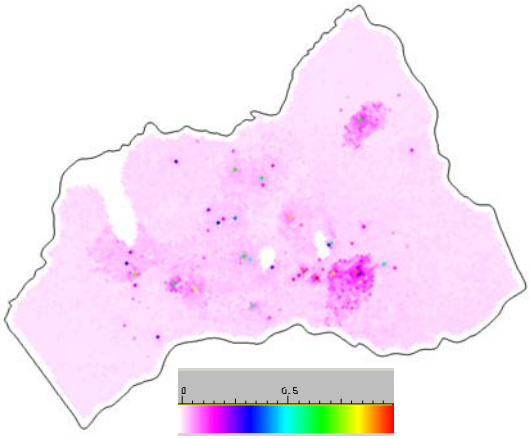

Minimum value per cell of the 200 SGS in both facies

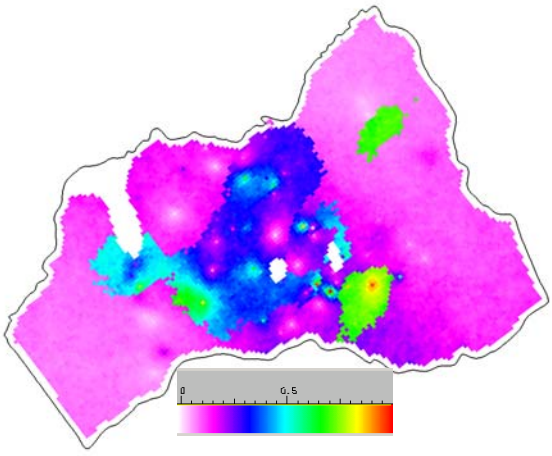

Mean per cell

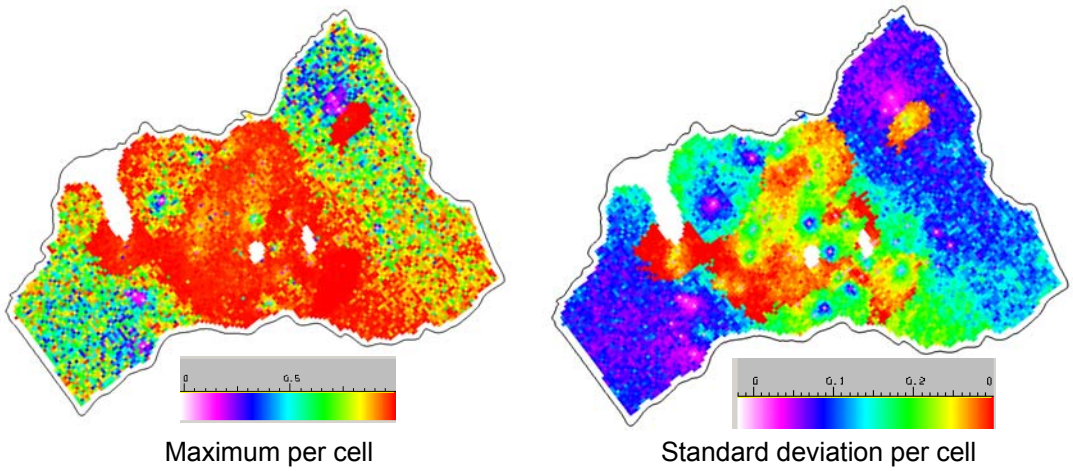

Figure 105: Percent mud modeling in the Congaree

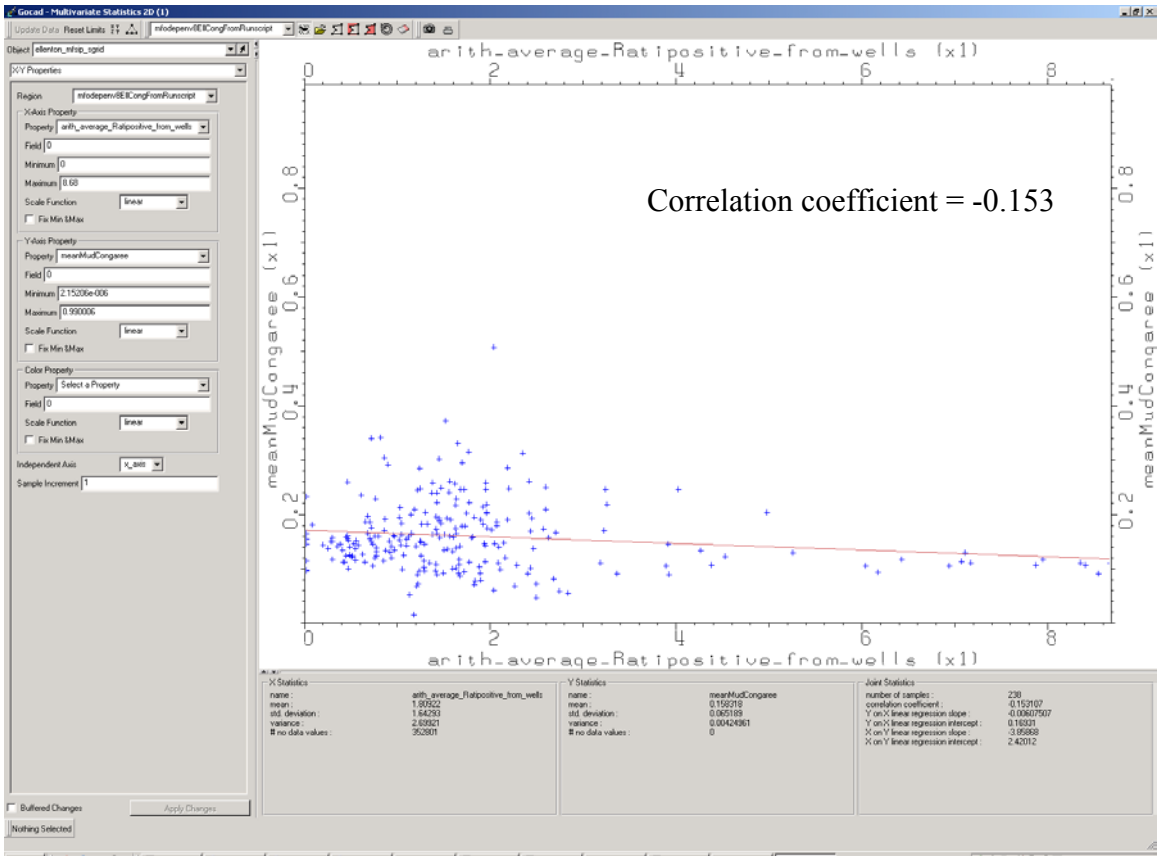

Figure 106: Cross-plot of the mean per cell of Percent mud against Friction Ratio from well logs at the logs location for the "Lower Shoreface" facies in the Congaree

The "Inner bay/Lagoonal" facies does not contain any Friction Ratio logs. The cross-plot cannot be calculated.

Conclusion and Recommendations

The document represents an intermediate project status report. Throughout the duration for this phase of the project, the modeling workflow was continuously improved as more was learned about modeling the various depositional systems.

Creating the structural surfaces was quite complex involving the use of variogram maps to assist in the computation and modeling of the experimental variograms. For each surface a multi-directional nested model was required to reproduce the general NE to SW strike of the coastal plain topography, requiring one anisotropic variogram model. To model an erosional pattern creating by paleochannels flowing roughly perpendicular to the coastal plain, it was necessary to created an additional anisotropic model, and add this model to that of the coastal plain model. Several of the Kriged surfaces appear dimpled, suggesting that additional editing of the horizon picks is needed.

The facies modeling yielded satisfactory results, but the use of the most commonly occurring facies per cell creates a slightly unrealistic result. It is not one of the simulations, but represents a result intermediate between Kriging and simulation. The true spatial scales are not fully preserved. Further work needs to be done to select one of the simulations by means of a ranking scheme, with the criteria for the ranking to be determined at a later stage of the project. One simulation from among the 200 will be selected and used as the template for the petrophysical simulations. This approach will preserve the spatial correlation scales and directionality modeled from the experimental variogram and variogram maps.

The different cross-plots made between the mean Percent mud per cell and the friction ratio well logs showed that the correlation between these two petrophysical properties is very poor, which was not expected. The poor correlation could be explained by the method that was used to get data at the same location for crossplot purpose. Although the friction ratio was used in the collocated cosimulation step and for only one facies, its influence on the final simulation is minimal, adding only a slight “texture” in the end product. Such a relationship does not bode well for the friction ratios use to help predict permeability (we are not sure if such a relationship truly exists, and any correlation may be by pure chance).

References

Boylan, D. C., 1982, *Stratigraphy and Depositional Environments of the Lower South Carolina Coastal Plain Between Charleston and Hilton Head Island.* M.S. Thesis, University of South Carolina.

Colquhoun, D. J., 1991, *Southeast Atlantic Transect.* American Association of Petroleum Geologists, Regional Transect Series #449.

Colquhoun, D. J., and Johnson, H. S., Jr., 1968, "Tertiary Sea-Level Fluctuation in South Carolina". *Palaeogeography, Palaeoclimatology, Palaeoecology, 5:105-126*.

Colquhoun, D. J., Oldham, R. W., Bishop, J. W., and Howell, P. D., 1982, *Updip Delineation of the Tertiary Limestone Aquifer, South Carolina*. Report No. 97, Clemson University Water-Resources Research Institute, Clemson, SC.

Colquhoun, D. J., Woollen, I. D., Van Nieuwenhuise, D. S., Padgett, G. G., Oldham, R. W., Boylan, D. C., Bishop, J. W., and Howell, P. D., 1983, *Surface and Subsurface Stratigraphy, Structure and Aquifers of the South Carolina Coastal Plain*. SCDHEC Report ISBN 0-9613154-0-7, Columbia, SC.

Colquhoun, D. J., Rine, J. M., Segall, M. P., Katuna, M. P., Cohen, A. D., and Siron, D. L., 1994, *Sedimentology and Stratigraphy of the Upland Unit*. Final Report for Task 110, SCUREF Cooperation Agreement AA00900T, Earth Sciences and Resources Institute, University of South Carolina, Columbia, SC 29201.

Cooke, C. W., 1936, *Geology of the Coastal Plain of South Carolina*. U.S. Geological Survey Bulletin 867.

Cooke, C. W. and MacNeil, F. S., 1952, "Tertiary Stratigraphy of South Carolina". *U.S. Geological Survey Professional Paper*, *243-B: l9-29*.

Davis, J. C., 1986, Statistics and data analysis in geology, 2nd ed.: New York, John Wiley, 646 p.

Dennehy, K. F., Prowell, D. C., and McMahon, P. B., 1989, *Reconnaissance Hydrogeologic Investigation of the Defense Waste Processing Facility and Vicinity*, *Savannah River Plant, South Carolina*. Water Resources Investigations Report 88-4221, U. S. Geological Survey, Columbia, SC.

Fallaw, W. C. and Price, V., 1995, "Stratigraphy of the Savannah River Site and Vicinity". *Southeastern Geology, 35: 21-58*.

Fallaw, W. C., Price, V., and Thayer, P., 1990, "Stratigraphy of the Savannah River Site, South Carolina". *Savannah River Region: Transition Between the Gulf and Atlantic Coastal Plains*, *Proceedings of the Second Bald Head Island Conference on Coastal Plains Geology*, University of North Carolina at Wilmington, pp 29-32.

Harris, W. B., Zullo, V. A., Laws, R. A. and Harris, M. K., 1990, "Paleogene Sequence Stratigraphy and Chronostratigraphy of a Core from Allendale County, South Carolina". *Geological Society of America Abstracts with Programs*, *22: 17-18*.

Harris, W. B., Zullo, V. A. and Laws, R. A., 1993, "Sequence Stratigraphy of the Onshore Paleogene, Southeastern Atlantic Coastal Plain, USA". *Sequence Stratigraphy and Facies Associations*. Special Publication 18, International Association of Sedimentologists, pp 537-561.

Hohn, M. E., 1988, Geostatistics and petroleum geology: New York, Van Nostrand Rienhold, 264 p.

Huddlestun, P. F., 1988, *A Revision of the Lithostratigraphic Units of the Coastal Plain of Georgia, the Miocene through Holocene*. Georgia Geologic Survey Bulletin 104.

Huddlestun, P. F and Hetrick, J. H., 1979, *The Stratigraphy of the Barnwell Group in Georgia:* Georgia Geologic Survey Open-File Report 80-1, pp 56-73.

Isaaks, E. H., and R. M. Srivastava, 1989, An introduction to applied geostatistics: Oxford, Oxford University Press, 561 p.

Krige, D. G., 1951, A statistical approach to some basic valuation problems on the Witwatersrand: Journal of the Chemical, Metallurgical and Mining Society of South Africa, no. 52, 1951, p. 119-139.

Krige, D. G., 1966, Two-dimensional weighted average trend surfaces for ore valuation, *in* Proceedings of the symposium on mathematical statistics and computer applications in ore valuation: South African Institute of Ming and Metallurgy, Johannesburg, South Africa, p. 13-38.

Logan, W. R. and Euler, G. M., 1989, *Geology and Groundwater Resources of Allendale, Bamberg, and Barnwell Counties and Part of Aiken County, South Carolina.* South Carolina Water Resources Commission Report 155, Columbia, SC.

Lyell, C., 1845, "Observations on the White Limestone and Other Eocene or Older Tertiary Formations of Virginia, South Carolina, and Georgia". *Quarterly Journal of the Geological Society of London*, *1: 429-442*.

Matheron, G. F., "La théorie des variables régionalisées et ses applications," Tech. Rep. Fascicule 5, Les Cahiers du Centre de Morphologie Mathématique de Fontainebleau, Ecole Supérieure des Mines de Paris, 1970.

Matheron, G. F., "Estimer et choisir," Fascicule 7, Les Cahiers du Centre de Morphologie Mathématique de Fontainebleau, Ecole Supérieure des Mines de Paris, 1978.

Nystrom, P. G., 1986, "Cretaceous-Tertiary Stratigraphy of the Updip Limit of the Coastal Plain Between Ward and Leesville, South Carolina". *Geological Society of America Abstracts with Programs*, *18: 258*.

Nystrom, P. G., Jr. and Willoughby, R. H., 1982a, "Cretaceous, Tertiary, and Pleistocene(?) Stratigraphy of Hollow Creek and Graniteville quadrangles, Aiken County, South Carolina". *Geological Investigations Related to the Stratigraphy in the Kaolin Mining District, Aiken County*, *South Carolina*. Carolina Geological Society 1982 Field Trip Guidebook, South Carolina State Development Board, Division of Geology, Columbia, SC, pp. 80-113.

Nystrom, P. G., Jr. and Willoughby, R. H., 1982b, "Early Tertiary (Jacksonian/Priabonian?) Stratigraphy in Graniteville and Hollow Creek Quadrangles, Aiken County, South Carolina". *Geological Society of America Abstracts with Programs*, *18: 68*.

Nystrom, P. G., Jr., Willoughby, R. H., and Price, L. K., 1989, "The Cretaceous and Tertiary Stratigraphy of the Upper Coastal Plain of South Carolina". *Upper Cretaceous and Cenozoic Geology of the Southeastern Atlantic Coastal Plain*. 28th International Geological Congress Field Trip Guidebook T171, American Geophysical Union., Washington, D.C., pp. 23-42.

Pooser, W. K., 1965, "Biostratigraphy of Cenozoic Ostracoda from South Carolina". *University of Kansas Paleontological Contributions, Arthropoda, 8: 80*.

Robertson, C. G., 1990, *A Textural, Petrographic, and Hydrogeological Study of the Congaree Formation at the Savannah River Site, South Carolina*. M.S. Thesis, University of North Carolina at Wilmington, Wilmington, NC

Robertson, C. G. and Thayer, P. A., 1992, "Petrology and Reservoir Characteristics of the Congaree Formation at the Savannah River Site, South Carolina". *Savannah River Region: Transition Between the Gulf and Atlantic Coastal Plains*, *Proceedings of the Second Bald Head Island Conference on Coastal Plains Geology*, University of North Carolina at Wilmington, pp. 54-55.

Siple, G. E., 1967, *Geology and Ground Water of the Savannah River Plant and Vicinity, South Carolina*. U.S. Geological Survey Water Supply Paper 1841.

Siple, G. E., and Pooser, W. K., 1965, *Proposal of the Name Orangeburg Group for Outcropping Beds of Eocene Age in Orangeburg County and Vicinity, South Carolina*. U.S. Geological Survey Bulletin 1395A.

Sloan, E., 1907, "Geology and Mineral Resources". *Handbook of South Carolina, Volume 2*, South Carolina State Department of Agriculture, Commerce, and Immigration, pp 77-145.

Sloan, E., 1908, *Catalogue of the Mineral Localities of South Carolina*, South Carolina Geological Survey, Series 5, Bulletin 2.

Smits, A.D., Harris, M.K., Hawkins, K.L., and Flach, G.P., 1997, *Integrated Hydrogeological Model of the General Separation Area, Hydrogeologic Famework*, Volume 1, Savannah River Site, pp. 1-35.

Willoughby, R. H., 1983, *Geologic Map of the Graniteville Quadrangle*. South Carolina Geological Survey Open-File Report 31, 1:24,000.

Willoughby, R. H., 1985, *Geologic Map of the Coastal Plain in Johnston and Edgefield Quadrangle*. South Carolina Geological Survey Open-File Report 46, 1:24,000.

Willoughby, R. H., 1986, "Stratigraphy of the Northwestern Edge of the Coastal Plain in Aiken and Lexington Counties, South Carolina". *Geological Society of America Abstracts with Programs*, *18: 272-273*.

Yarus, J. M. and Chambers, R. L., 1994, Stochastic Modeling and Geostatistics, Principles, Methods, and Case Studies: AAPG Computer Applications in Geology, No. 3, 371 p.

Appendix 1

- ***3D framework, base conformable***

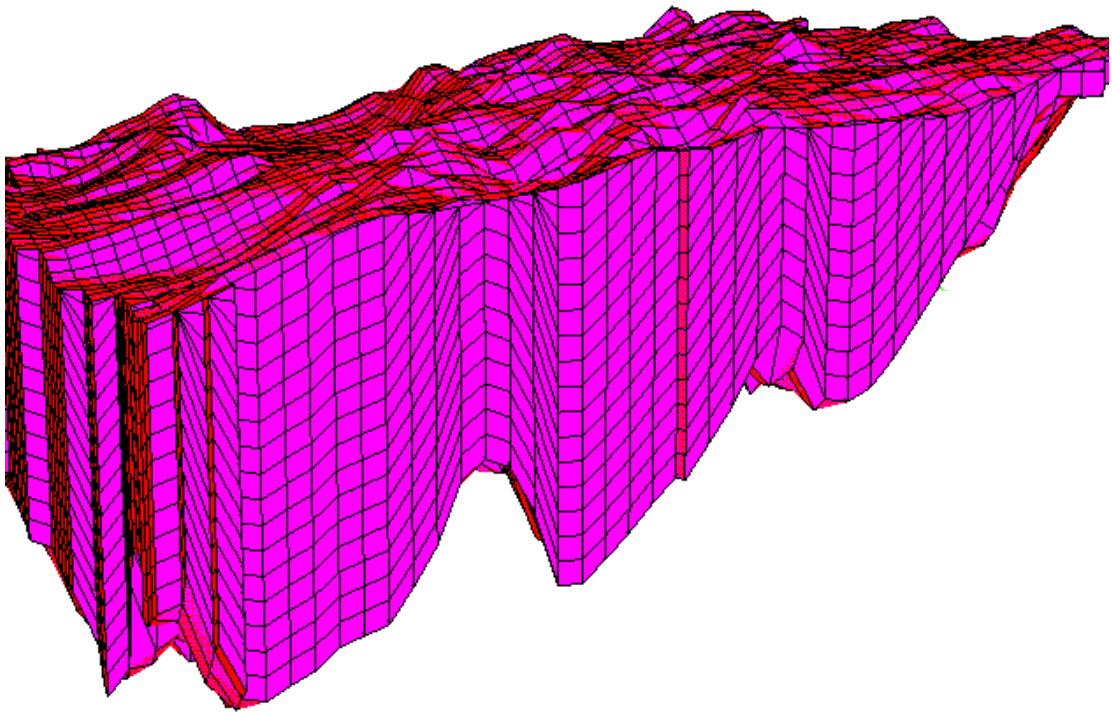

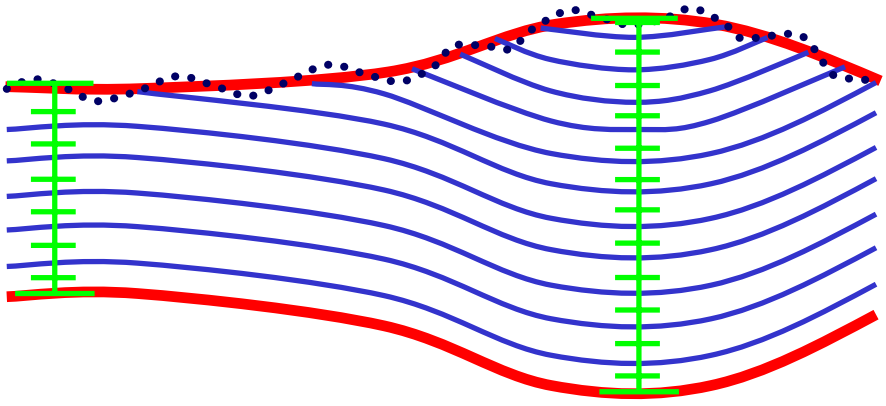

- ***3D framework, top conformable***

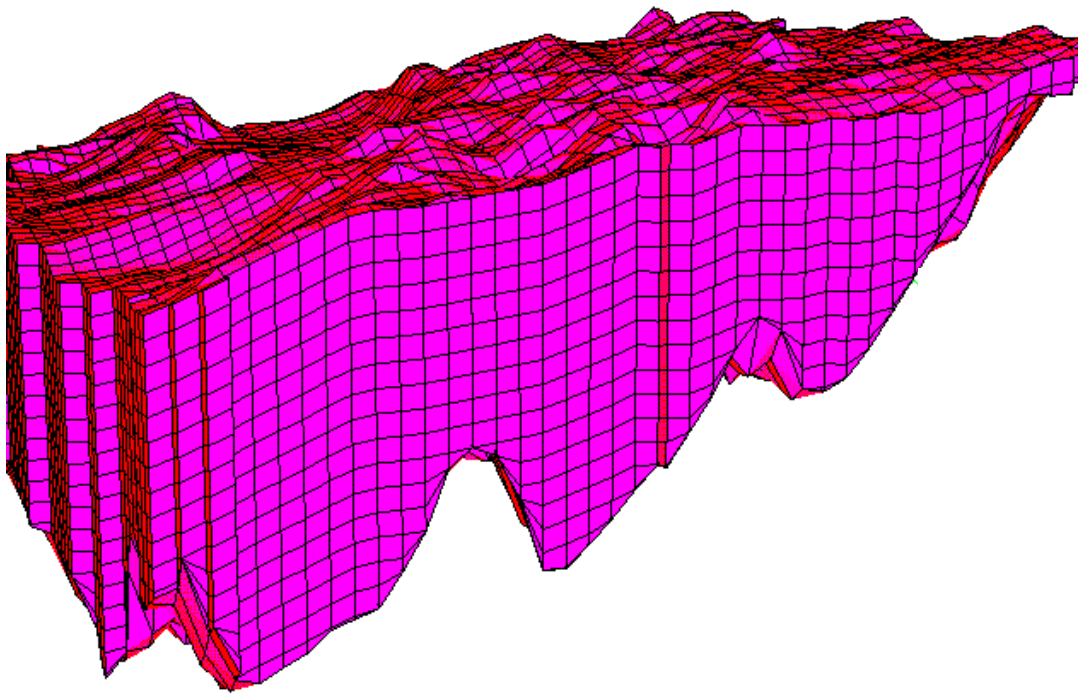

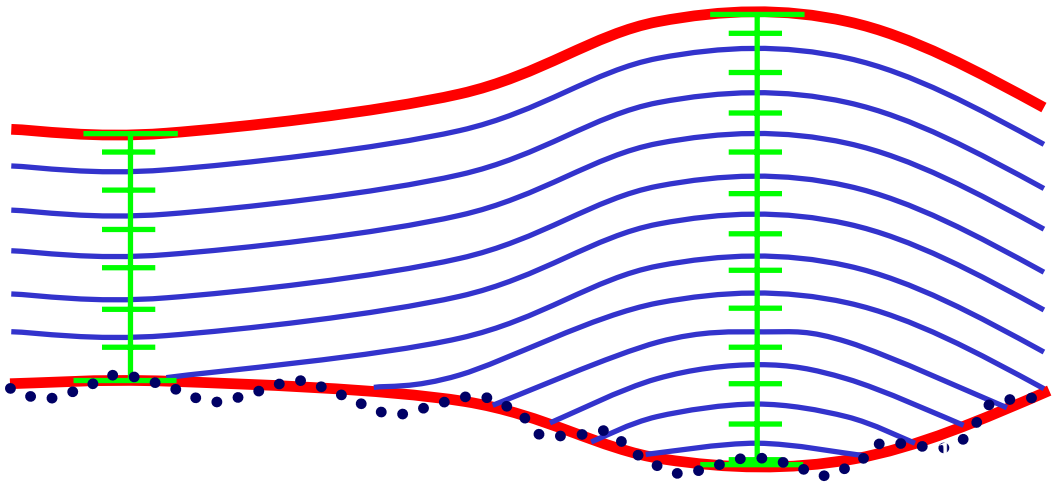

- ***3D framework, proportional***